AD-A186 878

NAVAL POSTGRADUATE SCHOOL
Monterey, California

DTIC
SELECTED
OCT 2 3 1987
D

THESIS

A PILOTED SIMULATION INVESTIGATING
HANDLING QUALITIES
AND PERFORMANCE REQUIREMENTS OF A
SINGLE-PILOT HELICOPTER
IN AIR COMBAT EMPLOYING A HELMET-DRIVEN
TURRETED GUN

by

Jeffrey N. Williams

September 1987

Thesis Advisor   Donald M. Layton

87   14   448

AD-A186878

REPORT DOCUMENTATION PAGE

1a REPORT SECURITY CLASSIFICATION	1b RESTRICTIVE MARKINGS
Unclassified	

2a SECURITY CLASSIFICATION AUTHORITY	3 DISTRIBUTION/AVAILABILITY OF REPORT
	Approved for public release; distribution is unlimited.
2b DECLASSIFICATION/DOWNGRADING SCHEDULE	

4 PERFORMING ORGANIZATION REPORT NUMBER(S)	5 MONITORING ORGANIZATION REPORT NUMBER(S)

6a NAME OF PERFORMING ORGANIZATION	6b OFFICE SYMBOL (If applicable)	7a NAME OF MONITORING ORGANIZATION
Naval Postgraduate School	67	Naval Postgraduate School

6c ADDRESS (City, State, and ZIP Code)	7b ADDRESS (City, State, and ZIP Code)
Monterey, California 93943-5000	Monterey, California 93943-5000

8a NAME OF FUNDING/SPONSORING ORGANIZATION	8b OFFICE SYMBOL (If applicable)	9 PROCUREMENT INSTRUMENT IDENTIFICATION NUMBER

8c ADDRESS (City, State, and ZIP Code)	10 SOURCE OF FUNDING NUMBERS			
	PROGRAM ELEMENT NO	PROJECT NO	TASK NO	WORK UNIT ACCESSION NO

11 TITLE (Include Security Classification)

A Piloted Simulation Investigating Handling Qualities and Performance Requirements of a Single-Pilot Helicopter in Air Combat Employing a Helmet-Driven Turreted Gun.

12 PERSONAL AUTHOR(S)
Williams, Jeffrey N.

13a TYPE OF REPORT	13b TIME COVERED	14 DATE OF REPORT (Year Month Day)	15 PAGE COUNT
Master's Thesis	FROM ___ TO ___	1987 September	113

16 SUPPLEMENTARY NOTATION

17 COSATI CODES			18 SUBJECT TERMS (Continue on reverse if necessary and identify by block number)
FIELD	GROUP	SUB-GROUP	Helicopter, Helicopter Air Combat, Maneuverability, Helmet-Mounted Sight, Turreted Gun, Handling Qualities, Flight Control System, Performance Envelopes

19 ABSTRACT (Continue on reverse if necessary and identify by block number)

The development, implementation, and results of a pilot-in-the-loop fixed-base simulation investigating yaw-axis handling qualities and vehicle maneuverability requirements for the task of single-pilot helicopter air combat at terrain-flight altitudes are presented. Experimental variables included yaw-axis natural frequency and damping. Weapon system type was also varied to include a full- and limited-traverse turret driven by a helmet-mounted sight and a fixed-forward gun. Results indicated that a high yaw natural frequency ($\omega_n = 1.5$-2.0 rad/sec) and high yaw damping ($\zeta \sim 1.4$) were desirable for Level 1 handling qualities. Pilot ratings generally decreased and the effect of the yaw dynamic characteristics became more pronounced as the weapon system became more restrictive. Other analyses discussed are the vehicle maneuver envelope usage, turret envelope usage, tracking performance, and pilot commentary.

20 DISTRIBUTION/AVAILABILITY OF ABSTRACT	21 ABSTRACT SECURITY CLASSIFICATION
☒ UNCLASSIFIED/UNLIMITED ☐ SAME AS RPT ☐ DTIC USERS	Unclassified

22a NAME OF RESPONSIBLE INDIVIDUAL	22b TELEPHONE (Include Area Code)	22c OFFICE SYMBOL
Donald M. Layton	(408) 646-2997	67Ln

DD FORM 1473, 84 MAR
83 APR edition may be used until exhausted
All other editions are obsolete

A Piloted Simulation Investigating Handling Qualities
and Performance Requirements of a Single-Pilot Helicopter
in Air Combat Employing a Helmet-Driven Turreted Gun

by

Jeffrey N. Williams
Captain, United States Army
B.S., United States Military Academy

Submitted in partial fulfillment of the
requirements for the degrees of

MASTER OF SCIENCE IN AERONAUTICAL ENGINEERING
and
AERONAUTICAL ENGINEER

from the

NAVAL POSTGRADUATE SCHOOL
September 1987

Author: _____
Jeffrey N. Williams
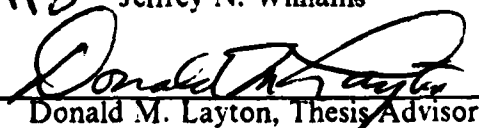
Approved by: _____
Donald M. Layton, Thesis Advisor

_____
J. Victor Lebacqz, Second Reader

_____
Max F. Platzer, Chairman,
Department of Aeronautical Engineering

_____
G. E. Schacher,
Dean of Science and Engineering

2

ABSTRACT

The development, implementation, and results of a pilot-in-the-loop fixed-base simulation investigating yaw-axis handling qualities and vehicle maneuverability requirements for the task of single-pilot helicopter air combat at terrain-flight altitudes are presented. Experimental variables included yaw-axis natural frequency and damping. Weapon system type was also varied to include a full- and limited-traverse turret driven by a helmet-mounted sight and a fixed-forward gun. Results indicated that a high yaw natural frequency (ω_n = 1.5-2.0 rad/sec) and high yaw damping ($\zeta \sim$ 1.4) were desirable for Level 1 handling qualities. Pilot ratings generally decreased and the effect of the yaw dynamic characteristics became more pronounced as the weapon system became more restrictive. Other analyses discussed are the vehicle maneuver envelope usage, turret envelope usage, tracking performance, and pilot commentary.

3

TABLE OF CONTENTS

LIST OF TABLES

8

LIST OF FIGURES

ACKNOWLEDGEMENTS

I. INTRODUCTION

The combat helicopter has evolved into one of the most powerful weapon systems on the modern battlefield. Its incorporation into the combined arms team has enhanced the commander's capability of projecting combat power through mobility, speed, and flexibility. History has shown that the most effective method of countering a developing technology is through that very same technology. In light of the helicopter's evolving lethality and combat potential, it has become apparent that air-to-air combat is inevitable.

There exists a great deal of evidence that the Threat recognizes the value of a anti-helicopter capability. Recent information released regarding the Threat's newest helicopters, the Havoc and the Hokum, has shown that both have a significant anti-helicopter capability. It has been suggested that the Hokum may even be optimized for that role.

There are many factors which influence a combat helicopter's success in the air combat role. Among those factors, the aircraft must have the maneuverability and agility to gain a firing position first and the weapon systems must be able to get first round hits for successful air combat. Air-to-air combat at terrain flight altitudes requires continual precision of control. Critical to success is the ability of the pilot to maneuver the aircraft quickly and precisely and bring the weapons to bear on the threat aircraft.

One of the current issues of concern is the type/combination of weapon systems that should be implemented for air combat and how that type effects the required handling qualities. For example, for the shorter engagement ranges what type of gun is most effective and should it be turreted. If so, how is it best driven; i.e., head-driven, eye-driven, hand controller? What maneuverability and agility characteristics effect the pilots ability to employ a turreted gun?

In an attempt to address these questions, this report documents a piloted simulation investigating helicopter handling qualities requirements in air combat employing a turreted gun driven by a helmet-mounted sight.

12

II. PREVIOUS RESEARCH IN HELICOPTER AIR COMBAT

In 1982, the capability to perform the helicopter air combat mission was identified as a high priority deficiency in the U.S. Army. Subsequently, the air combat mission has been among the most significant factors driving military rotary-wing research, both analytical and flight test. Research has focused equally on both near-term programs such as developing an air-to-air capability on aircraft in the current inventory, and long-term programs such as the Family of Light Helicopters (LHX). Analytical research has included many non-realtime computer simulations which have looked at mission success and combat survivability as functions of parameters such as performance, agility, armament, signatures, tactics, countermeasures, and aircraft configurations. Several of these simulations are documented in References 1 - 4.

Flight research has included the series of Air-to-Air Combat Tests (AACT) at Patuxent River Air Test Center which investigated clear-air one-on-one maneuvering against dissimilar aircraft [Ref. 5] and the Air-to-Air Combat (ATAC) tests at Fort Hunter Liggett which focused on the verification of current doctrine, short-term hardware fixes, and current weapon system effectiveness [Ref. 6].

Several man-in-the-loop simulations have also been developed in support of helicopter air combat research. At NASA's Ames Research Center, the Vertical Motion Simulator (VMS) has been used for a series of investigations into handling qualities requirements for a helicopter in air combat. During 1984, the Helicopter Air Combat (HAC) simulation facility consisting of a single-pilot generic cockpit and a terrain data base appropriate for the air combat task was developed on the VMS [Ref. 7]. Several experiments have since been conducted utilizing the HAC facility focusing primarily on the handling qualities required for various tasks, including the air-to-air combat task.

NASA TN-D-5153 defines handling qualities as "those qualities or characteristics of an aircraft that govern the ease and precision with which a pilot is able to perform the tasks required in support of an aircraft role" [Ref. 8]. For military operations, Handling Qualities are specified in terms of levels where the allowable level for each rotorcraft normal state is [Ref. 9]:

a)   Operational Flight Envelope -- Level 1

b)   Service Flight Envelope --Level 2

c)   Emergency Flight Envelope -- Level 3

Levels are related to the Cooper-Harper Pilot Ratings in that ratings 1-3.5 constitute level 1, ratings 3.5-6.5 constitute level 2, and ratings 6.5-8.5 constitute level 3, as depicted in Figure 2.1.
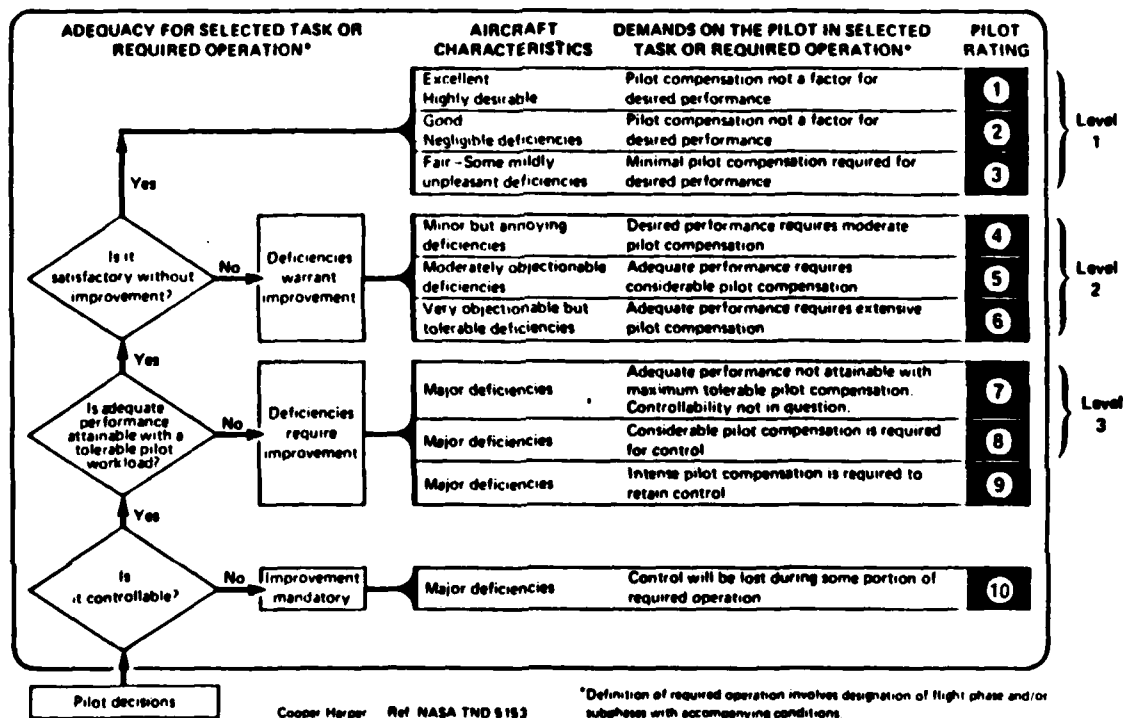
Figure 2.1   Cooper-Harper Rating Scale and Handling Qualities Levels
(From Reference 8).

The ability to define the required handling qualities characteristics of future combat helicopters is critical for the task of helicopter air combat. Two experiments have been conducted on the VMS which were dedicated to the investigation of handling qualities for helicopter air combat. The most recent, Helicopter Air Combat II (HAC II) conducted January 1986, investigated control response characteristics using a fixed-forward gun with emphasis placed on the yaw axis dynamics [Ref. 10, 11].

The subject of this report is a man-in-the-loop simulation experiment designated Helicopter Air Combat III (HAC III). The remainder of the report is divided into five

14

primary sections. Section III defines the nature of the problem and describes the developmental goals and the experimental objectives. Section IV describes the algorithms and models developed prior to the simulation period which were originally intended to be incorporated into the simulation. Section V explains the procedure used to implement and validate the various components of the model, and documents the modifications, omissions, and additions made during the validation phase. Section VI is an analysis of the results of the experimental portion of the simulation. Finally, Section VII presents some conclusions made based on the analysis and offers some suggestions for future investigations into handling qualities requirements for helicopter air combat.

III. NATURE OF THE PROBLEM

Previous man-in-the-loop simulations for handling qualities research in helicopter air combat have employed maneuver and tracking tasks utilizing a fixed-forward gun. Additionally, with the exception of HAC I and II, the majority of the research has concentrated in the pitch and roll axis. HAC II demonstrated that the yaw axis is very important in terms of handling qualities for the task of engaging a threat helicopter with a fixed gun. The experiment to be discussed here (HAC III) extended the previous work to examine the effect of varying yaw dynamics in the employment of a turreted gun in helicopter air combat.

For the development phase of the HAC III experiment for implementation on the VMS, the following principal goals were established:

- To develop the capability to employ a turreted gun with specified capabilities and limitations.

- To incorporate ballistics modeling to include tracer representation on the visual scene and recoil forces.

- To integrate the Honeywell IHADSS (Integrated Helmet and Display Sighting System) with the VMS facility.

- To develop and implement a lead computing fire control which would account for ownship and target states.

- To improve the texture and contrast of the visual scene to provide better visual cues for near-earth tactical flight altitudes.

Assuming the successful achievement of the developmental goals, the following experimental objectives were sought:

- To establish the boundary between level 1 and level 2 flying qualities in terms of yaw-axis dynamics (natural frequency and damping) employing a turreted gun in helicopter air combat.

- To establish variations in task performance and workload for different types of gun weapon systems; i.e., full- and limited-traverse turret, and fixed-forward.

- To establish the use of the maneuver envelope on helicopter air combat maneuvering employing a turreted gun.

IV. DEVELOPMENT OF THE EXPERIMENT

This section provides a brief description of the simulator architecture and the HAC facility developed during previous years. The different aspects of the experimental design and the algorithms for the various subroutines necessary to meet the specific experimental goals and objectives of HAC III are described.

A. VMS FACILITY

HAC III was performed on the NASA Ames Vertical Motion Simulator (VMS) in a fixed-base mode. The cockpit (Blue-ship) used (designated R-CAB) was a single-pilot configuration with conventional controllers, a standard instrument panel, and a panel-mounted situational display. A three-window, wide-field-of-view, high resolution, computer generated image (CGI) was displayed to the pilot. The Honeywell Integrated Helmet and Display Sighting System (IHADSS) was used to present flight symbology and targeting information to the pilot.

A fourth available window (visual channel) provided a single window view to a second cab (designated S-CAB) from a second eyepoint located at the CG of the threat aircraft (Red-ship). The Red-ship was equipped with a head-up display (HUD) and piloted using a four-axis pencil controller. On the visual scene, the Red aircraft was depicted as a MI-24 Hind and the Blue aircraft, as a generic UH-60 silhouette.

The VMS facility is composed of several major components. The computer model was run using a CDC 7600 mainframe as the host computer. The computer generated imagery (CGI) was generated using a Singer-Link Digital Image Generator (DIG) computer. The display information was calculated on a PDP 11/55 computer. The head-up and panel-mounted displays were generated on a Evans and Sutherland Picture System One (PS1) computer. The IHADSS display was generated on a Integrated Raster Imaging System (IRIS). Figure 4.1 illustrates the system architecture used for the experiment.
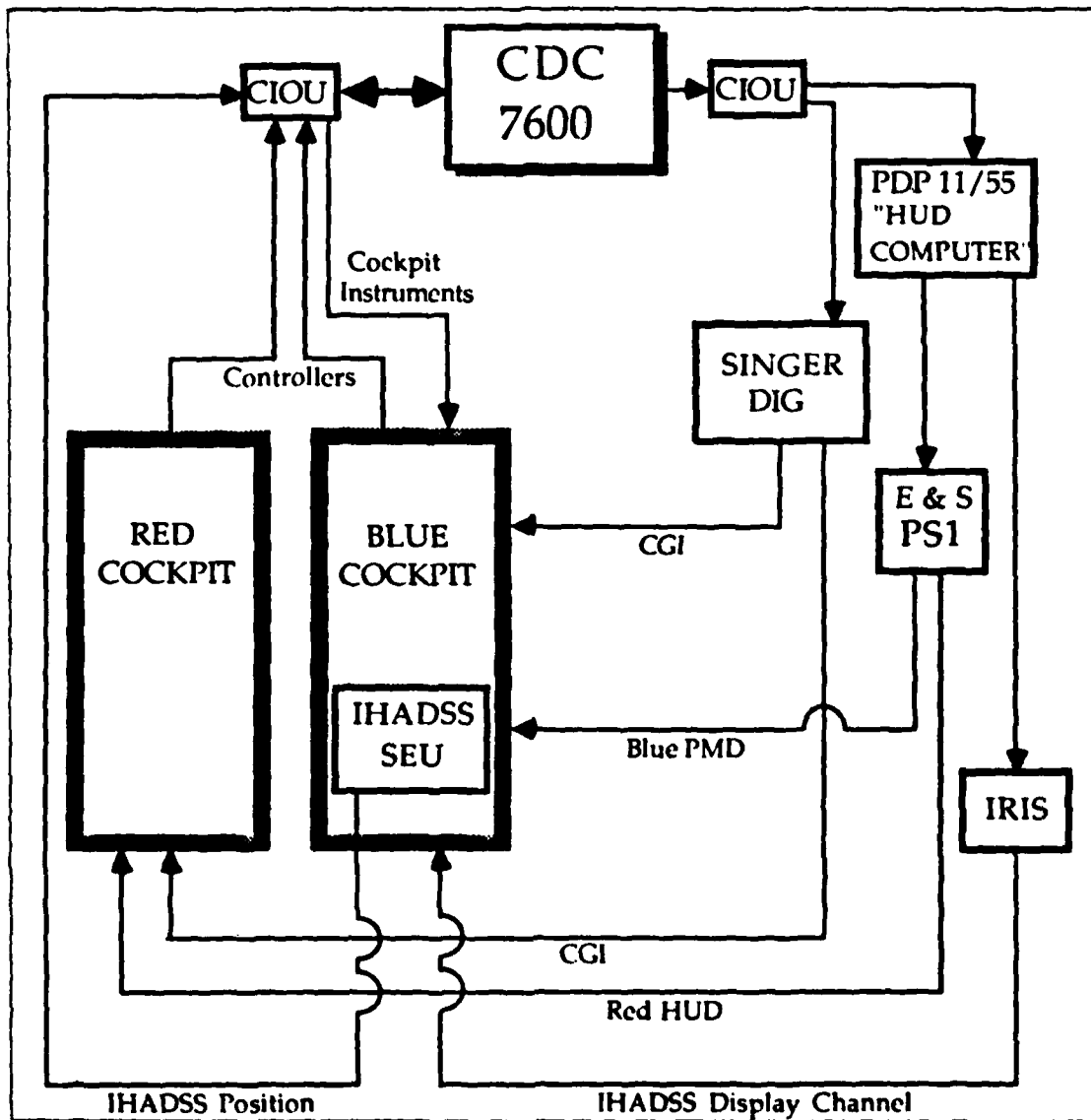
Figure 4.1   Simulation System Architecture.

B.   THE HELICOPTER AIR COMBAT (HAC) FACILITY

1. Blue Aircraft

a. Cockpit

The ownship cockpit was a single pilot configuration with conventional controllers. Artificial force-feel characteristics were provided to the controls by electro-hydraulic loaders. The values for control displacements, friction settings, breakout

18

forces, and force gradients for each of the controls was adjustable. The seat was equipped with four degree-of-freedom adjustments for the pilot. The pedal position was also adjustable to the pilot.

The standard instrument panel included the following flight instruments:

1) airspeed indicator

2) altimeter

3) vertical speed indicator

4) turn and slip indicator

5) attitude indicator

6) radio magnetic indicator

7) magnetic compass

8) collective trim

9) g-meter

10) clock

Additionally, a torque meter was included in the cockpit.

A panel-mounted situation display, explained in more detail later, provided range and relative position and altitude of the threat aircraft to the pilot when the line of sight condition was satisfied. Figure 4.2 depicts the arrangement of the cockpit instrument panel, to include the instruments, location of the panel-mounted display, and the boresight reticle unit (discussed later).

b. Aircraft model

The own-ship or Blue aircraft was driven by a generic conventional helicopter model using quasi-static linear stability and control derivatives and the complete nonlinear kinematic and gravitational terms. The model, explained in more detail in Appendix A, facilitated the assignment of particular combinations of natural frequency and damping in each independent axis. The model was uncoupled but allowed the addition of dihedral and automatic turn coordination. The model also utilized either a rate command/attitude hold or an attitude command control system in the pitch and roll axes and a rate command control system for yaw and the vertical axis. A complete description of the aircraft model can be found in Reference 11, Appendix A.

For HAC III, non-linear limits for normal load factor, rates of climb and descent, and sideslip were added to the model to facilitate the investigation of maneuverability contraints. The steady-state normal load factor limit, adopted from HAC II, is shown in Figure 4.3. The capability is similar to the AH-64 Apache.

19
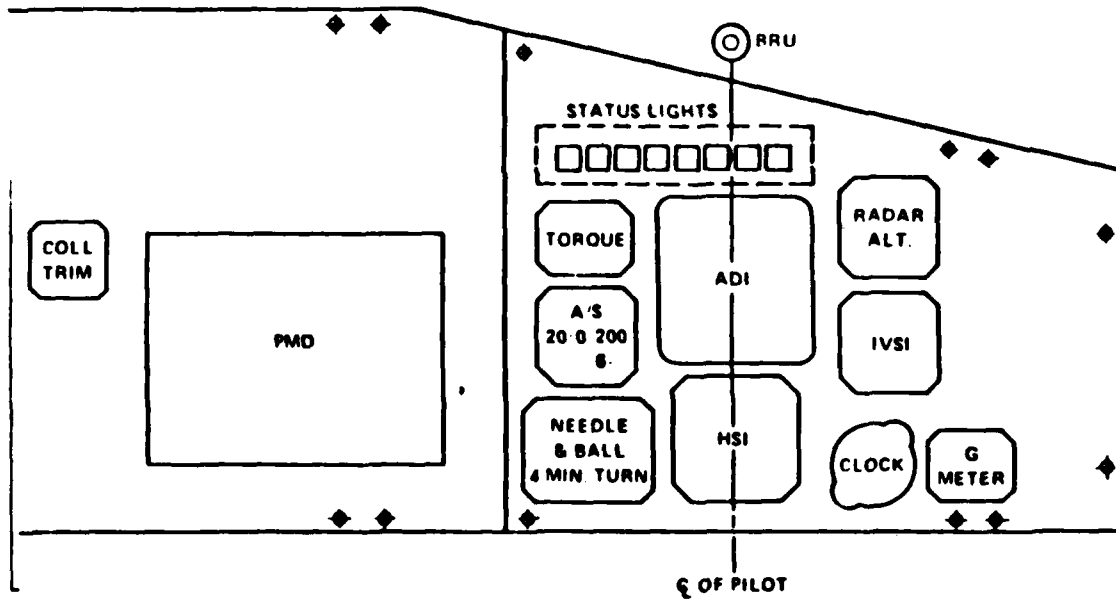
Figure 4.2   Blue Cockpit Instrument Panel.
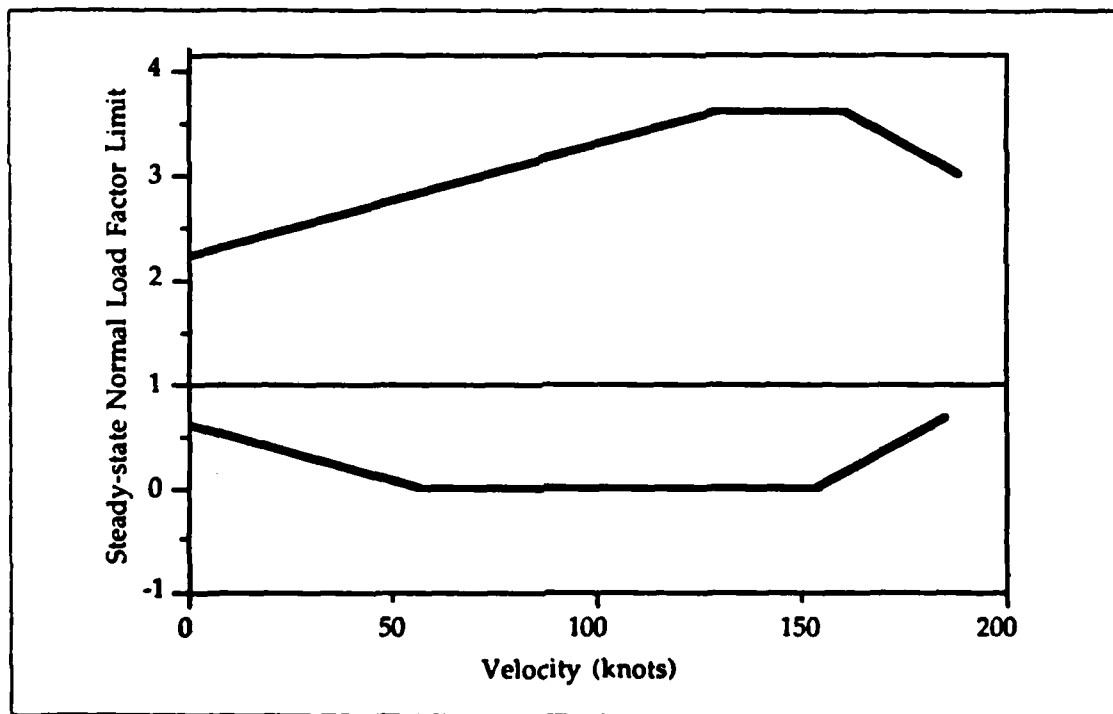
Figure 4.3   Steady State Normal Load Factor Limit.

The maximum steady-state rates of climb and descent added to the aircraft model are shown in Figure 4.4 . The rate of descent limit curve, added to the HAC II model, is a linear approximation to values obtained from reports documenting flight tests of the AH-1G [Ref. 12] and UH-1 [Ref. 13]. The steady-state sideslip limit is shown in Figure 4.5 and is comparable to the limits of the UH-60 and AH-64.
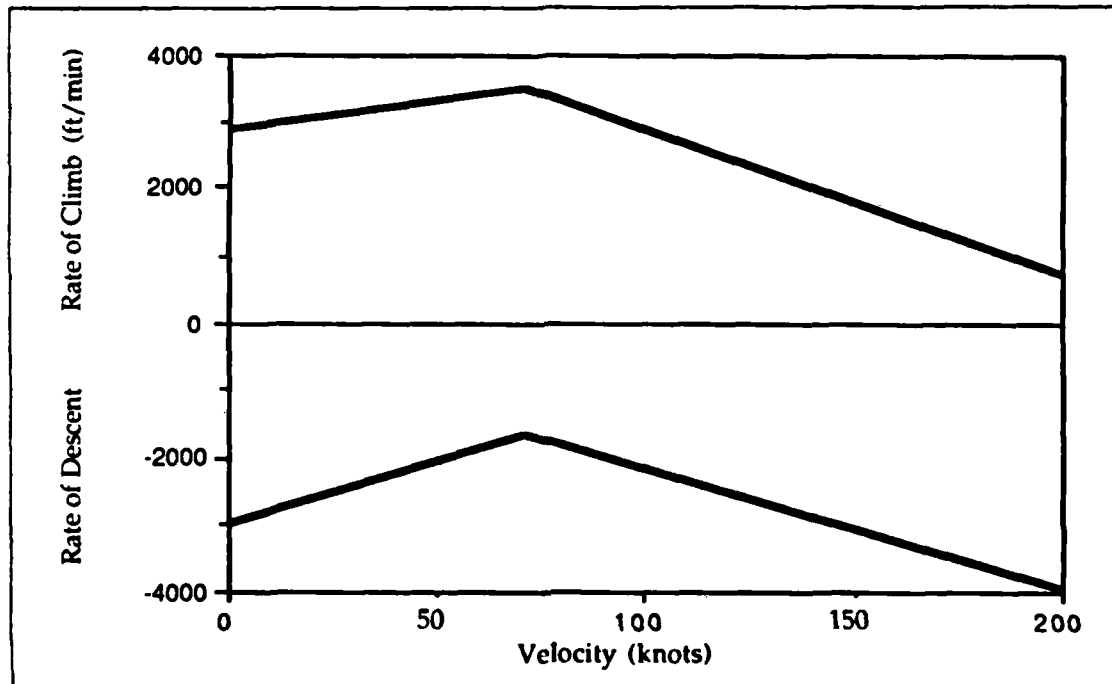
Figure 4.4 Maximum Steady-State Rates of Climb and Descent.
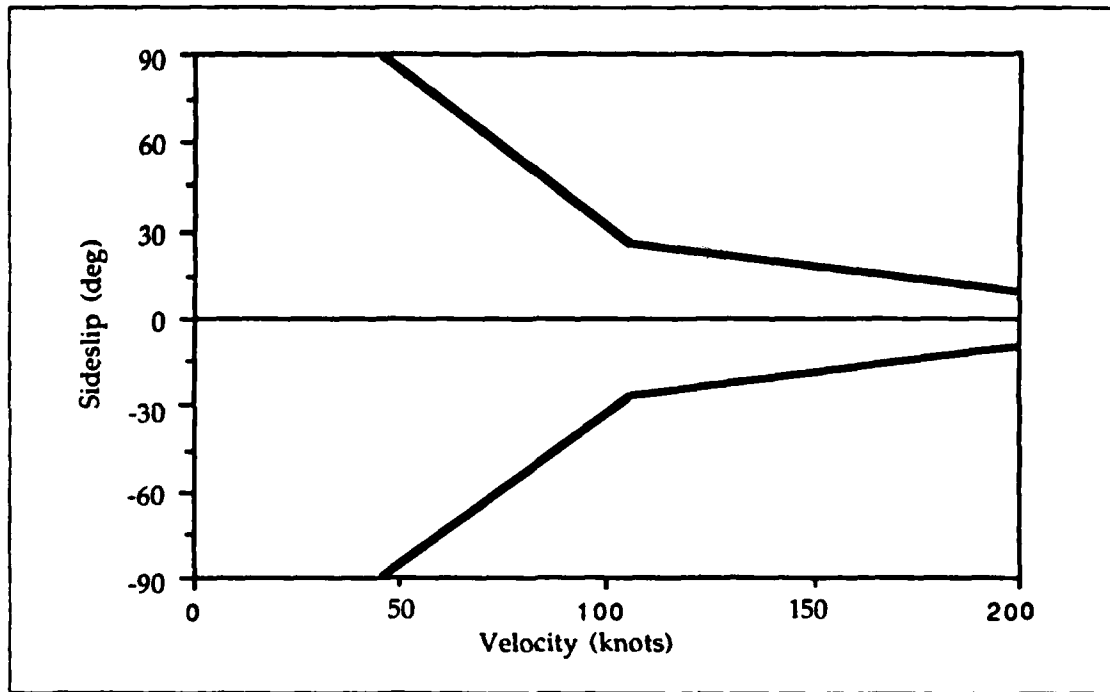
Figure 4.5   Steady-State Sideslip Limit.

2. Red Aircraft

a. Cockpit

The right window/seat arrangement of the VMS S-Cab was utilized for piloting the threat aircraft. The pencil controller and the head-up display (HUD) hardware of the Red cab are visible in Figure 4.6.

The HUD, shown in Figure 4.7, was used to display airspeed and altitude and the relative position of the Blue Aircraft. The display for relative position used two scales, one for ranges greater than 1000 meters and one for ranges less than 1000 meters. Figure 4.7 depicts the scale for ranges greater than 1000 meters.

b. Red-ship Model

The red-ship utilized essentially the same model as the blue-ship but using a attitude command flight control system.

Figure 4.6   Red-Ship Cockpit.

3. Terrain Database

The terrain database used for the previous HAC was adopted for HAC III. The database consisted of a 3 km by 3 km square terrain area modeled geometrically. A significant shortcoming identified in previous experiments was the lack of sufficient depth perception cues available to the pilot on the visual scene. Depth perception cues were especially important in HAC III to enable the task to be performed at terrain flight altitudes. To help provide those cues, a significant amount of ground texturing and objects such as trees and building were added. Several shades of green and brown as well as black were used.

C.   THE HELMET SIGHTING SYSTEM

The helmet sighting system utilized for the HAC III simulation was the Honeywell IHADSS (Integrated Helmet and Display Sighting System) which is also the system currently used on the AH-64 Apache. Figure 4.8 depicts the IHADSS component architecture for the simulation.
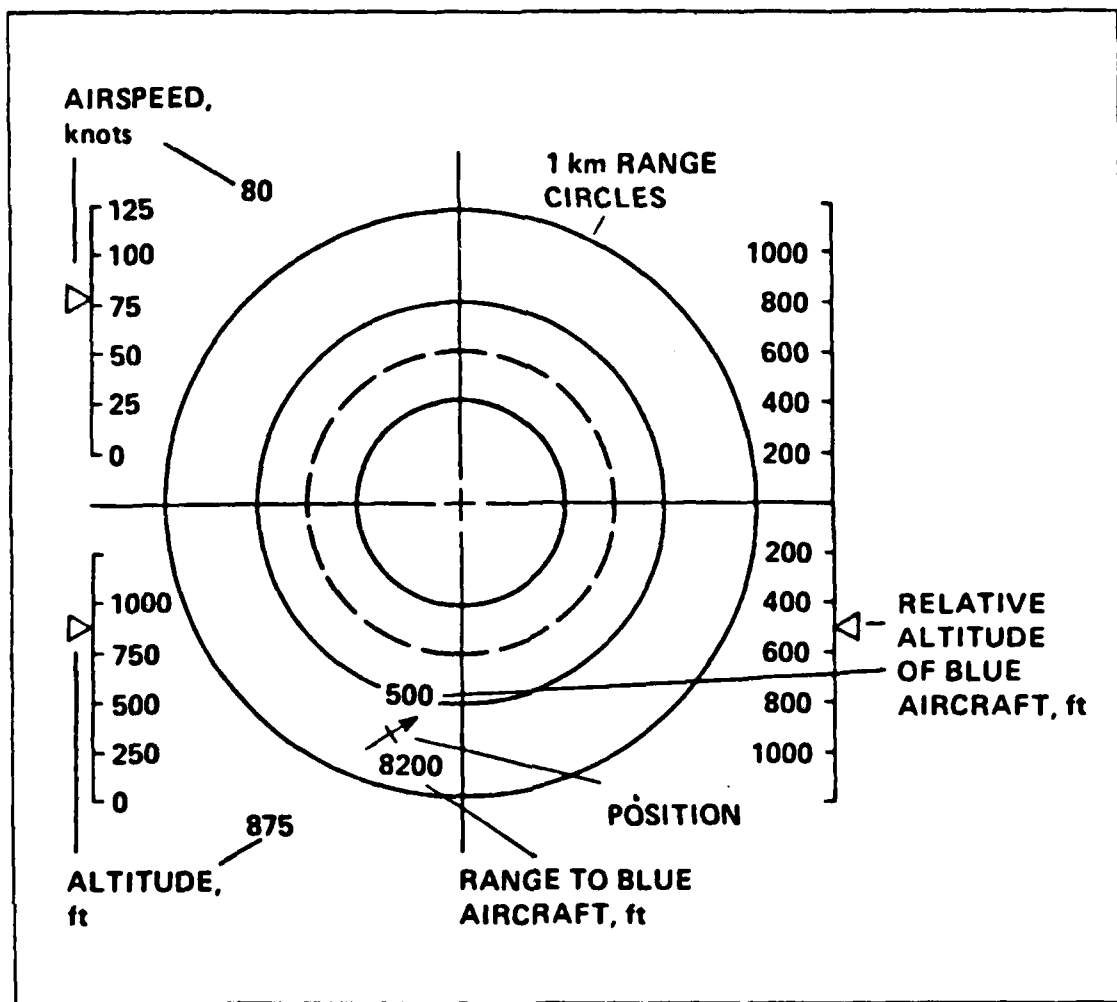
Figure 4.7 Red-ship Head-up Display.

The major functional components of the IHADSS were the Integrated Helmet Unit (IHU) which consisted of the helmet and the Helmet Display Unit (HDU), the Sensor Surveying Units (SSU) which measured the helmet position, the Sight Electronics Unit (SEU) which digitized the helmet position to provide pilot line-of-sight (LOS) information to the host computer. The system measured the pilot's head position in pitch and azimuth (2 DOF) by means of an infrared source and receiver on the SSU and the reflection of that source on the helmet, the information from which was processed by the SEU. The symbology display was sent to the monocle from the IRIS computer. The Boresight Reticle Unit (BRU) provided a fixed source to which the system position could be referenced during the preflight phase.

24
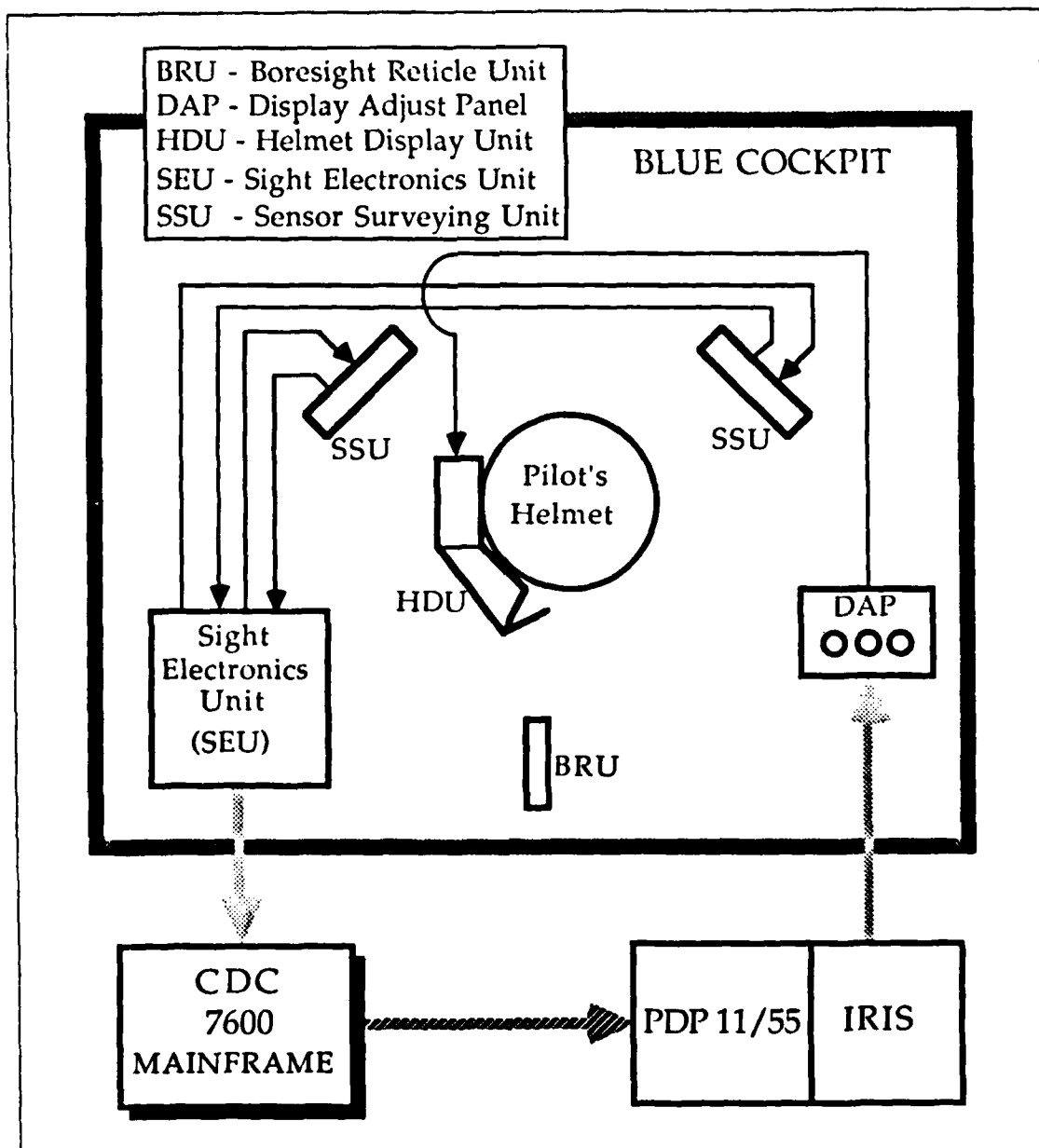
Figure 4.8   IHADSS Component Architecture.

The development of the sight display was patterned after the AH-64 format. It was desired to present to the pilot only information needed to accomplish the tasks of maneuvering and engaging. The final format of the display used for the simulation is shown in Figure 4.9. Following are descriptions of each item of the display:

25
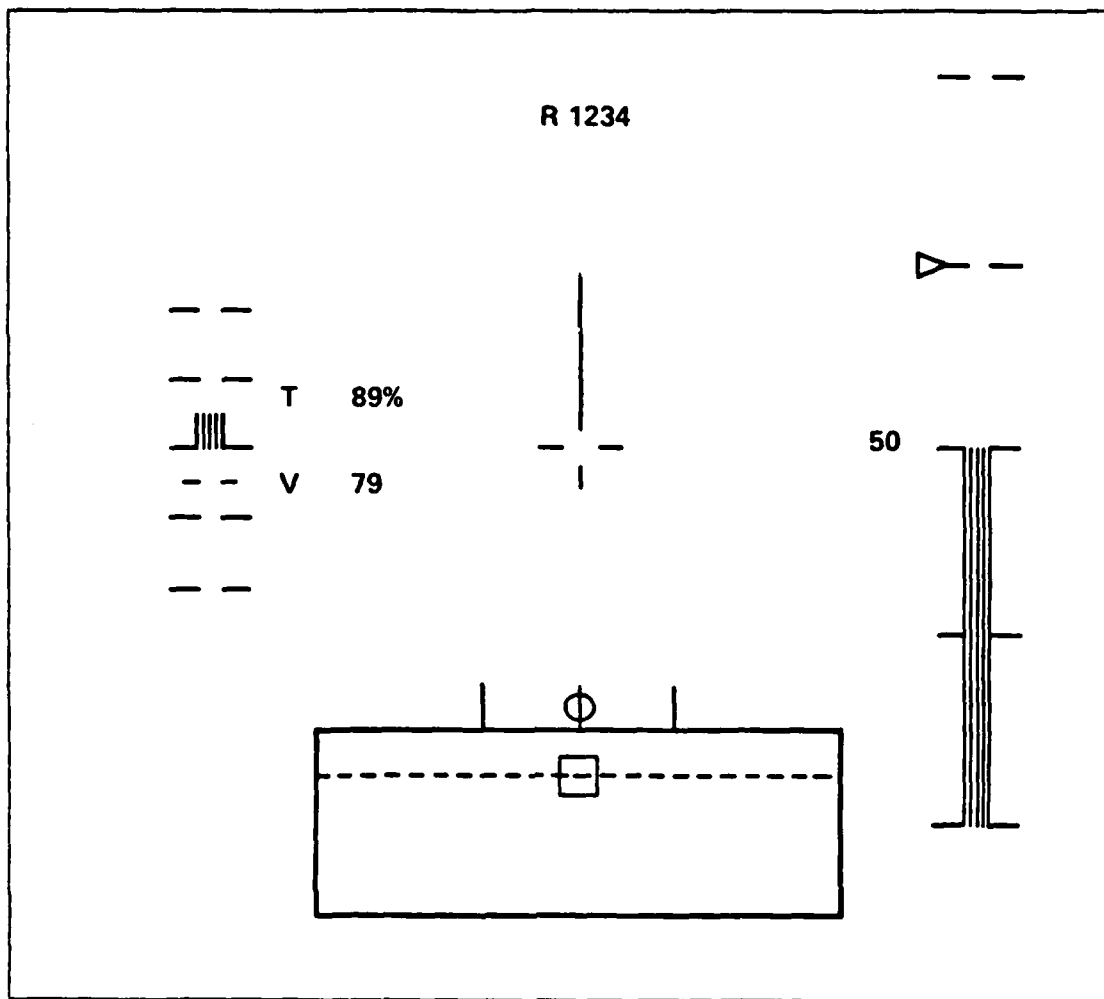
Figure 4.9   IHADSS Symbology Display Format.

1)   Percent Torque: A four character readout (three decimal digits and the %
     sign). The box appears above 98% torque and flashes at two Hertz.

2)   Digital Velocity: A three character readout of airspeed (three decimal digits)
     indicating the magnitude of velocity in knots.

3)   Normal Load-Factor Analog Tape: A solid bar which increases linearly in
     magnitude up for loads greater than 1-g and down for loads less than 1-g.
     The solid bar disappears at 1-g flight.

4)   Sideslip Ball: Open ball which moves left or right for with the presence of a
     sidewards velocity component to the left or right, respectively. Sensitivity
     changes as a function of velocity (as the sideslip limit changes) so that vertical
     bars represent 100% sideslip capability at any velocity.

5) Turret Constraints Box: Rectangular box representing the plus-minus azimuth and elevation limits of the turret. Two sizes were used corresponding to the full traverse and limited traverse turrets, respectively. For fixed-gun simulation, no contraints box is displayed.

6) IHADSS Position and Field-of-View: A square box representing the field of view (FOV) relative to the turret contraints box. Located at its relative position in the turret contraints box which correlates to the present head position. The box flashes when turret limits are reached.

7) Digital Altitude: Digital display of altitude (four digits) representing the height above the datum plane.

8) Analog Altitude Tape: A solid bar which increases in height as altitude above the ground increases. The scale is linear from 0 ft to 200 ft altitude.

9) Instantaneous Vertical Speed Indicator: Solid triangle which moves up and down vertically along the analog altimeter scale. The scale for vertical speed is linear with zero at the center and full-scale values of $\pm$ 2000 ft/min.

10) Digital Range: Four character readout (four decimal digits) of range to the target aircraft in meters.

11) Target Pipper: Single-line cross open in the center representing the ballistic solution. Also the origin of the velocity vector.

12) Velocity Vector: Single-line vector scaled from zero at the display center to 200 knots at the edge of the display. Represents the addition of the x and y-components of velocity.

D. TURRET AND BALLISTICS

1. Turret

The weapon system modeled was a generic turreted gun driven by the IHADSS system. Two configurations of the turret were used. The first, modeled similar to the AH-64, had azimuth limits of $\pm$110 degrees, 20 degrees up, and 60 deg. down in elevation. Designated the 'full-traverse turret,' the configuration virtually encompassed the entire visual scene. The second modeled a turret with an arbitrary $\pm$40 degrees in azimuth capability, and 10 degrees up and 60 degrees down for elevation limits. Designated the 'limited-traverse turret,' its constraints were well inside the visual scene. Varying the maneuver envelopes of the turret had two primary purposes. First, a significant limiting factor inherent in a conventional helicopter configuration is the main rotor tip-path-plane constraining the up-elevation of a turreted gun. This limit becomes especially important because of the nose-down attitude necessary for forward acceleration. The two turret configurations could be used to investigate the impact of that limit in the performance of the air-to-air task.

27

The second purpose for the limited traverse turret was to investigate the use of off-axis engagements. It was hypothesized that in the nap-of-the-earth (NOE) environment, the pilot may not be willing to make significant off-axis engagements which could complicate aircraft control and obstacle avoidance.

The drive system of the XM197 three-barrel 20 mm automatic gun on the AH-1 attack helicopter has been found to have a natural frequency of 191 rad/sec in elevation and 155 rad/sec in azimuth [Ref. 14]. Assuming a calculation time of 30 msec for the simulation model, the dynamics of the turret would be calculated at 33.3 Hz or 209 rad/sec. The ratio of sampling frequency to system natural frequency would be approximately 1.1. In other words, the bandwidth of the turret would be nearly the bandwidth of the host computer. Results listed in Reference 15 indicate that when the ratio of cycle time to system natural frequency is less than 8-10, undesired oscillations and instabilities are introduced. Therefore, the turret position was assumed to be equal to the helmet sight position, subject to a rate limit of 80 deg/sec and acceleration limit of 120 deg/sec.

2. Ballistics

The turreted weapon was nominally chosen to be a 25 mm gun. The characteristics of the round were assumed to be:

weight	0.409 lbs
frontal area	0.005284 ft2
muzzle velocity	3610 ft/sec

The assumed maximum range for the simulation was 5000 feet. The zero-yaw axial drag coefficient of a 25 mm M793 round is nearly linear in the supersonic region [Ref. 16] and, assuming sea level conditions, results in a function of velocity of the round as given in Equation 4.1.

$$C_D = 0.605 - V(8.476 \times 10^{-5}) \qquad \text{(eqn 4.1)}$$

where: V   ■   round velocity (ft/sec)

The round is supersonic at ranges well beyond 5000 ft, so the relationship holds over the desired range.

An algorithm for the round trajectory was adopted from software documentation for the AH-64 Combat Mission Simulator [Ref. 17]. The process calculates the point mass two degree-of-freedom equations-of-motion and applies a

28

spin degree-of-freedom linear approximation as a linear function of time-of-flight of the round.

If the yaw angle of the projectile is assumed to remain zero over the time of flight, the projectile equation of motion can be represented by a one-dimensional wind axis where the x-axis is coincident with the round velocity vector. The axial force (wind axis) of the projectile is expressed in Equation 4.2:

$$F_X(I) = -(0.5)\, \rho\, [V_p(I)]^2\, S\, C_D(I) \qquad (lb) \qquad (eqn\ 4.2)$$

where:
ρ ≡ sea level density (slugs/ft^3)
$V_p(I)$ ≡ projectile velocity (ft/sec)
S ≡ projectile frontal area (ft^3)
$C_D(I)$ ≡ drag coefficient (eqn 4.1)

Then the deceleration of the projectile is given in Equation 4.3:

$$A_p(I) = \frac{F_X(I)}{m} - g\, \sin[\gamma_w(I)] \qquad (ft/sec^2) \qquad (eqn\ 4.3)$$

where: $\gamma_w(I)$ ≡ wind-axis Euler pitch angle

The velocity would then be given numerically by:

$$V_p(I) = V_p(I-1) + \Delta t\, [1.5\, A_p(I) - 0.5\, A_p(I-1)] \qquad (ft/sec)\ (eqn\ 4.4)$$

The position and velocity of the projectile can be tranformed to an earth-axis coordinate system in terms of Euler pitch and yaw angles. The gravity drop of the round and the spin degree-of-freedom results in a Euler wind-axis pitch and yaw rate, respectively. The Euler wind-axis pitch rate is given by Equation 4.5:

$$\dot{\gamma}_w(I) = \frac{-F_{wz}(I)}{m\, V_p(I)} \qquad (rad/sec) \qquad (eqn\ 4.5)$$

where:
F_{wz} ≡ $mg\, \cos[\gamma_w(I)]$
m ≡ round mass (slugs)

29

The Euler wind-axis yaw rate was given as a linear approximation of projectile time-of-flight by:

$$\dot{\psi}_w(I) = 0.00135 + 0.00005 \ t_{tof}(I) \quad \text{(rad/sec)} \quad \text{(eqn 4.6)}$$

The rate of fire of the gun was selected to be 750 rd/min. The algorithm calculated the position, velocity, and acceleration at each time step for every fifth round.

Since the gun was turreted, the recoil force could potentially effect the aircraft handling qualities. The force was modeled using the change in momentum of a round during the impulse of firing. The impulse for each round is given by:

$$F_I = mV_f - mV_i \quad \text{(lb-sec)} \quad \text{(eqn 4.7)}$$

where: F_I $\equiv$ recoil impulse

V_f $\equiv$ final velocity after impulse

V_i $\equiv$ initial velocity (zero)

Substituting into equation 4.7:

$$F_I = (0.0127 \ \text{slugs})(3610 \ \text{ft/sec}) = 45.9 \ \text{lb-sec}$$

Since the firing rate is 750 rd/min or 12.5 rd/sec, the equivalent steady recoil force during the cycle time is:

$$F_R = (46 \ \text{lb-sec/rd}) \ (12.5 \ \text{rd/sec}) = 575 \ \text{lbs} \quad \text{(eqn 4.8)}$$

The series of impulses during a burst is therefore approximately equivalent to a steady force of 575 lbs.

Because of the inertial characteristics of an automatic gun mechanism, the rate of fire and, hence, the recoil force was assumed not to be instantaneous. A spin-up time of 0.4 seconds was assumed. The rate of spin-up was also assumed to be exponential. Therefore, the effective time constant of the recoil force was 0.1334 seconds and the recoil force could be expressed as:

$$F_R = 575 \ [1 - \exp(-t/0.1334)] \quad \text{(lbs)} \quad \text{(eqn 4.9)}$$

30

Figure 4.10 depicts the assumed location of the turret relative to the aircraft center of gravity.
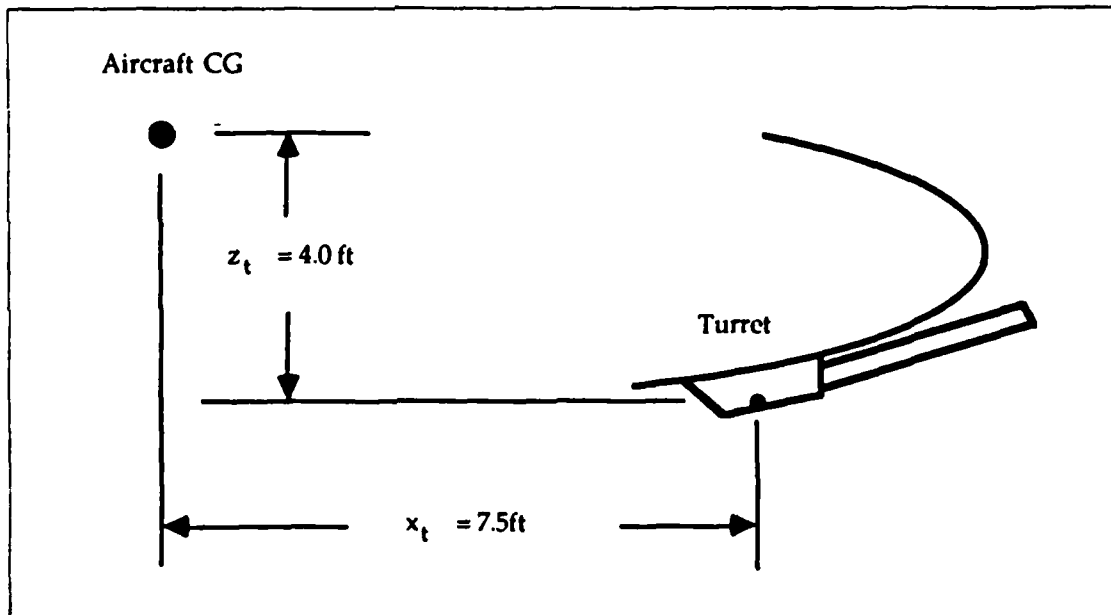
Figure 4.10   Turret Location Relative to Aircraft CG.

The recoil force resolved into components is given by:

$$\begin{Bmatrix} F_{rx} \\ F_{ry} \\ F_{rz} \end{Bmatrix} = |\bar{F}_r| \begin{bmatrix} \cos\theta_t \cos\psi_t \\ \cos\theta_t \sin\psi_t \\ \sin\theta_t \end{bmatrix} \qquad \text{(eqn 4.10)}$$

The moments about the aircraft center of gravity are then:

$$\begin{Bmatrix} L_r \\ M_r \\ N_r \end{Bmatrix} = \begin{bmatrix} x_t & F_{rx} \\ y_t & F_{ry} \\ z_t & F_{rz} \end{bmatrix} = \begin{vmatrix} \bar{i} & \bar{j} & \bar{k} \\ x_t & y_t & z_t \\ F_{rx} & F_{ry} & F_{rz} \end{vmatrix} = \begin{Bmatrix} -z_t F_{ry} \\ z_t F_{rx} - x_t F_{rz} \\ x_t F_{ry} \end{Bmatrix} \text{(eqn 4.11)}$$

The recoil forces and moments were then added to the three translational and three rotational aircraft equations of motion of the model.

E. FIRE CONTROL

In order for the pilot to put rounds on the target accurately, a lead-computing fire control needed to be incorporated. By estimating the current states of the ownship and target, a future position of the target can be determined based on the time of flight of the round and aiming corrections could be applied. For minimal pilot workload, the targeting pipper would be fixed in the center of the display and the lead aiming corrections can then be applied to the turret. The algorithm used was adopted from Reference 18. Simplifications were possible because of the simulation environment and the availability of realtime positions, rates, and accelerations for both aircraft.

The future position of the target can be estimated by the simple kinematic equation:

$$\overline{X}_T = 0.5 \overline{A}_T \, t_{tof}^2 + \overline{V}_T \, t_{tof} + \overline{X}_{T0} \qquad \text{(eqn 4.12)}$$

where $\overline{X}_T$ = future position vector of the target

$\overline{A}_T$ = current acceleration vector of the target (angular and linear)

$\overline{V}_T$ = current velocity vector of the target (angular and linear)

$\overline{X}_{T0}$ = current position vector of the target

t_{tof} = time of flight of the round to the target

The unknowns in equation 4.12 are $\overline{X}_T$ and t_{tof}. In the simulation environment, the range was computed realtime by subtracting the own-ship position vector from the target aircraft future position vector.

If the Blue-ship position is expressed in earth coordinates as:

$$\overline{X}_B = x_b \overline{i} + y_b \overline{j} + z_b \overline{k} \qquad \text{(eqn 4.13)}$$

the round position as:

$$\overline{S} = S_x \overline{i} + S_y \overline{j} + S_z \overline{k} \qquad \text{(eqn 4.14)}$$

and the Red-ship future position as:

$$\overline{X}_T = x_t \overline{i} + y_t \overline{j} + z_t \overline{k} \qquad \text{(eqn 4.15)}$$

Then define the position vector between the Blue-ship and the round position as:

32

$$\overline{B} = \overline{S} - \overline{X}_T = (S_x - x_b)\overline{i} + (S_y - y_b)\overline{j} + (S_z - z_b)\overline{k} \quad \text{(eqn 4.16)}$$

and the position vector between the Blue-ship and Red-ship as:

$$\overline{R} = \overline{X}_T - \overline{X}_B = (x_t - x_b)\overline{i} + (y_t - y_b)\overline{j} + (z_t - z_b)\overline{k} \quad \text{(eqn 4.17)}$$

The ballistics algorithm, explained previously, was utilized by the fire control. The unknown in the ballistics and the future target position calculations was t_{tof} to the target. To calculate time-of-flight from the ballistics equations explicitly would be very complicated but convergence of an iterative approach between time-of-flight to the target range and the target future-position was very rapid. In other words, given the present range to the target, calculate realtime the trajectory of the projectile to the target range and use the resulting time-of-flight to calculate the target future position. For that trajectory calculation, define the initial velocity vector in the aircraft reference frame so that it passes through the CG of the Red aircraft; that is, coincident with the LOS to the Red-ship. The future position yields a new time-of-flight and the procedure is repeated until convergence to the time-of-flight and future range. Given the relative velocities of the projectile and aircraft and the ranges involved, the number of iterations necessary is on the order of 2-3. The time-of-flight, future position of the target (X_T), ownship position (S_B), and round position (S) in earth coordinates are then known so the angle between the three points can be calculated by the simple trigonometric relationship:

$$\delta = \cos^{-1}\left\{ \frac{R \quad B}{|R| \, |B|} \right\} \quad \text{(eqn 4.18)}$$

The angle (δ) constitutes the correction angle for the fire control and has components in the aircraft-axis x-y plane (azimuth), and x-z plane (elevation) which can be resolved and rotated to the aircraft coordinates in which the turret operates. The gun angle is then computed by adding the correction angle (δ) in aircraft coordinates to the sight direction of the IHADSS. The gun angle then defines the initial velocity vector of the round in the aircraft reference frame.

33

F. SCORING

To adequately assess pilot performance in the task of air combat, a method of scoring needed to be applied. The first level of scoring was tracking accuracy; that is, the accuracy that a pilot could keep a head-tracked ballistic pipper on target. To determine tracking accuracy, both aircraft positions and orientations in earth coordinates were needed and were easily accessible in the simulation environment. From the position vectors of the Blue and Red aircraft, the pitch-off and angle-off angles from each respective aircraft to the other were determined. The IHADSS SSU sent head position information to the host computer in terms of azimuth and pitch angles relative to the nose of the aircraft. The tracking error was then, simply, the difference between the pitch-off and angle-off angles to the target and the head position pitch and azimuth angles, respectively, which is given by:

$$\theta_e = \theta_{turret} - \theta_{BtoR} \qquad \text{(eqn 4.19)}$$

$$\psi_e = \psi_{turret} - \psi_{BtoR} \qquad \text{(eqn 4.20)}$$

where:
θ_e	$\equiv$	tracking error in pitch
ψ_e	$\equiv$	tracking error in azimuth
θ_{turret}	$\equiv$	turret position in pitch
ψ_{turret}	$\equiv$	turret position in azimuth
θ_{BtoR}	$\equiv$	pitch-off angle from Blue-ship to Red-ship
ψ_{BtoR}	$\equiv$	angle-off (azimuth) from Blue-ship to Red-ship

Total errors are also a function of range to the target. Therefore, the perpendicular distance from the track line-of-sight and target position is also of interest and is given by the simple relationships:

$$x_{miss} = R \, \tan(\psi_e) \qquad \text{(eqn 4.21)}$$

$$y_{miss} = R \, \tan(\theta_e) \qquad \text{(eqn 4.22)}$$

where: R $\equiv$ range to the target

34

Yielding a total tracking miss distance (magnitude) of:

$$E_{miss} = [(x_{miss})^2 + (y_{miss})^2]^{1/2} \qquad \text{(eqn 4.23)}$$

The next level of scoring was the hits of the rounds. To measure the ballistic accuracy of a hit, the target was assumed to be an ellipsoid, for simplicity. The major radius was assumed to be 27.25 ft and the minor radius was 7.0 ft. Only the tracers were computed and there was one tracer for every five rounds. A line was defined in earth coordinates between each new tracer and the subsequent one. A test determined whether the line passed through the target ellipsoid. If the test was positive, a hit was recorded.

The probability of kill of the target (P_K) is a function of the number of hits (n) during an engagement and the single-shot probability-of-kill given a hit $(P_{k/h})$ [Ref. 19]:

$$P_k(n) = 1 - \prod_{j=1}^{n} [1 - P_{k/h}^{(j)}] \qquad \text{(eqn 4.24)}$$

Then the probability of survival (P_s) of the target is:

$$P_s(n) = 1 - P_k(n) \qquad \text{(eqn 4.25)}$$

The single-shot-probability of kill is the ratio of vulnerable area to projected area (A_v/A_p) of the target aircraft. The complete development of $P_{k/h}$ can be found in Reference 19, pages 154-183. For HAC III, the vulnerable area was nominally assumed to be 22 ft^2 and the projected area, 300 ft^2, yielding a single-shot-probability of kill of:

$$P_{k/h}^{(j)} = 0.0733$$

The resulting curve for kill probability as a function of number of hits is shown in Figure 4.11.

The final level of scoring developed was the miss distance of the round if no hit occurred. Simply, as the round passed the target, the miss distance between the round and target center of gravity would be recorded.

The figure shows a plot with the following equation:

$$P_k^{(n)} = 1 - \prod_{j=1}^{n} (1 - P_{k/h}^{(j)})$$

Where: $P_{k/h}^{(j)} = 0.733$

The plot axes are labeled "Probability of Kill" (y-axis, 0.0 to 1.0) and "Number of Hits" (x-axis, 0 to 60).
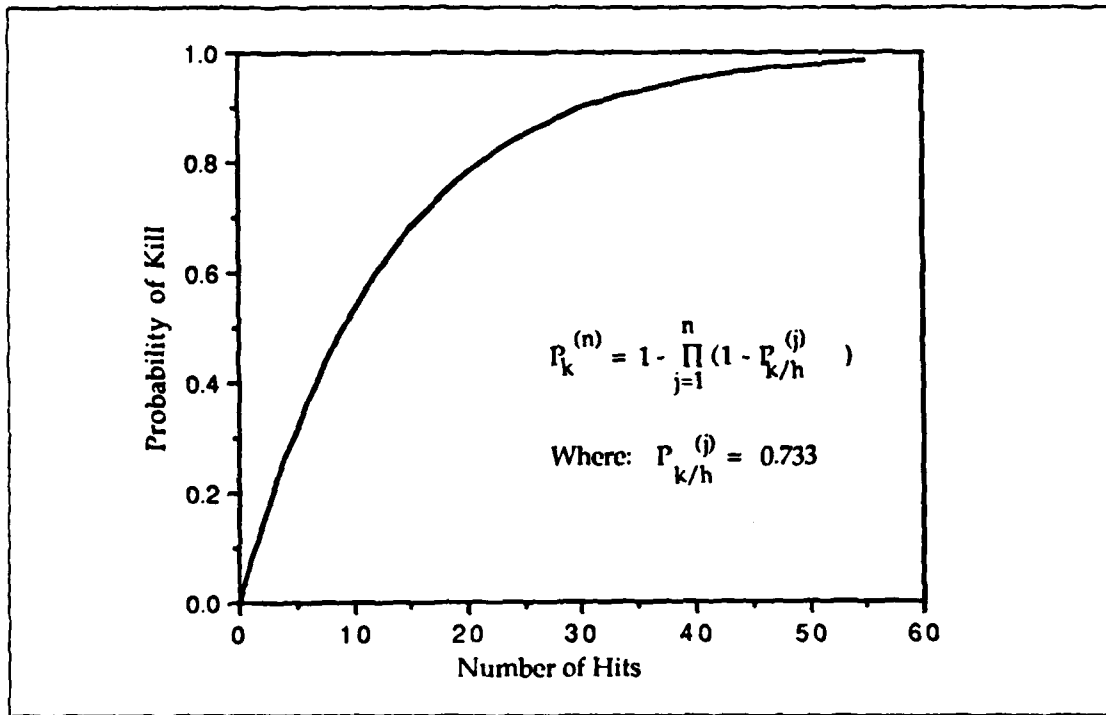
Figure 4.11   Probability of Kill vs. Number of Hits.

G.   GROUND-TO-AIR THREAT

An additional goal of the experiment design was to ensure the task would be performed at realistic tactical flight altitudes. To assist in accomplishing that goal, a ground-to-air threat umbrella was designed. Figure 4.12 depicts the planview of the ground-to-air missile umbrella.

When the own-ship entered the umbrella upon reaching the specified altitude (150 ft and 300 ft, respectively), a strobe illuminated on the PMD at an azimuth corresponding to the relative azimuth from the nose of the aircraft to the ground threat. Concurrently, an audio warning tone would be heard over the pilots headset. For 10 seconds the tone would be a series of pulses, representing a radar acquisition mode, and then the tone would be steady representing a radar track mode. The steady tone would continue until the pilot 'broke the lock' by descending below the threats umbrella.

36

ABOVE
300 ft ALT.

ABOVE
150 ft ALT.

GROUND AD
THREAT LOCATION
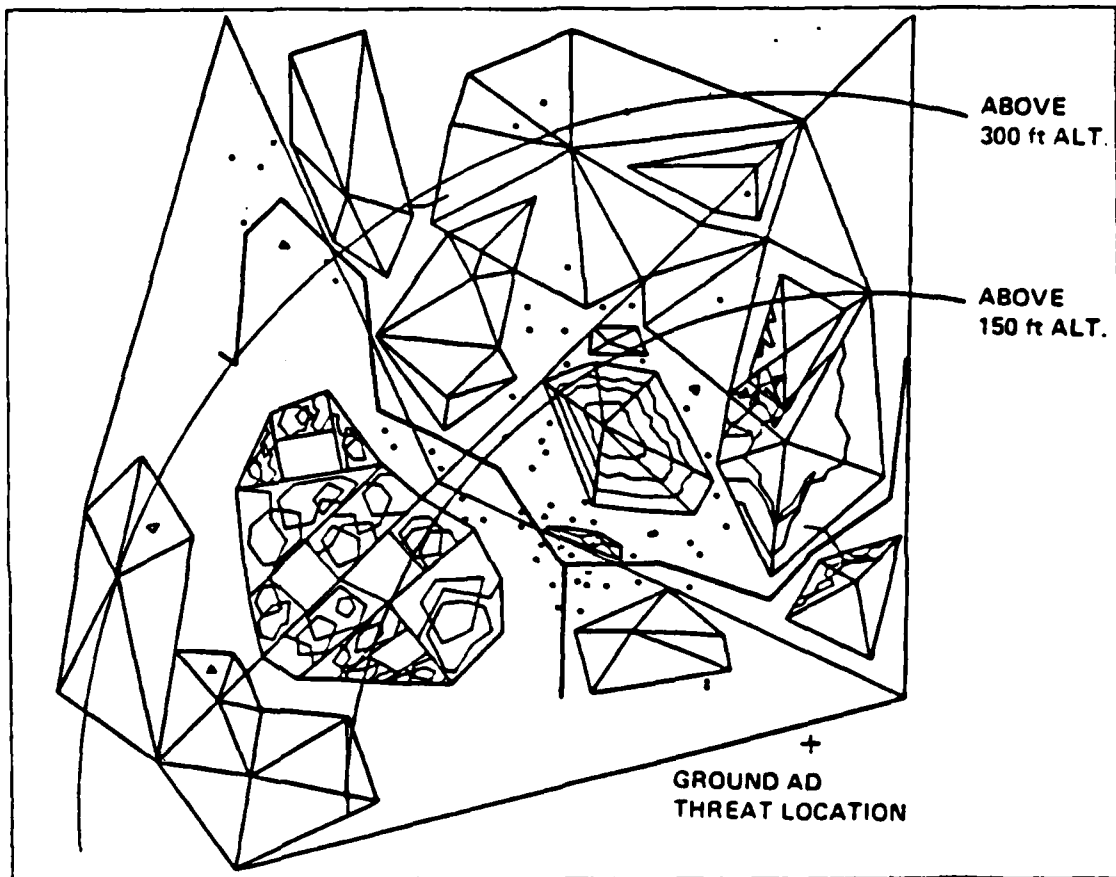
Figure 4.12   Ground-to-Air Threat Umbrella.

V. EXPERIMENTAL PROCEDURE

HAC III was conducted on the VMS fixed base during the period 16 March to 28 April 1987. Approximately three weeks were spent integrating and validating the various subroutines of the simulation model with the cockpit. Figure 5.1 depicts the original software architecture which was to be integrated into the facility.
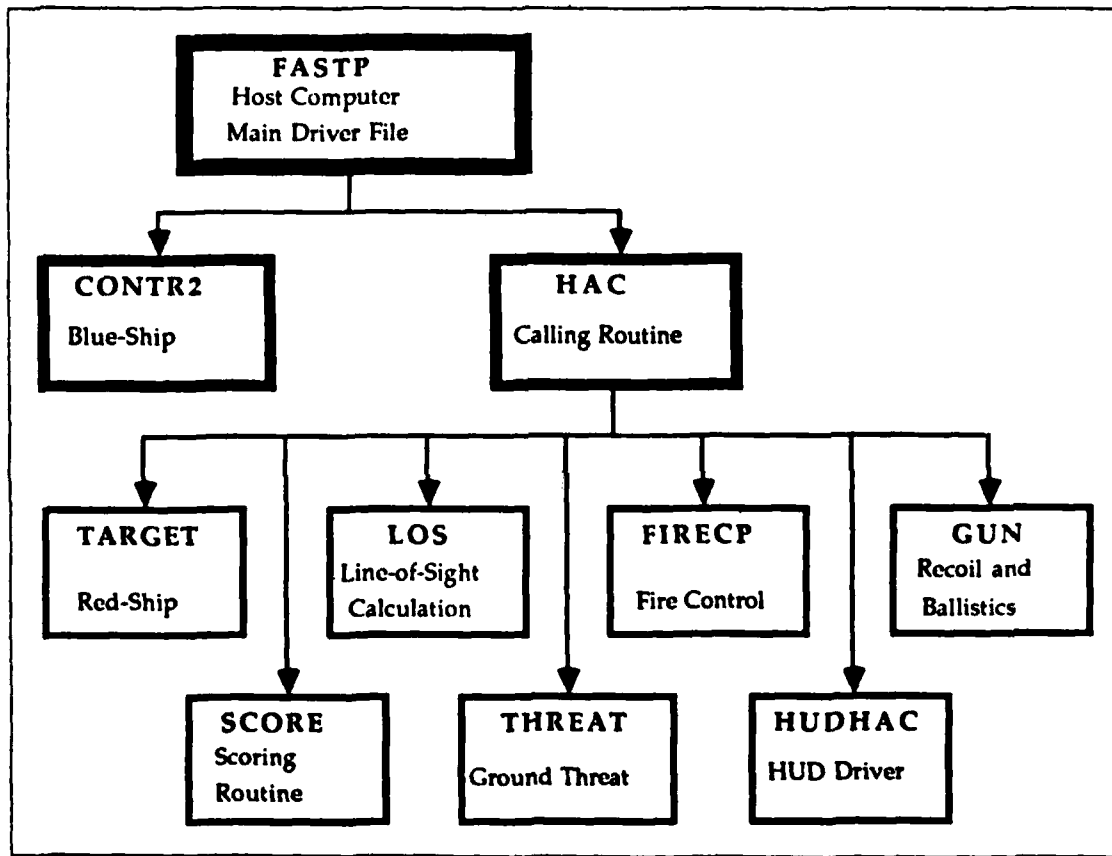
Figure 5.1   Simulation Software Architecture.

The remaining two and one-half weeks were utilized for experimental evaluation runs. The experimental portion of the simulation was organized so that two guest pilots were participating at a time for a duration of 3-4 days.

A. IMPLEMENTATION ONTO THE FACILITY

1. Cockpit Checkout

The cockpit layout is shown in Figure 5.2, where the CGI windows, the format of the instruments, the controls, and the HADDS SSU's are visible.
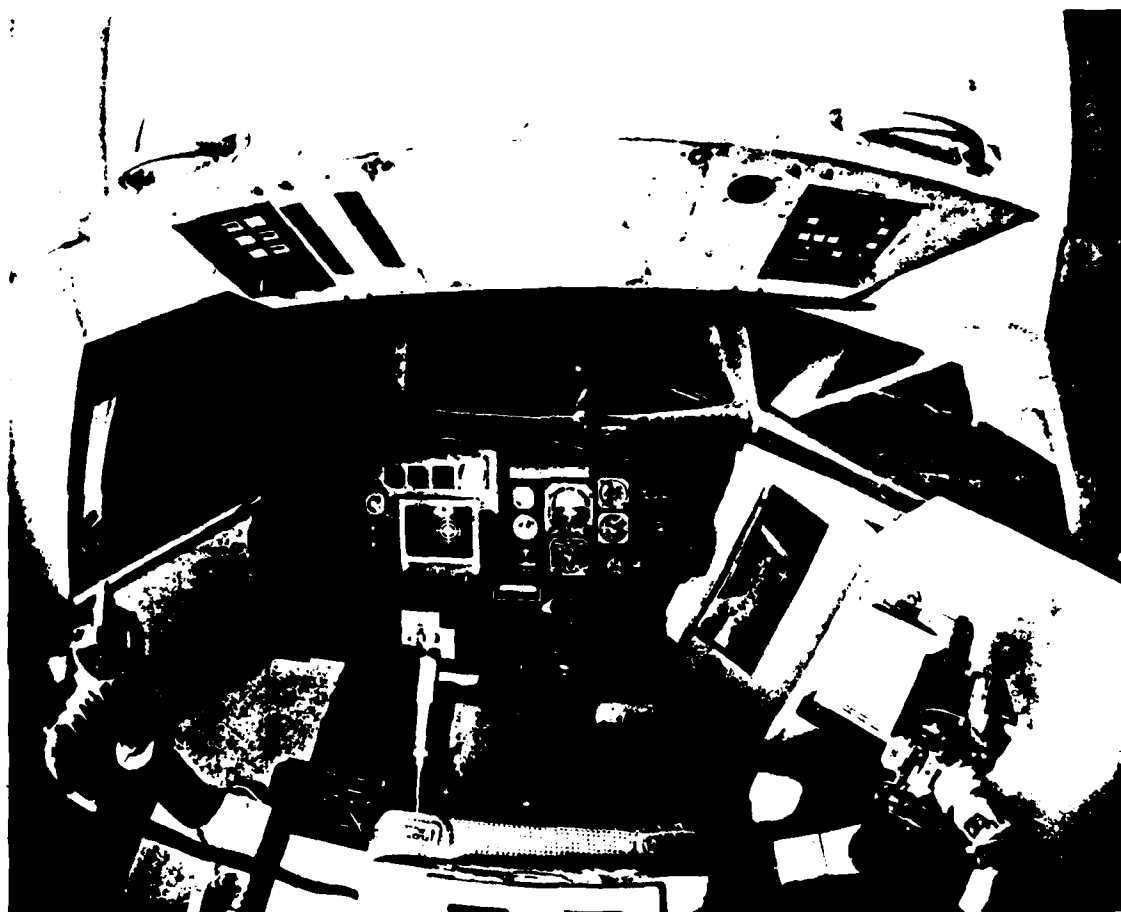
Figure 5.2   Blue-ship Cockpit.

The cockpit development and checkout consisted of the adjustment and assignment of control friction, force gradient, and breakout force values, the assignment of switches and warning lights, verifying cockpit instrument indications, assignment of noises and tones, and improvement of the CGI visual scene.

a. Cockpit Controls

In an effort to maximize the fidelity of the simulation and thereby reduce adverse influences on the pilot ratings, it was important to adjust the control forces to

as close as possible represent an actual helicopter. It was desirable to optimize the artificial control forces for the task to minimize the effects on pilot ratings. After several flight hours of iteration on the control force-feel the values of friction, gradient, and breakout in Table 1 were set and held constant throughout the remainder of the simulation. It should be noted that the force gradient decided upon for the pedals (2.0 lb/in) was below the range of 4-8 lb/in given in the proposed handling qualities specification [Ref. 9, p. 44].

<div style="border:1px solid">

TABLE 1

CONTROL FORCE-FEEL SETTINGS

Control	Friction	Gradient	Breakout
Lateral Cyclic	0	1.0 lb/in	0.25 lb
Longitudinal Cyclic	0	1.0 lb/in	0.25 lb
Collective	4.0 lb	0	0
Pedals	0	2.0 lb/in	2.0 lb

</div>

Hysterisis values for all controls were set to zero. The artificial force-feel could not be disabled as an option during the experiment.

b. Cockpit Switch Assignments

The cockpit switches used by the pilot during the simulation were located principally on the cyclic grip, collective grip, a overhead control panel, the instrument panel, and a control panel located on the floor to the left of the pilot seat.

(1) *Cyclic Grip.* Figure 5.3 shows the switch assignment for the cyclic. Included were switches to initiate the operate mode (OP) and to return to the initial condition mode (IC). The two-detent trigger switch was used to simulate activation of the fire control and firing of the gun, respectively. Engaging the trigger switch activated flags in the continuous data recording routine, so that the engagement windows could be isolated for post-simulation analysis.

40
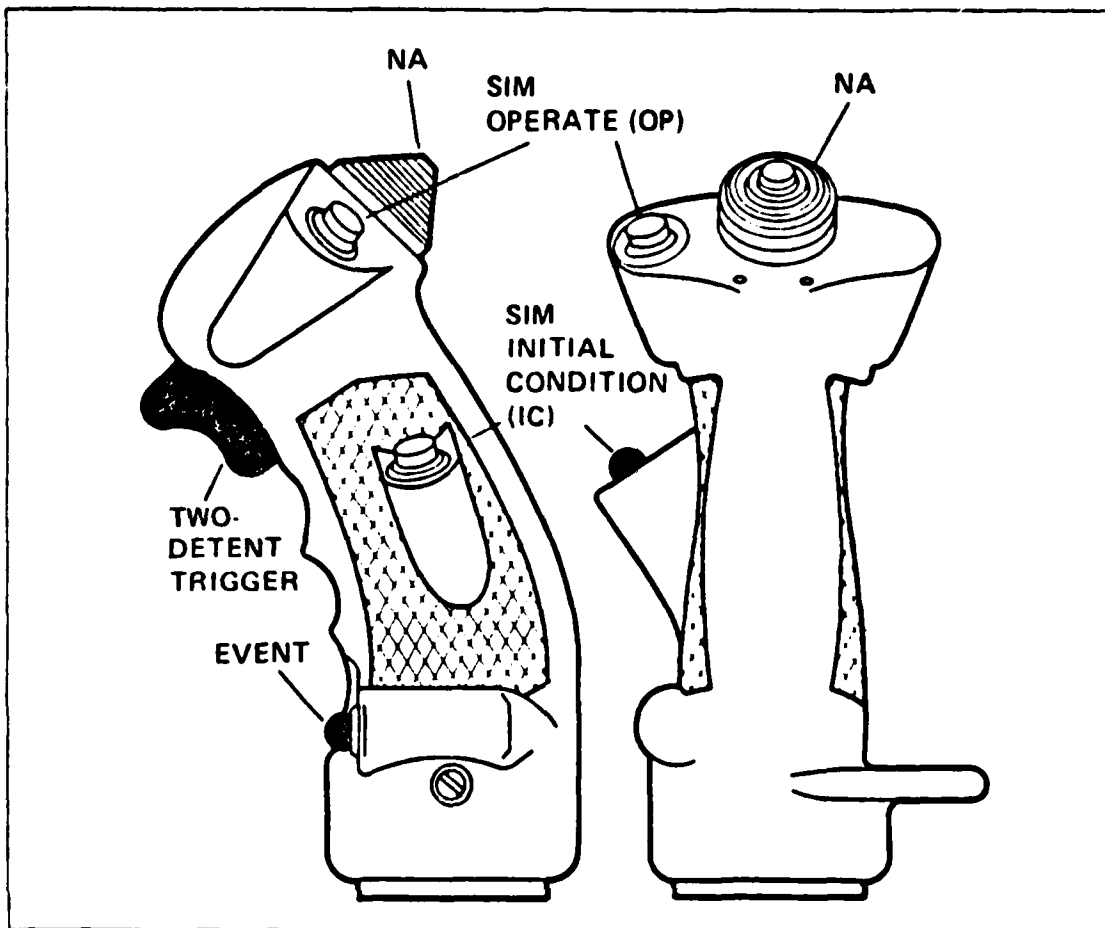
Figure 5.3 Cyclic Grip Switch Assignments.

(2) *Collective Grip.* Two switches were used on the collective grip as shown in Figure 5.4. Both switches were used for the IHADDS boresight procedure. The left switch activated the boresight select mode in the IHADDS sight electronics unit (SEU). The right switch activated the boresight store mode in the SEU.

(3) *Overhead Control Panel.* The overhead panel switches included activation/reset switches for the pilot controls hydraulic loader pumps and intensity adjustment knobs for the instrument panel lighting and overhead cab lighting.

(4) *Instrument Panel.* The altitude setting for the low-altitude light was adjustable to the pilot. A knob for adjusting the intensity of the panel-mounted display was located adjacent to the PMD. Additionally, the on/off switch for the boresight reticle unit (BRU) was mounted on the right side of the instrument panel, available to the pilot during the boresight procedure.

41
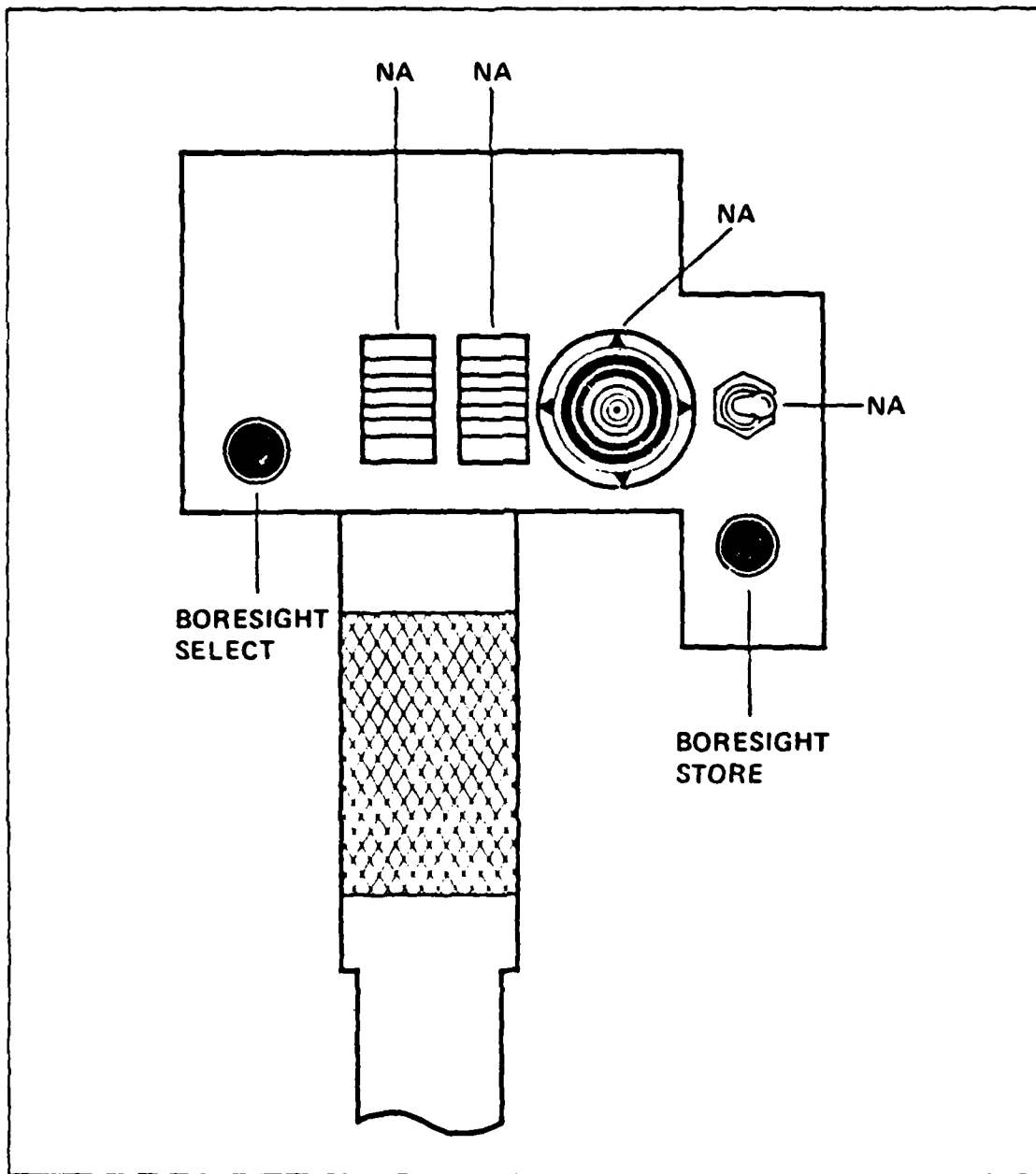
Figure 5.4 Collective Grip Switch Assignments.

(5) *Floor-mounted Control Panel.* Adjacent to the seat to the pilots left was the simulation control panel with push-buttons for the operate and initial-condition modes. Additionally, a hold-mode button allowed the simulation to be stopped and frozen in place without returning to the initial condition.

Also mounted on the floor panel were switches and adjustments for the pilot intercom system and the IHADSS symbology intensity and contrast.

c. *Cockpit Warning Lights, Noises, and Tones*

(1) *Warning Lights.* It was considered that the availability of the IHADSS sight to present flight information reduced the requirement for multiple warning lights inside the cockpit. Because the task to be evaluated was very much an out-of-the-cockpit task, it was desirable to minimize the time needed inside the cockpit to interpret warning lights. Therefore, the final configuration included only an engine-torque warning light which illuminated at 98% torque and the low-altitude light on the altimeter.

(2) *Noise Generation.* To simulated the noise environment in-flight, external speakers were present inside the simulator cab. Noises produced for the experiment included rotor noise and engine noise which varied with collective input, and gun burst noise which was activated by the second detent of the pilot's trigger.

(3) *Tone Generation.* A tone generator was available to send tones with variable pitches, frequencies, and modulation over the pilot's headset. For the experiment, tones were produced for the radar warning system for the different radar modes of the ground threat.

d. *Communications*

Communications during the simulation was accomplished over an intercom connecting the blue cab, red cab, and the simulation control room. Also monitering the communication net were support personnel maintaining the host computer and the DIG to facilitate rapid response to system problems during the simulation.

2. Aircraft Model

The simulator was flown extensively to insure the proper functioning of the desired control responses and maneuverability limits. The rate-command/attitude-hold flight control system was utilized for the experiment. Because the model had been used on several previous experiments, no significant problems were expected nor encountered.

As a verification that the simulator was responding as predicted by the theoretical mathematic model, a frequency-sweep flight-testing technique and data analysis was conducted for one configuration at hover for the yaw axis. The configuration used test cell eight explained later.

The technique involved saw-tooth control inputs over time starting with a period of about 20 seconds, gradually increasing the frequency, and ending with a frequency of about 4 Hz. The entire frequency sweep took about 90 seconds. [Ref. 20] Figure 5.5 depicts the time history of the pedal input and yaw rate output for the sample test.
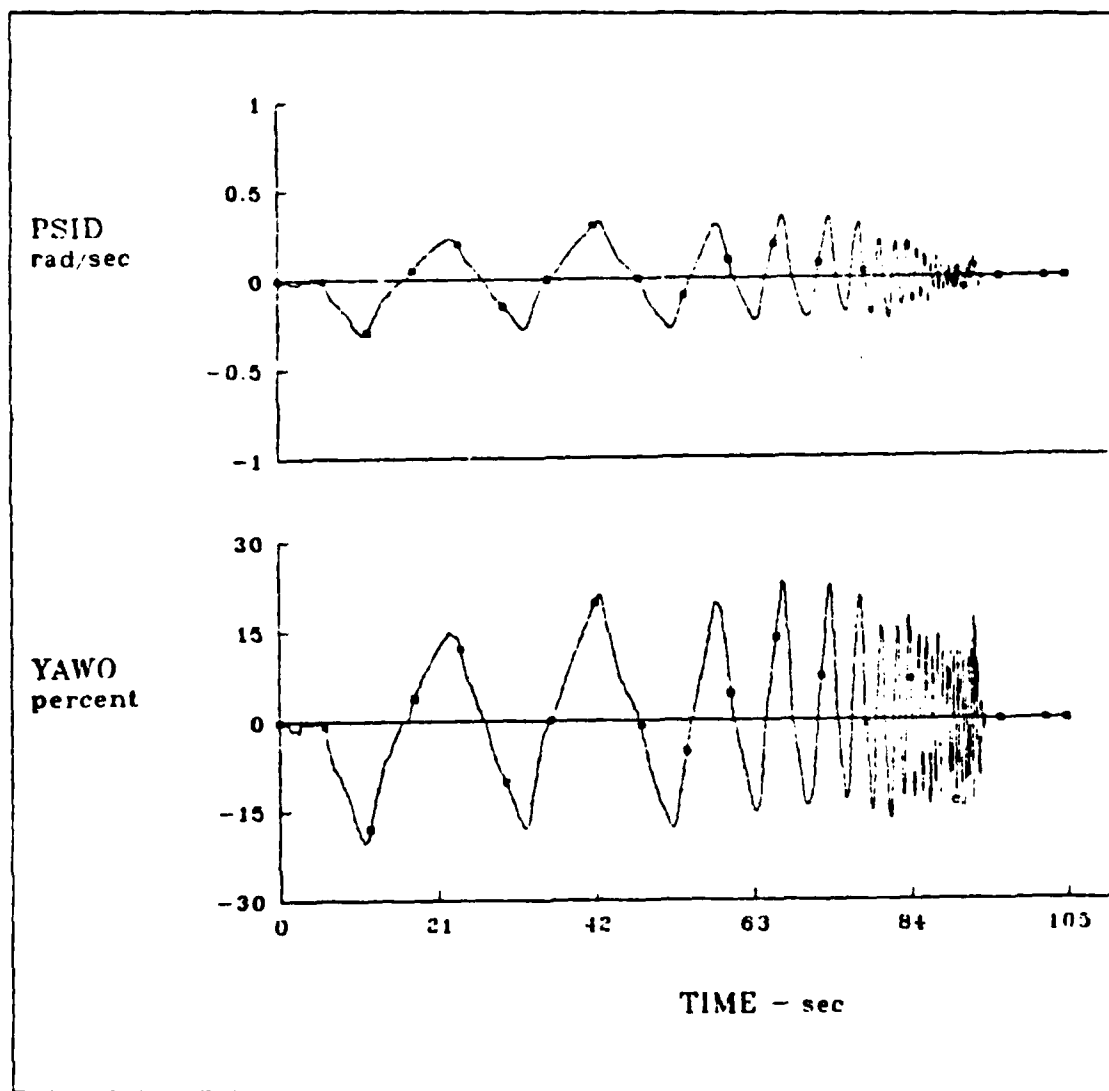
Figure 5.5   Frequency Sweep Input and Output Time Histories.

A simple Fortran program was developed to reformat the input/output data files for input into a frequency-response identification program (FRESPID) developed

by M.B. Tischler of the U.S. Army Aeroflightdynamics Directorate at NASA's Ames Research Center. TRESPID contains an algorithm implementing Fast Fourier Transforms for the system identification. The outputs of TRESPID included a time history, Bode magnitude and phase plots, the system transfer function, and a tabular data file. The frequency-sweep transfer function and the theoretical transfer function for yaw rate to pedal input are listed in Table 2 and support the validity of the model.

TABLE 2
COMPARISON BETWEEN THEORICAL AND FREQUENCY-SWEEP TRANSFER FUNCTIONS

$$\text{Theoretical Transfer Function} \qquad \frac{r}{\delta_p} = \frac{0.0836}{s + 5.38}$$

$$\text{Frequency Sweep Analysis} \qquad \frac{r}{\delta_p} = \frac{0.0843}{s + 5.42}$$

The intent of the frequency sweep analysis was not to be a thorough verification of the aircraft model but a spot-check of the model and an exercise in the testing technique.

3. IHADSS Development and Checkout

The IHADSS was installed in the VMS ICAB prior to the simulation by Honeywell Corporation of Minneapolis, MN under contract to NASA. Subsequent to the system installation an error map over the range of the visual scene was contructed and is shown in Figure 5.6.

a. IHADSS Symbology

During the simulation development several iterations were made on the display format in an attempt to present only flight and weapon system information necessary for the task to be evaluated and in a format easily applied.

```
┌─────────────────────────────────────────────────────────────────────┐
│  -0.21        -0.24      0.06       0.35      -0.15        -0.16      │
│  □-0.88       □-0.65     □-0.15     □0.37     □-0.29       □-0.22     │
│                                                                       │
│       0.05                   0.09                   0.11             │
│       □-0.43                 □-0.22                  □-0.04           │
│                                                                       │
│  0.12         0.03       0.01       0.11      -0.08        0.24       │
│  □-1.04       □-0.75     □0         □0.15     □-0.29       □-0.17     │
│    left window             center window           right window      │
└─────────────────────────────────────────────────────────────────────┘

            Y         X = azimuth error (deg)
     KEY:   □ X
                      Y = elevation error (deg)
```
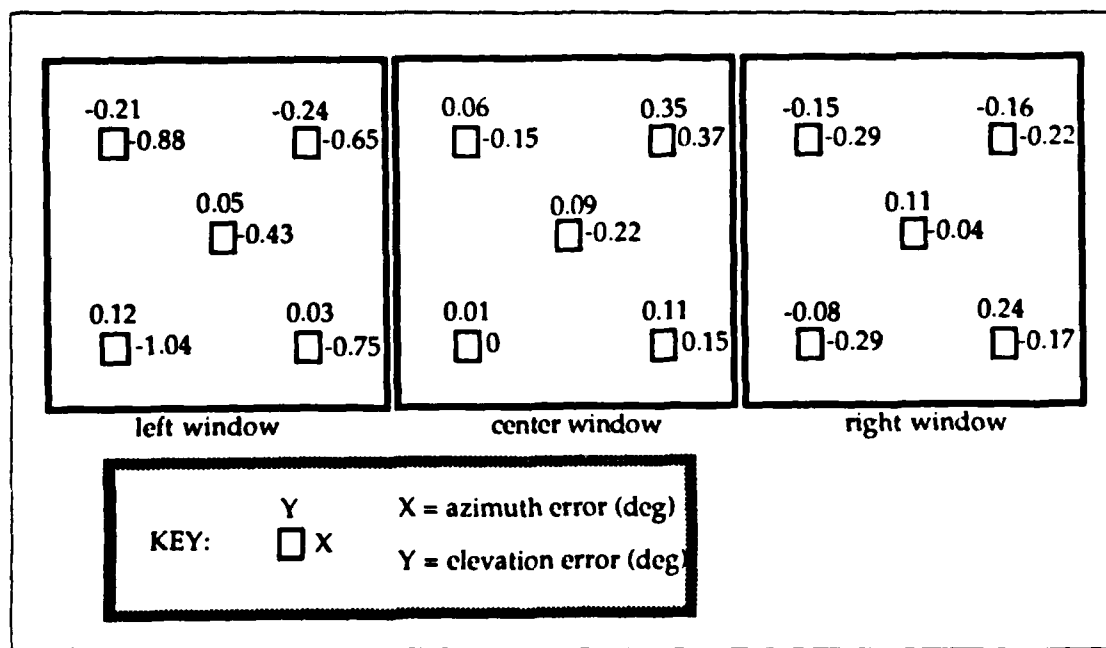
Figure 5.6   IHADSS Pointing-Error Map Over the FOV.

Significant changes to the display during the first three weeks of simulation and the rationale for the changes were:

1) The ballistic pipper (open cross) was removed from the display completely leaving only the center reference cross. It was found that the larger open cross cluttered the targeting area making tracking difficult. Contributing to this difficultly was most likely the relative lack of resolution of the CGI scene.

2) The scaling (sensitivity) of the velocity vector was adjusted to be from zero to 200 knots full scale. Because of fairly good visual cues for hovering flight it was decided not to change the sensitivity for low velocities.

3) The sideslip ball was driven by beta (β) instead of sideforce (Y_v). The full scale bars represented 100 percent sideslip capability at the present airspeed. Therefore, the sensitivity was a function of airspeed and was determined from the sideslip capability defined in the aircraft model (Fig 4.5).

4) The sensitivity of the altitude tape was adjusted to be from 0 to 200 ft full scale. That scaling provided the best cuing for the low-level terrain flight task.

5) The IVSI was set to be from zero to ± 2000 ft/min full scale. Increased sensitivities (± 1000 ft/min) were tried but resulted in the instrument indicating full scale for a significant percentage of the time during maneuvering flight.

6) To provide an additional cue, the IHADSS FOV box was flashed when the turret reached an angular position limit.

b. *Boresight Procedure*

The boresight procedure was very simple and caused no significant problems during the simulation. Important to gaining and maintaining an accurate boresight, however, was a properly fitted helmet and the monocle adjusted properly to the pilot's eye. The pilot's steps for boresighting were:

1) Turn on the BRU.

2) Activate the boresight select button (Figure 5.4). A "Boresight Select" message appeared in the turret constraints box in the pilot's IHADSS display.

3) Position the head so that the center pipper of the pilot's display overlayed the columated reticle of the BRU.

4) Push the boresight store button (Figure 5.4). The head alignment with the BRU had to be held for approximately one second for the boresight. Upon successful boresighting, a "Boresight Good" message was displayed for about two seconds in the turret constraints box of the pilot's display.

4. Panel-Mounted Display

The PMD symbology, shown in Figure 5.7, was adopted from the HAC II experiment. At ranges greater than 1000 meters, each of the three range circles represented 1000 meters. When the range to the target became less than 1000 meters, the format changed to two range circles of 500 and 1000 meters radii, respectively. The target aircraft was displayed only when line-of-sight was satisfied.

The only addition to the PMD was the strobe displaying relative bearing to the ground threat when the threat's umbrella was entered.

5. Fire Control, Turret, and Ballistics

a. *Fire Control*

During the integration and validation period on the simulation facility, attempts to debug the fire control subroutine were unsuccessful. The actual source of the problem was not isolated but it was assumed to be caused by logic errors in coordinate transformations and/or poor stability characteristics of the discrete computation of the turret correction angle. Consequently, the fire control was not used for the experiment.

b. *Turret*

The turret model, as defined previously, resulted in unwanted oscillations when ran on the digital computer. A satisfactory method of limiting the turret to 80 deg/sec in rate and 120 deg/sec^2 and implementing those limits in the computer model was not found during the simulation validation period. Consequently, it was decided

47
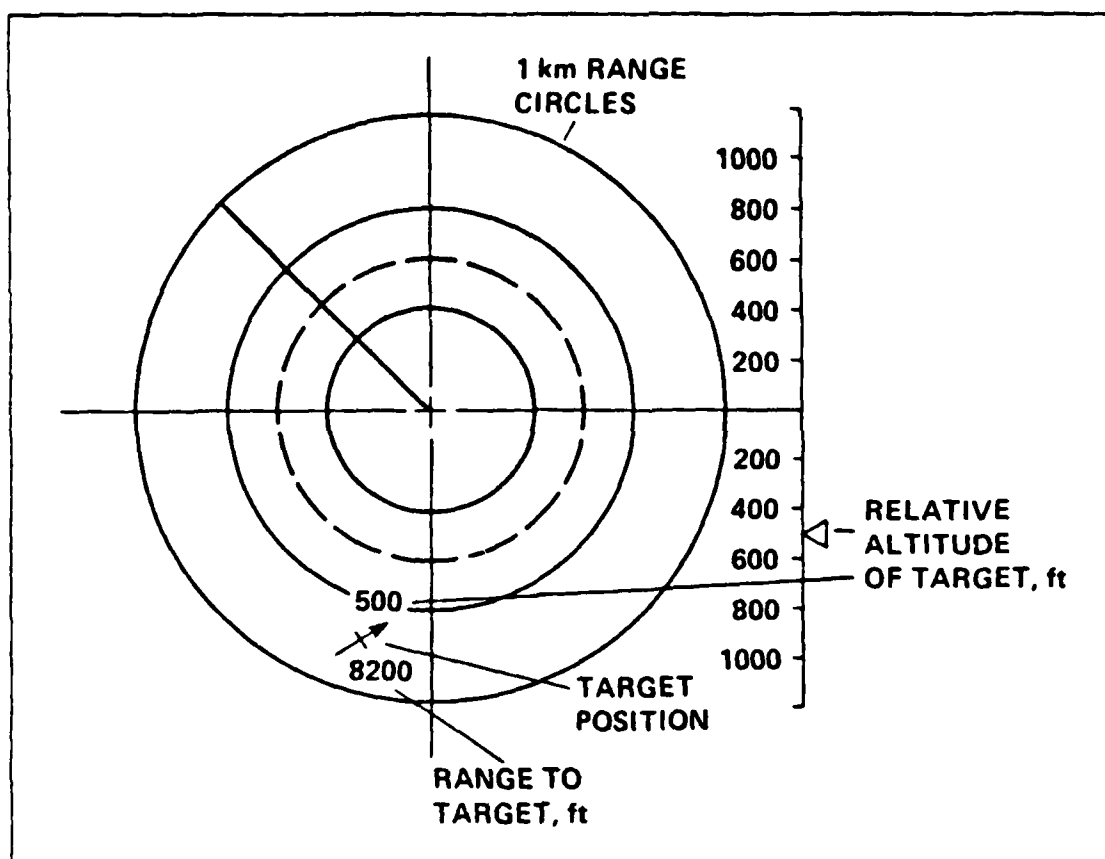
Figure 5.7   Blue-Ship Panel-Mounted Display.

not to attempt to model rate and acceleration delays in the turret. Instead, the turret position was assumed to be equal to the head position. The actual rates and accelerations of the pilot head motion were determined during post-simulation analysis and will be discussed later.

c. Ballistics

The implementation of the ballistic subroutine was very successful, both in the calculation of trajectories and in the presentation of the visual tracers. It was presumed prior to the simulation that the high velocity of the round would cause problems with seeing the rounds on the CGI but it was found not to be the case.

6. Utilization of the Terrain Database

The CGI terrain database used for HAC III is shown in Figure 5.8. The terrain database was found to be suitable for the terrain flight environment except in some of the peripheral areas. A great deal of detail in the form of buildings and trees

48

was added to the most usable areas near the center of the database. Texturing, in the form of geometry shapes of varying colors, was also added to aid in depth perception and terrain clearance in the low-level flight environment. Several iterations on the quantity of the detail and scaling of the texture were necessary during the experimental workup because too much detail was found to induce problems with the regeneration of the CGI during aggressive maneuvering. The problems were made less severe by slightly decreasing the detail and increasing the scaling of the texture of the CGI.

SAMPLE DIMENSIONS

HILL	HEIGHT OF PEAK, ft
A	900
B	1000
C	400
D	900
E	700
F	150
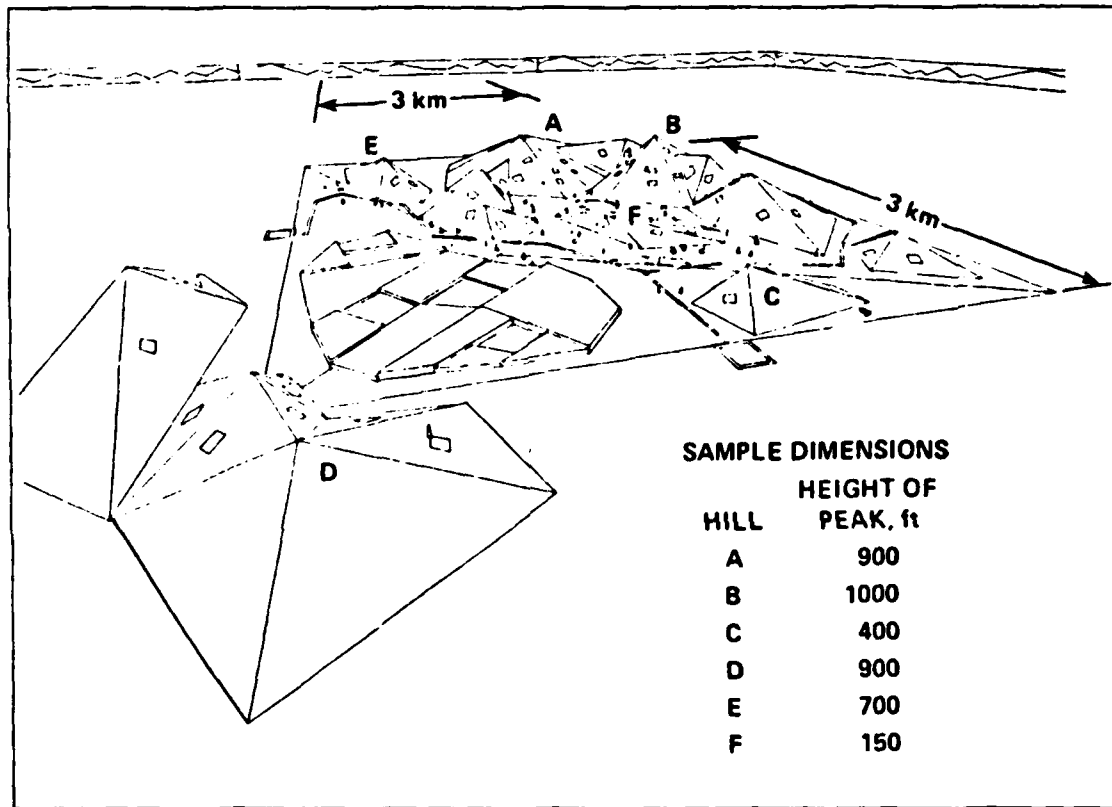
Figure 5.8   HAC III Terrain Database.

Adjustments in the coloring of the Red-ship image were made to help compensate for the reduced visual acuity in the simulation environment. A medium blue color was added to the lower portion of the fuselage so that the image could be more easily detected at longer ranges. The Red-ship image is shown in Figure 5.9.

The detail of the scene of the second eyepoint in the red cockpit also contributed to the computational times of the CGI regeneration. To further reduce the
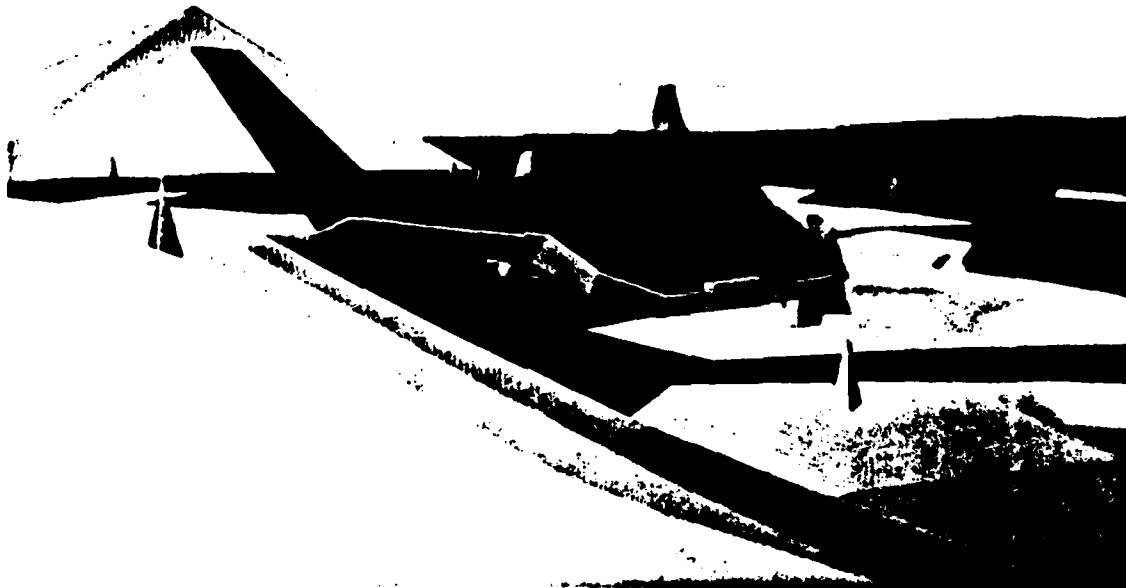
Figure 5.9 Red-Ship CGI Image.

computational and transport loads, the blue aircraft was significantly reduced in detail (Figure 5.10).

The relatively high hills on two sides of the terrain database were found to be nearly unusable because of the severe elevation gradients. Instead, they became virtually a boundary limiting the maneuver area of the aircraft.

Despite the improvements made in the terrain environment, however, the depth and rate of closure cues were still far from being as strong as in actual flight. An additional compensation for that deficiency was found to be the use of the altitude tape and IVSI on the IHADSS display to prevent flying in contact with the terrain.

Figure 5.10   Blue-Ship CGI Model.

7. Data Acquisition

a. Strip Charts

Three strip chart recorders were used to record the analog variation of a total of 48 variables during the simulation. The strip charts were used extensively during the validation phase for dynamic checks of the various subroutines of the simulation model.

b. Initial Configuration and Post-Run Summaries

The summaries were printed prior to and immediately after each simulation run on a Versatec plotter. Common information included the date and time, run number, model configuration, and pilot.

The initial configuration summary included the position, heading, and velocity of each aircraft. The configuration was also printed to include control system type, turret type, and initial values for the stability derivatives for calculation of the equations of motion.

The post-run summary listed a statistical summary of a single run, including the maximum and minimum values for ownship velocity, altitude, body angles and angular rates, and linear accelerations. Additionally, control reversals were summed and maximum turret azimuth and elevation was recorded.

c. Realtime Variable Recording

Seventy-eight variables listed in Table 3 were recorded continuously on magnetic tape at a cycle time of 30 msec. The variables were recorded in a format for post-run analysis on a VAX 11/750 computer system.

52

TABLE 3

RECORDED REALTIME VARIABLES

TIME	Total time into run	seconds
XCG	X-position of Blue-ship CG (earth coordinates)	feet
YCG	Y-position of Blue-ship CG (earth coordinates)	feet
HCG	Z-position of Blue-ship CG (earth coordinates)	feet
ALTD	Blue-ship rate of climb	feet/sec
FTX	Sum of forces in x-axis of Blue-ship (body axes)	lbf
FTY	Sum of forces in y-axis of Blue-ship (body axes)	lbf
FTZ	Sum of forces in z-axis of Blue-ship (body axes)	lbf
UB	X-component of Blue-ship velocity (body axes)	ft/sec
VB	Y-component of Blue-ship velocity (body axes)	ft/sec
WB	Z-component of Blue-ship velocity (body axes)	ft/sec
VEQ	Blue-ship Airspeed	knots
PHIRDM	Blue-ship Euler roll angle	degrees
THET	Blue-ship Euler pitch angle	degrees
PSI	Blue-ship heading	degrees
BETA	Blue-ship sideslip angle	degrees
PHID	Blue-ship roll rate	rad/sec
THED	Blue-ship pitch rate	rad/sec
PSID	Blue-ship yaw rate	rad/sec
ROLLO	Blue-ship lateral cyclic input	percent
PITCHO	Blue-ship longitudinal cyclic input	percent
COLO	Blue-ship collective input	percent
YAWO	Blue-ship pedal input	percent
VN	Blue-ship north component of velocity	ft/sec
VE	Blue-ship east component of velocity	ft/sec
XCGT	X-position of Red-ship CG (earth coordinates)	feet
YCGT	Y-position of Red-ship CG (earth coordinates)	feet
HCGT	Z-position of Red-ship CG (earth coordinates)	feet
FTXT	Sum of forces in x-axis of Red-ship (body axes)	lbf
FTYT	Sum of forces in y-axis of Red-ship (body axes)	lbf
FTZT	Sum of forces in z-axis of Red-ship (body axes)	lbf
UBT	X-component of Red-ship velocity (body axes)	ft/sec
VBT	Y-component of Red-ship velocity (body axes)	ft/sec
WBT	Z-component of Red-ship velocity (body axes)	ft/sec
VEQT	Red-ship airspeed	knots
PHIT	Red-ship Euler roll angle	degrees
THETAT	Red-ship Euler pitch angle	degrees
PSIT	Red-ship heading	degrees
BETAT	Red-ship sideslip angle	degrees
PBTDEG	Red-ship roll rate	deg/sec
QBTDEG	Red-ship pitch rate	deg/sec
RBTDEG	Red-ship yaw rate	deg/sec
ROLLT	Red-ship lateral cyclic input	percent
PITCHT	Red-ship longitudinal cyclic input	percent
YAWT	Red-ship pedal input	percent
COLT	Red-ship collective input	percent
VNT	Red-ship north component of velocity	ft/sec
VET	Red-ship east component of velocity	ft/sec
VDT	Red-ship vertical component of velocity	ft/sec
ALTDT	Red-ship rate of climb	ft/sec
UTURB	X-component of turbulence (body axes)	ft/sec
VTURB	Y-component of turbulence (body axes)	ft/sec
WTURB	Z-component of turbulence (body axes)	ft/sec
ISEE	Clear line-of-sight flag	
SRANGE	Distance from Blue- to Red-ship	feet
AOFFO	Azimuth from Blue- to Red-ship (Blue-ship axes)	degrees
POFFO	Pitch from Blue- to Red-ship (Blue-ship axes)	degrees
AOFFT	Azimuth from Red- to Blue-ship (Red-ship axes)	degrees
POFFT	Pitch from Red- to Blue-ship (Red-ship axes)	degrees
TOTAL	Total rounds fired by Blue-ship	
SCORSUM	Total hits by Blue-ship on Red-ship	
TYMISS	Horizontal miss distance of round from Red-ship CG	feet
TZMISS	Vertical miss distance of round from Red-ship CG	feet
OWNTIMS	Total tracking time	seconds
TURTIME	Total time target within turret envelope	seconds
TRDIST	Total miss distance of the round	feet
PSIRTD	IHADSS position in azimuth (body axes)	degrees
THETRTD	IHADSS position in elevation (body axes)	degrees
EPSID	IHADSS tracking error in azimuth	degrees
ETHETD	IHADSS tracking error in elevation	degrees
IFIRECP	Fire control activation flag	
IFIREB	Gun trigger flag	
FRX	X-component of the recoil force (body axes)	lbf
FRY	Y-component of the recoil force (body axes)	lbf
FRZ	Z-component of the recoil force (body axes)	lbf
ITHR2	Ground threat activation flag (above 150 ft)	
ITHR3	Ground threat activation flag (above 300ft)	
IEVENT	Event marker flag	

d. Pilot Commentary

A voice activated audio tape recorder was used to record pilot commentary and communications among the blue cockpit, red cockpit, and control room. Commentary during the simulation was encouraged at any time and was solicited after experimental runs for a particular configuration were completed to include a Cooper-Harper rating of the tasks. Post-run commentary was somewhat standardized by a pilot's questionaire present in the cockpit as shown in Table 4. A comment summary sheet was maintained at the engineers station in the control room to record a summary of events and highlighting commentary.

Finally, after each session in the cockpit, the pilot was solicited for general and detailed comments on all aspects of the simulation. Comments were prompted using a post-session questionaire as shown in Table 5.

8. Task Definition

NASA TN D-5153 defines the task as "the actual work assigned a pilot to be performed in completion of or as representative of a designated flight segment" [Ref. 8, p. 4]. For consistancy and validity in pilots ratings and commentary, the task to be evaluated needed to be precisely defined. For HAC III, the air-to-air gun engagement was divided into two control tasks and a auxiliary task, as defined in Table 6. The auxiliary task was specified to encourage the use of realistic terrain flight tactics and altitudes.

TABLE 4

HAC-III POST-RUN PILOT QUESTIONAIRE

1. GROSS-MANEUVERING SUBTASK (Maneuver to gain a firing position)

   (a) MANEUVERABILITY (Gross aircraft maneuver performance)
       -GOOD / FAIR / POOR -- Comment
       -Were you constrained by concerns for apparent maneuver
        envelope limits (ie., torque,load factor, sideslip) ?
   (b) AGILITY (Ability to quickly and precisely change flight path):
       -CONTROL RESPONSE: GOOD / FAIR / POOR --Comment
       -PREDICTABILITY: GOOD / FAIR / POOR --Comment
   (c) COOPER-HARPER PILOT RATING
   (d) What feature(s) (good or bad) most influenced your rating?

2. PRECISION TRACKING SUBTASK (Weapon utilization)

   (a) ABILITY to keep pipper on target
   (b) PREDICTABILITY of aircraft system
   (c) Use of Aircraft Control vs. IHADSS Turret
   (d) COOPER-HARPER PILOT RATING
   (e) What feature(s) (good or bad) most influenced your rating?

3. COMMENT where applicable:

   (a) IHADSS (display format, display dynamics)
   (b) Recoil force -- noticed? -- effect on task?
   (c) Situational Awareness: Airborne target, ground threat, terrain-
       - Use of PMD
   (d) Ability to judge if you have attained a satisfactory:
       - Firing position
       - Track
       - Hit
   (e) Power management -- effect on:
       - Closure with target
       - Terrain avoidance
   (f) Target maneuvering and aggressiveness

4. How do you feel about your performance?
   What techniques would have improved your performance?

MAKE COMMENTS AT ANY TIME

TABLE 5

HAC-III POST-SESSION PILOT QUESTIONAIRE

1. During this series of evaluation runs, what features (aircraft characteristics, fire control system -- including turret drive, displays, tactical scenario, simulator cab features) most contributed to your task performance?

2. What features most degraded your task performance?

3. During these runs, what was the easiest axis to control? What was the hardest?

4. During this session, how would you rate your use of terrain? How did your terrain use in the simulator relate to the real world?

5. What were the primary problems you encountered in low-level air-to-air combat (tactical situation, ground threat, air opponent, aircraft control, fire control system type, instrument symbology, visual system cueing)?

6. Was the display symbology useable? What was the best symbol feature? What was the least used symbol feature?

7. Where appropriate, comment on your relative use of aircraft and fire control system for placing rounds on target -- what was your control strategy?

8. Any additional comments?

56

TABLE 6

EXPERIMENT CONTROL AND AUXILLIARY PILOTING TASKS

Control Tasks:

    (1)   To maneuver the aircraft and/or gun turret (IHADSS LOS) so as to obtain a successful firing position.

    (2)   To gain and maintain the ballistic pipper (IHADSS LOS) on the target for a 3 second track and gun burst.

Auxiliary Task:

    Maintain situational awareness with regard to:

        (1) Red Aircraft

        (2) Ground threat

        (3) Terrain

---

9. Fixed-Forward Gun

During the previous HAC II experiment, it was found that the yaw damping and natural frequency and maneuver envelope played a significant role in the pilot ratings and the performance of the task. Since the design of the HAC III simulation was significantly different than HAC II, the results could not be directly compared with regard to one set of variables such as yaw dynamics. Therefore, to gain an insight into the influence of the turreted weapon and to relate the results to HAC II it was desirable to conduct evaluations with a simulated fixed-forward gun.

The fixed-forward gun sight was mechanized by adding a object in the form of a ring to the blue-ship CGI image. The ring was located a simulated distance of 30 feet forward of the CG and 4 degrees up from the body x-axis of the blue-ship. The resulting image on the CGI is shown in Figure 5.11. The 3 foot diameter resulted in a half-angle of 2 degrees from the pilot's viewpoint which was equivalent to the IHADSS gunsight pipper used for the turreted gun.

10. Environmental Factors

Adjustable environmental factors included visibility, wind, and turbulence. For the simulation, the visibility was set to 10000 feet and the net wind was set to zero. The turbulence was set to values shown in Table 7 which resulted in a random and alternating wind in three axes over time as shown in Figure 20.
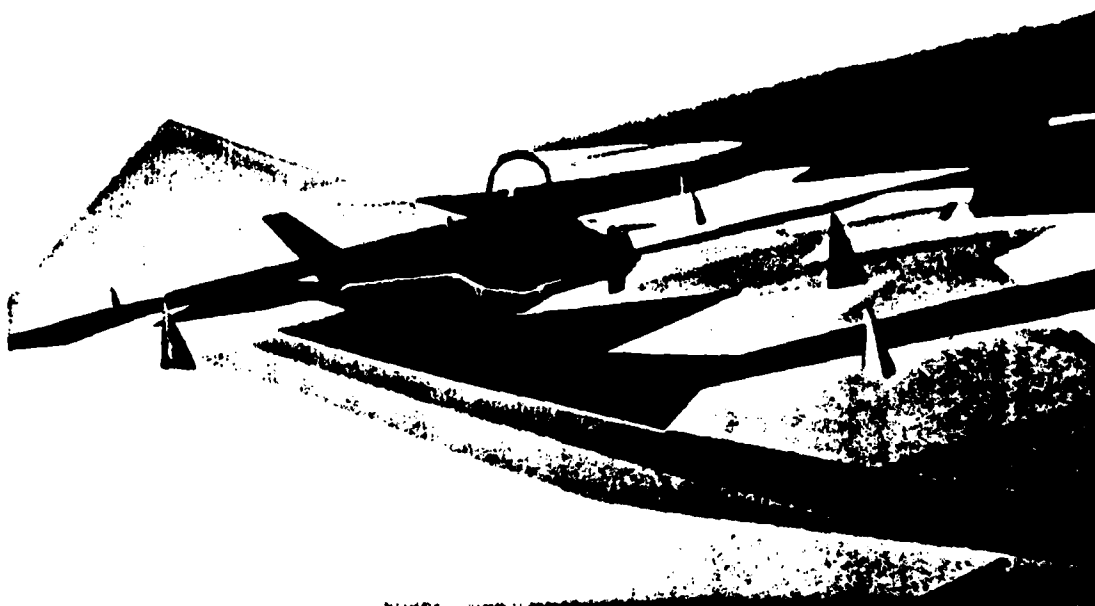
Figure 5.11   Fixed-Gun Reticle CGI Image.

TABLE 7
TURBULENCE PARAMETERS

Turbulence Response Derivatives   RMS

Derivative	Value	Units		Body Axis	Value (ft/sec)
Lv	-.0283	rad/ft-sec		U	2.025
Mu	.00267	rad/ft-sec		V	2.025
Mw	-.011	rad/ft-sec		W	3.038
Nv	.05127	rad/ft-sec			
Xu	-.010	1/sec			
Yv	-.100	1/sec			
Zu	-.107	1/sec			
Zw	-.374	1/sec			
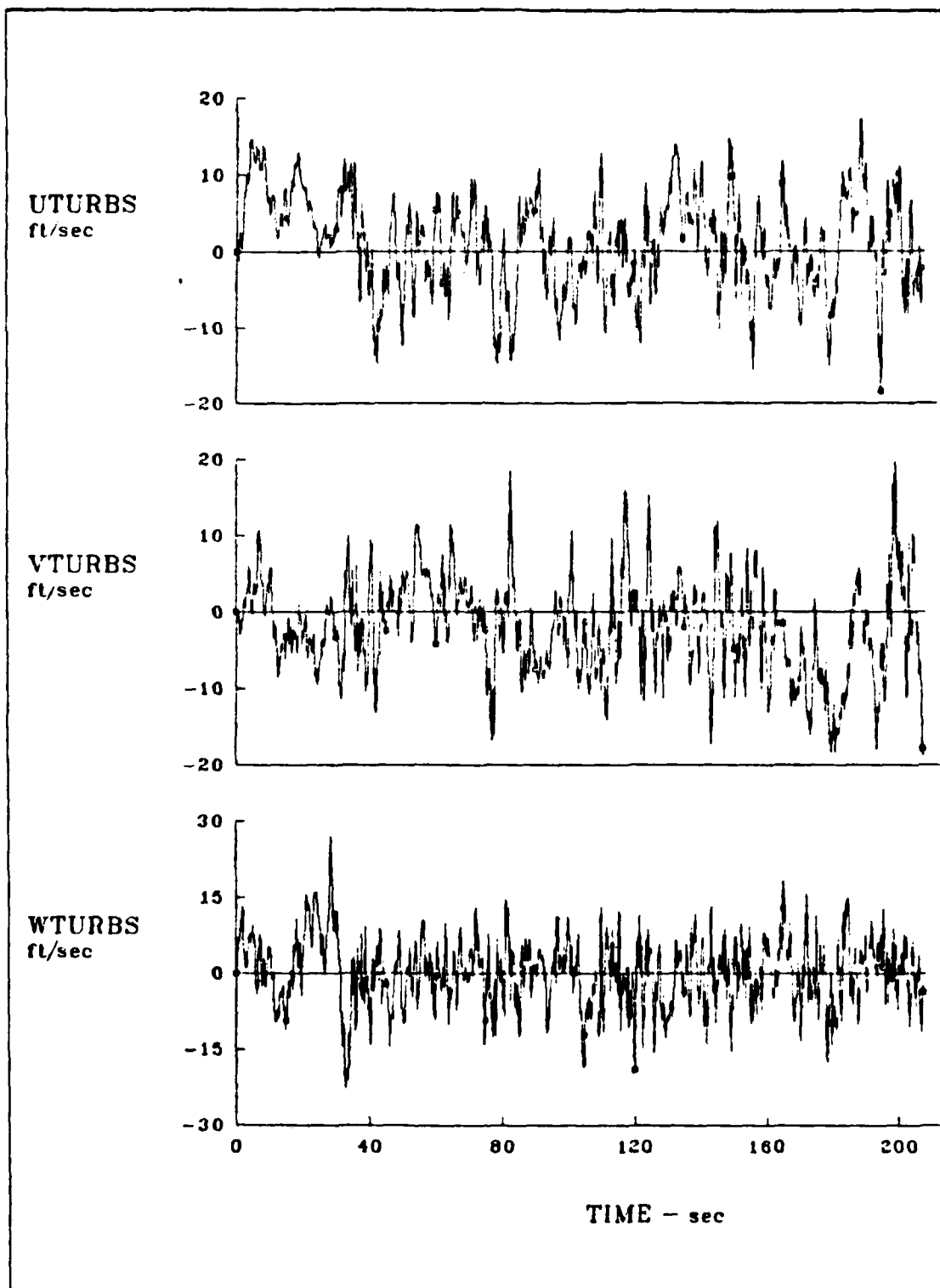
Figure 5.12   Velocities Due to Turbulence Over Time.

B. EXPERIMENTAL VARIABLES

1. Yaw Axis Dynamics

The primary variables for the experiment were yaw natural frequency and damping. Three values of each were used making a 3×3 test matrix.

From the equations of motion discussed in Appendix A, the transfer function for sideslip to pedal input above 50 knots is shown in Equation 5.1:

$$\frac{\beta}{\delta_p} = \frac{-N_{\delta p}}{s^2 - (Y_v + N_r)s + (Y_v N_r + U_o N_v)} \qquad \text{(eqn 5.1)}$$

For the simulation Y_v had a constant value of -0.1 sec^{-1}. Above 50 knots, the derivative N_v was set equal to $K_{Nv} U_o$ resulting in constant coefficients. The second order system denominator or its respective characteristic equation could also be written as:

$$s^2 + 2\zeta\omega_n s + \omega_n^2 = 0 \qquad \text{(eqn 5.2)}$$

Therefore:

$$\omega_n^2 = Y_v N_r + K_{Nv} \qquad \text{(eqn 5.3)}$$

$$2\zeta\omega_n = -(Y_v + N_r) \qquad \text{(eqn 5.4)}$$

During the previous HAC II experiment, a damping ratio of 0.7 was found to be unsatisfactorily low for the air combat task. Higher damping ratios (1-1.5) were found to be desirable. As for natural frequency, HAC II found no definitive trends over a range of 1-2 rad/sec.

The proposed specification for handling qualities states that, for Level 1 handling qualities, the lateral-directional natural frequency be greater than 1.0 rad/sec and the damping be greater that 0.35 [Ref. 9, p. 40]. To assist in the formulation of a more definitive specification, the damping ratios chosen for HAC III were 0.7, 1.4, and 2.0 with 1.4 as the baseline damping ratio, and the yaw natural frequencies were 1.0,

<div align="center">60</div>

1.5. and 2.0 rad sec with 1.5 rad sec as the baseline natural frequency. The combinations of natural frequency and damping which made up the test cells, as well as the respective values of N_r and K_{Nv} are shown in Table 8.

Test Cell	w_n	ζ	N_r	K_{Nv}
		TABLE 8		
		YAW DYNAMICS TEST CELLS		
1	1.0	0.71	− 1.32	0.868
2	1.0	1.37	− 2.64	0.736
3	1.0	2.03	− 3.96	0.604
4	1.5	0.71	− 2.03	2.05
5	1.5	1.37	− 4.01	1.85
6	1.5	2.03	− 5.99	1.65
7	2.0	0.71	− 2.74	3.73
8	2.0	1.37	− 5.38	3.46
9	2.0	2.03	− 8.02	3.20

2. Turret Envelope Size

To investigate the effect of turret maneuver envelope size on the task of air combat, two envelopes were used during the simulation. The depiction of the IHADDS display (Figure 4.9) has on it the representation of the 'full traverse' turret with limits of ± 110 degrees in azimuth, 15 degrees up, and 60 degrees down. A second 'limited traverse' turret was defined with limits of ± 40 degrees. in azimuth, 10 degrees up and 60 degrees down.

3. Fixed-forward versus Turreted Gun

As previously mentioned, to relate the results of HAC III with previous experiments, a method to simulate a fixed-gun as a variable was employed. The primary purpose of this set of discrete variables was to be able to relate the results of HAC III with previous fixed-forward gun simulations.

C. EXPERIMENTAL CONDUCT

1. Participating Evaluation Pilots

Pilots who participated in the experimental portion of the simulation varied significantly in background and represented a variety of users. Each of the pilots, their affiliation, and their background are shown in Table 9.

TABLE 9

PARTICIPATING EVALUATION PILOTS

CW 2 John Burt, U.S. Army
 ACM Instructor Pilot, Utah ANG
 Total Time: 3000 hrs
 Total Rotary Wing Time: 3000 hrs
 Primary Aircraft: AH-1, OH-6

MAJ Eric L. Mitchell, U.S. Army
 Test Pilot, U.S. Navy Test Pilot School
 Total Time: 3000 hrs
 Total Rotary Wing Time: 2400 hrs
 Primary Aircraft: UH-1, UH-60,
 OH-6, OH-58

Mr. Robert Gradle, Boeing Vertol
 Test Pilot
 Total Time: 2800 hrs
 Total Rotary Wing Time: 1700 hrs
 Primary Aircraft: HH-53, CH-47
 UH-1, AH-1, OH-58

Mr. Chan Morse, MDHC
 Test Pilot
 Total Time: 5000 hrs
 Total Rotary Wing Time: 3500 hrs
 Primary Aircraft: H-53, H-3, AH-1
 AH-64, OH-6, OH-58

Mr. Nicholas D. Lappos, Sikorsky
 Test Pilot
 Total Time: 4000 hrs
 Total Rotary Wing Time: 4000 hrs
 Primary Aircraft: S-76, UH-60,
 AH-1, H-53, H-3, XH-59A

Mr. Robert Williams, Bell Helicopter
 Test Pilot
 Total Time: 7500 hrs
 Total Rotary Wing Time: 6200 hrs
 Primary Aircraft: UH-1, UH-60

2. Methodology

a. Facility Preparation

Prior to evaluations, the various components of the simulation were brought on-line and checked out. The cockpit controls' force-feel system was verified and balanced. The proper functioning of the visual scene, instruments, and displays during flight as well as the sound and tone generation was insured. Finally, the functioning of the data acquisition systems and the assignment of values to the software variables was checked. It became evident early on in the simulation that, because of the complexity of the system, a systematic check of all of the facility components was necessary to insure that nothing was overlooked and valid results were obtained.

b. Pilot Preparation

(1) *Pilot Briefing.* Upon arrival, the subject pilots were given a standard briefing by the simulation project pilot. Included in the briefing were the program

objectives and a general description of the simulation facility with emphasis on the cockpit. The format of the cockpit instruments, switchology, and IHADSS and panel-mounted displays were described. The scenario and simulation conduct under which the experiment would be conducted was briefed, to include the tasks to be evaluated. To assist in the standardization of pilot ratings and commentary a list of definitions of key words was briefed to the pilots and referenced throughout the simulation. The established definitions are shown in Table 10 .

(2) *Helmet Fitting and Cockpit Orientation.* The proper fitting of the IHADSS helmet was critical to insure no relative movement of the helmet on the pilot's head occurred during a flight. The helmets could be tailored to the pilot's head through the use of pads and adjustable straps. The fitting was accompliched in accordance with the procedure outlined in the IHADSS helmet technical manual. Once the helmet was successfully fitted, the pilot kept that helmet for the duration of his participation.

Once fitted, the pilots were oriented to the cockpit to include the location of instruments and switches, seat and pedal adjustments, and the lighting, communications. The operation of the IHADSS HDU and its adjustments was also demonstrated.

(3) *Pilot Training.* Prior to evaluations, one or two cockpit sessions, each of 45-60 minutes in duration, were flown so that the pilots could gain familiarity with the aircraft model, visual scene, and the displays. After the pilot indicated that he felt he had gained a familiarity with all of the available cues, a target aircraft was presented and flown manually in a free engagement to allow the integration of the cues (i.e., CGI, instrument, and displays) into the tasks of maneuvering and tracking in air combat. The primary objective for the training period was for the pilot to accomplish that integration.

c. Scenario and Evaluations

Upon completion of the training phase, experimental runs for evaluation were conducted. The Blue aircraft was initialized at a hover near the edge of the database facing toward the center. When ready, the pilot initiated the run by engaging the OP button on the cyclic stick. After 5-10 seconds, the red-ship appeared on the visual scene and the PMD at varying locations, airspeeds, and headings. The pilot then commenced the maneuver and engagement, continuing the tasks until the end of the run.

TABLE 10
KEY WORD DEFINITIONS

Maneuverability
Measure of the ability to change the aircraft velocity vector or energy state. Total aircraft performance, size of envelope.

Agility
Measure of the time required to precisely change the aircraft energy state. Control response; control power, damping.

Task
The actual work assigned a pilot to be performed in completion of or as representative of a designated flight segment.

Performance
The precision of control with respect to aircraft movement that the pilot is able to achieve while performing the task.

Workload
The total physical and mental effort required to perform the specified task.

Compensation
Measure of additional pilot effort and attention required to maintain a given level of performance because of deficient aircraft characteristics.

Cockpit Interface
The means provided for the flow of information to the pilot. Includes IHADSS, PMD, cockpit instruments, and control characteristics.

Configuration
The total aircraft/weapon system defined by the dynamic characteristics, the type of flight control system, and the type of fire control/weapon system.

Handling Qualities
Those qualities or characteristics of an aircraft that govern the ease and precision with which a pilot is able to perform the tasks required in support of an aircraft role.

Because of the desire to control the task and the relatively small size of the terrain database, the runs were normally kept at or below 90 seconds in duration. Commentary was encouraged at any time, however several runs were conducted for a given configuration before a Cooper-Harper rating was given. The pilot was requested to step methodically through the flow chart of the rating scale as shown in Figure 2.1. For each new configuration, the pilot was given time to get accustomed to the handling

characteristics of response of the aircraft model. Then a relatively unaggressive target red-ship was flown over a standard course at a constant airspeed of 90 knots and 20-50 feet above the terrain. Finally one of two free-engagement runs were conducted. Upon completion of the runs, the pilot responded to the in-cockpit comment card (Table 5) and rated the tasks before moving on to the next configuration.

Each session was begun using test cell 5 (ω_n = 1.5, ζ = 1.4) as a baseline. Then test cells were chosen at random without informing the pilot of which configuration he was flying. Each session was roughly one hour in duration, which produced results for 4-6 test cells. After each in-cockpit session, written comments were solicited, in particular, in response to the post-session questionaire (Table 5).

d. Red-ship Strategy and Piloting Technique

The fundamental purpose of the Red-ship in HAC III was to force the use of the full potential of the Blue-ship aircraft and weapon system while engaging in air combat at terrain flight altitudes. At the same time, it was desirable to standardize the threat aircraft's performance throughout the experiment so that the Red-ship's aggressiveness did not become a variable for the different configurations.

The Red-ship was also flown consistent with the desire to have the tasks performed at tactical terrain flight altitudes. The majority of the maneuvering stayed below 50 feet above the terrain and utilized the micro-terrain features when possible. Infrequently, flight excursions above 150 feet were made but were kept to a few seconds in duration.

VI. RESULTS AND ANALYSIS

A. GENERAL

The approach to the analysis of the results was divided into three primary parts. First, the pilot commentary was used to focus on potentially significant aspects of the experiment where further analysis may have been appropriate. Second, the CHPR's were analyzed and trends or the lack of trends were identified. Finally, analysis of the time history of recorded data was made to support or dispute the commentary and ratings. The approach was not to perform an exhaustive analysis of all runs for all pilots but to look at the majority of the experimental runs for one pilot. The pilot chosen had flown the most complete set of test cells and configurations and had previous experience with the HAC II simulation.

1. Configurations Completed

During the experiment, the yaw dynamics portion of the test matrix was completed by four out of the six visiting pilots. Of the remaining two, one pilot completed all but two cells and, the other, all but four. As a result, a good sampling of pilots for the yaw dynamics test matrix utilizing a full traverse turret was accomplished.

Three pilots flew configurations employing the limited-traverse turret. Of those three, two completed the yaw dynamics test matrix and the third completed five out of the nine cells. Only two pilots flew configurations using the fixed-forward gun completing five and seven cells of the nine, respectively.

The resulting data could generally support the influence of yaw dynamics on the employment of a turreted gun in helicopter air combat and possibly help define required yaw-axis handling qualities characteristics. That is, the number of samples were statistically significant. The limited results of flights using limited-traverse and fixed-forward guns could possibly identify but not define any significant influences those variables had on the task.

2. Experimental Fidelity and Pilot Commentary

a. Aircraft Model

Generally, the simple aircraft math model used was found to be well suited for the study of air combat. Unlike more complex models, the HAC model provided the robustness necessary for the aggressive maneuvering inherent in the task.

66

There were several adverse comments during the experiment however, regarding the aircraft model. In at least some of the configurations, the yaw control power was less than realistic at a hover. The reason for this was identified during the course of the experiment. To isolate the effects of yaw dynamics on the task, it was desirable to hold all other vehicle characteristics constant. To preclude the steady-state control power from being variable with changes in N_r and K_{Nv}, the numerator of the transfer function for sideslip to pedal input ($N_{\delta p}$) was calculated so that it equaled a constant (0.0209) times the s^0 coefficient of the denominator at velocities greater than 50 knots as shown in Equation 6.1.

$$N_{\delta p} = 0.0209 \, (Y_v N_r + K_{Nv}) \qquad \text{(eqn 6.1)}$$

As a result, the forward flight ($\geq$ 50 knots) steady-state value of sideslip was equal to 0.0209 rad/inch of the pedal input. To illustrate, if Equation 6.1 is substituted into Equation 5.1 and the final value theorem is then applied with a unit step input, the result in equation form is:

$$\frac{\beta}{\delta_{pss}} = 0.0209 \, \frac{(Y_v \, N_r + K_{Nv})}{(Y_v \, N_r + K_{Nv})} \quad \text{rad/inch} \qquad \text{(eqn 6.2)}$$

Using this methodology resulted in yaw control power being constant over the test cells, and therefore, not influencing the results.

This was not true at a hover, however, because the denominator was no longer second order, but reduced to a first order equation with a root at N_r. The calculation for $N_{\delta p}$ did not change with airspeed. Consequently, the yaw control power at hover was dependent on the test cell being flown because it was dependent on N_r as shown in Equation 6.3

$$\frac{r}{\delta_{pss}} = 0.0209 \, \frac{(Y_v \, N_r + K_{Nv})}{N_r} \quad \text{rad/sec/inch} \qquad \text{(eqn 6.3)}$$

where   r $\equiv$ yaw rate (rad/sec)

Table 11 lists the resulting steady-state yaw rate per pedal input (r/δ_{pss}) below 30 knots in rad/sec/inch of cyclic for each test cell. It is evident that the variation in pedal

control power was significant and may have influenced the pilot ratings. Further analysis of the experimental runs showed that the majority of the time was spent at airspeeds greater than 50 knots so the effect of the fault in the model was probably minimal.

TABLE 11

PEDAL CONTROL POWER PER TEST CELL AT HOVER

Test Cell	$N_{\delta p}$	N_r	$r\,\delta_{pss}$
1	0.0209	− 1.32	0.1583
2	0.0209	− 2.64	0.0792
3	0.0209	− 3.96	0.0528
4	0.0470	− 2.03	0.2316
5	0.0470	− 4.01	0.1173
6	0.0470	− 5.99	0.0785
7	0.0836	− 2.74	0.3051
8	0.0836	− 5.38	0.1554
9	0.0836	− 8.02	0.1042

b. Visual Scene and Field of View

Pilot comments indicated that generally the cues provided by the visual scene were good for the terrain flight operation, however, a relative lack of detail still caused problems in depth perception for some pilots. The degree of the problems seemed to lessen over time in the simulator.

The target aircraft was difficult to see at long ranges because of the relative lack of contrast with the terrain. Additional comments supported the idea that that difficulty was not unrealistic.

Another significant problem with the CGI inherent in the VMS system is the inability of the scene to update at a frequency high enough to keep up with high turn rates inherent in aggressive maneuvering. Figure 6.1 depicts the delays present in the simulation hardware, resulting in a total delay of 120 msec during the experiment. The subject of computational and transport delays and their effects on simulation fidelity has been investigated in numerous studies. Generally, the effects of excessive delays reduce the maximum rate at which a pilot can perform a task and cause a general decrease in handling qualities ratings [Ref. 21].

68
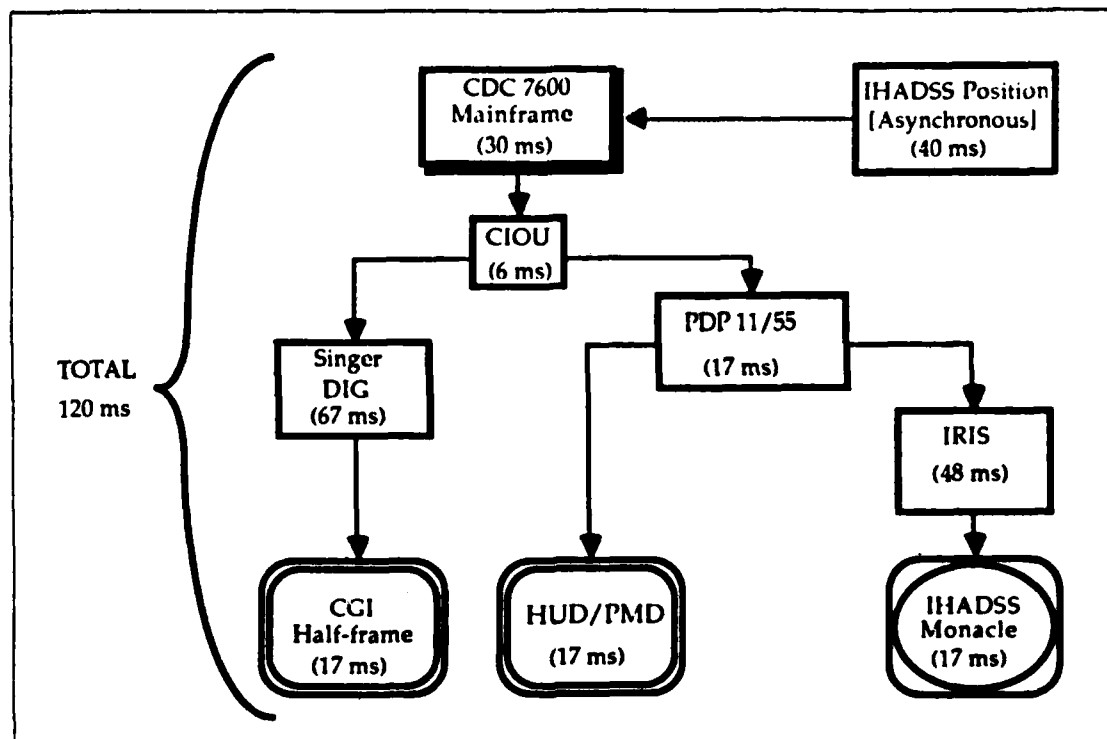
Figure 6.1   Simulation Hardware Timing Diagram.

The FOV was adequate except in up-elevation. The deficiency was a significant influence throughout the experiment because the necessity to pitch nose-down to accelerate prevented target engagements due to loss of visual contact. This restriction was partially compensated for by the integration of other cues from the IHADSS display and PMD, covered in a later section. The FOV was also restricted by the structural posts at ±25 degrees in azimuth. The restriction tended to discourage a gun engagement when tracking in the vicinity of the posts and may have forced a tendency to engage only in the center window.

c. IHADSS and the PMD

The integration of the IHADSS into the simulation and the experimental tasks was, generally, very good. Pilot commentary indicated that the portions of the symbology most used were the altitude tape and IVSI. Those cues helped compensate for the limited FOV, particularly while accelerating.

The primary deficiency noted by the pilots was the flashing of the IHADSS FOV box when the turret reached limits. Many times, the flashing FOV box was not seen during tracking. Because the high gain task of tracking the target required

concentration on the center pipper, it was felt that flashing the pipper when turret limits were exceeded would have been the best solution for providing the cue.

The g-meter was not used, generally, by any of the pilots, primarily because the normal load-factor limit was not normally an issue in the task flown at terrain flight altitudes.

Comments relating to the PMD indicated that the cues it provided were very useful for target acquisition and situational awareness, compensating somewhat for the deficiencies of the visual scene and FOV.

B. YAW DYNAMICS TEST MATRIX UTILIZING THE FULL-TRAVERSE TURRET

1. Cooper-Harper Pilot Ratings (CHPR)

Because of the task definitions, two CHPR's were taken for each run, one for the gross maneuvering subtask and one for the tracking subtask. The approach to determining significant trends in ratings was to perform separate analysis for each task. A word of caution should be given with regard to the approach taken, which included calculating the mean and standard deviation. The Cooper-Harper scale is ordinal, not interval; and determining the mean assumes a linear scale. Therefore, it is recognized that the statistical process is not strictly valid for large variations of ratings. With that in mind the following approach to the analysis of the CHPR's was taken.

Each test cell for the full-traverse turret contained from 4-7 data points. A mean rating for each cell was given by:

$$x_m = (1/n)\left[\sum_{i=1}^{n} x_i\right] \qquad \text{(eqn 6.4)}$$

where: n $=$ number of data points

x_i $=$ CHPR

x_m $=$ mean CHPR

Then a sample standard deviation was given by:

$$\sigma = \left[\frac{\displaystyle\sum_{i=1}^{n}(x_i - x_m)^2}{n-1}\right]^{(1/2)} \qquad \text{(eqn 6.5)}$$

An additional estimation of the accuracy associated with the result is the confidence interval. That is, the interval within which the true mean is expected to lie with a given probability (confidence level). The smaller the confidence level, the easier it is to interpret the experimental results. It can also be a measure of the quality control of the experiment. [Ref. 22: p. 7] For this analysis the probability level was assumed to be 90%. Then the confidence interval was given by:

$$CI/2 = \sigma\left[\frac{t_{\alpha/2}}{n^{(1/2)}}\right] \qquad \text{(eqn 6.6)}$$

where $\alpha \equiv$ 0.1 for 90% confidence

Table 12 gives the probability points of the t-distribution for t_{05} for the applicable number of data points (degrees of freedom).

TABLE 12

PROBABILITY POINTS OF THE T-DISTRIBUTION

DOF	4	5	6	7
t_{05}	2.132	2.015	1.943	1.895

Finally, in an attempt to insure that the means and standard deviations were somewhat accurate measures of a total pilot population, the data points were tested using Chauvenet's criterion presented in Reference 23, page 73. Chauvenet's Criterion

71

is a relatively restrictive test and "specifies that a reading [or data point] may be rejected if the probability of obtaining the particular deviation from the mean is less that $1/2n$." Table 13 lists the ratio of maximum acceptable deviation to standard deviation ($d_{i_{max}}/\sigma$) as a function of number of samples where $d_i = x_i - x_m$.

TABLE 13
CHAUVENET'S CRITERION

n	3	4	5	6	7
d_{max}/σ	1.38	1.54	1.65	1.73	1.80

---

a. Gross-Maneuvering Subtask

Table 14 lists the CHPR's and their respective statistical measures for the gross-maneuvering subtask by test cell. Not shown in Table 14 is one data point which was a CHPR of 5 for test cell 8 because it failed Chauvenet's Criterion explained above.

TABLE 14
CHPR AND STATISTICAL MEASURES FOR THE
FULL-TRAVERSE TURRET (GROSS-MANUEVERING SUBTASK)

Test Cell	ω_n	ζ	CHPR's	#pilots	x_m	σ	CI/2
1	1.0	0.7	7,7,7,6,5	5	6.4	0.9	.81
2	1.0	1.4	7,3,3,7,7,6	6	5.5	2.0	1.6
3	1.0	2.0	4,3,3,7	4	4.25	1.9	2.0
4	1.5	0.7	6,4,3,6,5,4,4	7	4.6	1.1	.79
5	1.5	1.4	4,3,2,4,5,4,4	7	3.7	1.0	.72
6	1.5	2.0	3,5,4,3,2,4,5	7	3.7	1.1	.79
7	2.0	0.7	5,6,5,2	4	4.5	1.7	1.8
8	2.0	1.4	3,2,2,2,3,2	6	2.3	0.5	.40
9	2.0	2.0	4,4,2,2,1	5	2.6	1.3	1.17

From the data, the approximate boundary band can be determined between Level one and Level two. Figure 6.2 shows a plot of the rating averages against yaw natural frequency and damping. Then overlaid on the plot is the approximated level boundary.
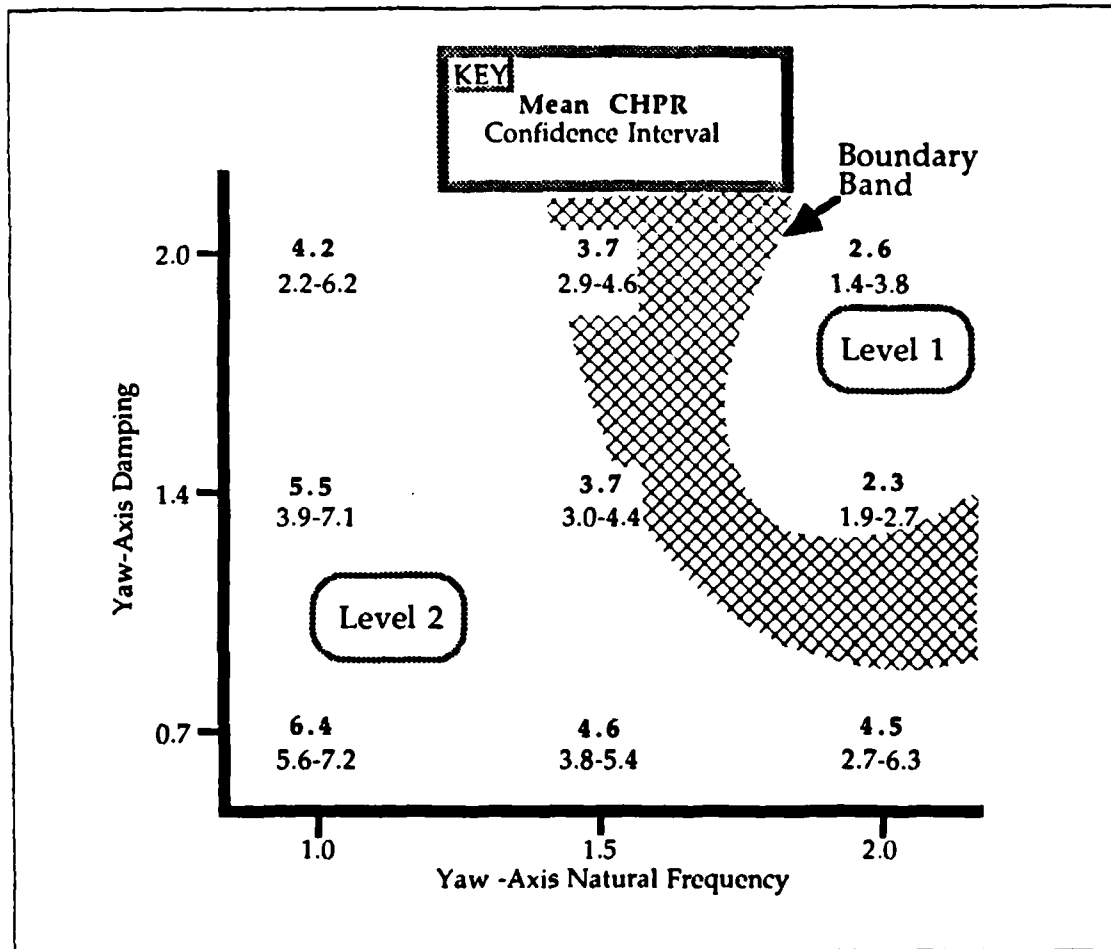
Figure 6.2   Level-Boundary Band for Full-Traverse Turret Gross-Maneuvering Subtask.

b. Tracking Subtask

Table 15 lists the Cooper-Harper Pilot Ratings and their respective statistical measures for the tracking subtask. For the tracking task, lower gradients of pilot ratings over the range of yaw dynamics would support a somewhat surprising conclusion that the yaw dynamics did not influence the tracking subtask as much as it did the gross-maneuvering subtask.

73

TABLE 15

CHPR AND STATISTICAL MEASURES FOR THE FULL-TRAVERSE TURRET (TRACKING SUBTASK)

Test Cell	ω_n	ζ	CHPR's	#pilots	x_m	σ	CI/2
1	1.0	0.7	4,6,8,5,5	5	5.6	1.5	1.4
2	1.0	1.4	4,5,6.3,4,5	6	4.5	1.05	0.83
3	1.0	2.0	4,4.5,3,5	4	4.1	0.85	0.91
4	1.5	0.7	3,5,7,5,3,5,3	7	4.4	1.5	1.07
5	1.5	1.4	3.5,3.3,4,4,3	7	3.6	0.79	0.56
6	1.5	2.0	3,4,3,3,4,2,4.5	7	3.4	0.85	0.61
7	2.0	0.7	2,7,5,2	4	4.0	2.45	2.6
8	2.0	1.4	3,3,2,2,3.3	6	2.67	0.52	0.41
9	2.0	2.0	4,6,3,2,1	5	3.2	1.92	1.73

c. Graphical Analysis of CHPR's

To help illustrate trends in pilot ratings with yaw natural frequency and damping, the means of the ratings are plotted for each test cell in Figure 6.3 for both the gross-maneuvering and tracking subtasks. Figures 6.3a-c plot ratings over the damping ratio holding natural frequency constant and Figures 6.3d-f plot ratings over natural frequency holding the damping ratio constant.

Disregarding the confidence intervals, several trends are apparent. First, the ratings for the tracking task are not as sensitive to damping and natural frequency as the gross-maneuvering task, however the ratings generally follow the same trend for both tasks. Second, to achieve Level 1 handling qualities, both a high natural frequency ($\omega_n \geq$ 1.5) and high damping ($\zeta \geq$ 1.4) are desirable. Finally, it is apparent that the two variables are interdependent. That is, the sensitivity of the CHPR to natural frequency is much greater for $\zeta = $ 1.4 than either of the other two values. Also, the sensitivity of the CHPR to damping is greater for $\omega_n = $ 2.0 rad. sec than the values of 1.0 and 1.5 rad sec. All of the data analysis supports the conclusion that test cell 8 ($\omega_n = $ 2.0, $\zeta = $ 1.4) resulted in the most favorable handling qualities.
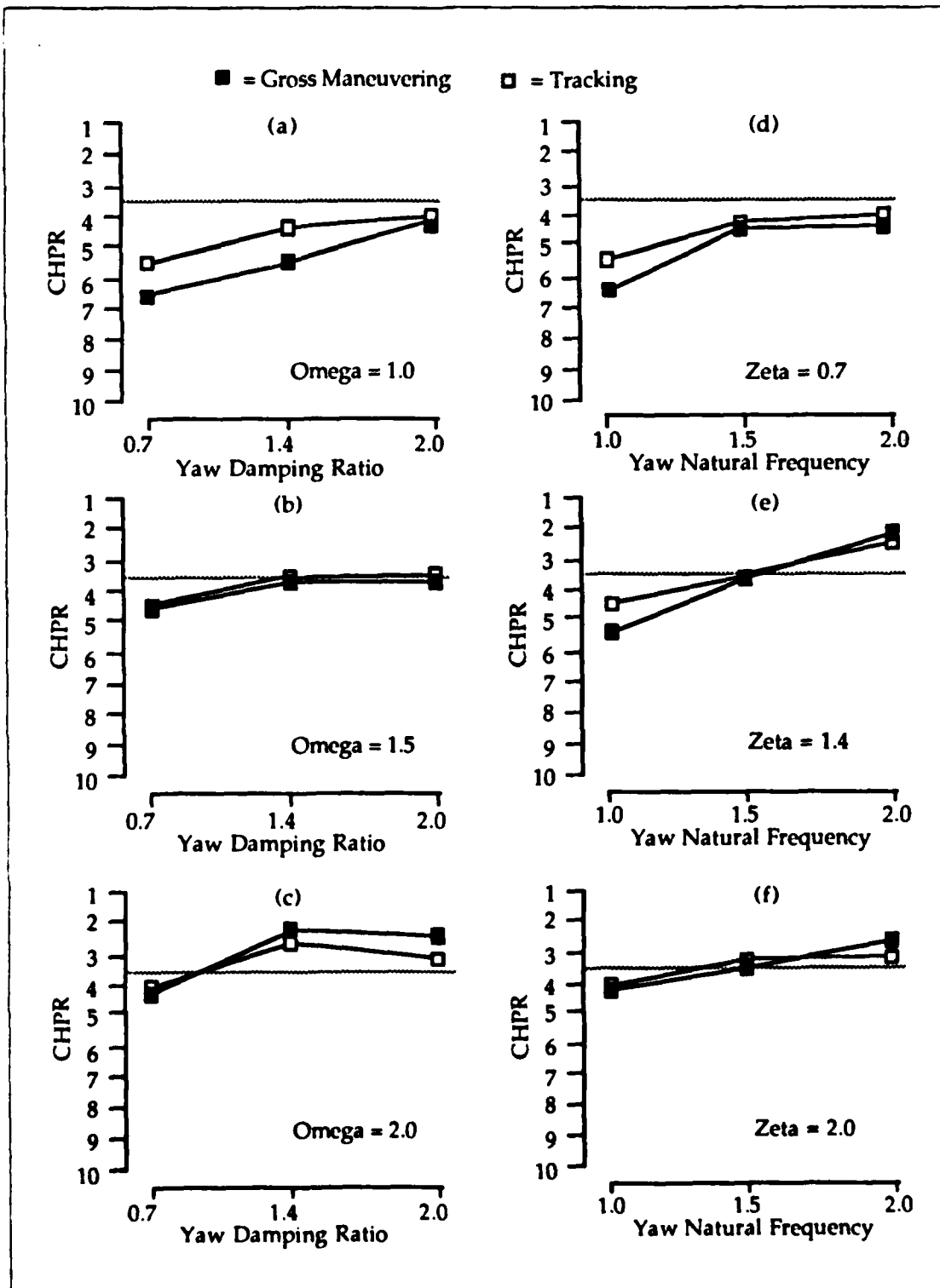
Figure 6.3   CHPR Means for the Full-Traverse Turret.

2. Tracking Performance

The tracking performance was analyzed graphically and statistically. A graphical representation of a time history of a tracking sequence over ten seconds is shown in Figure 6.4.
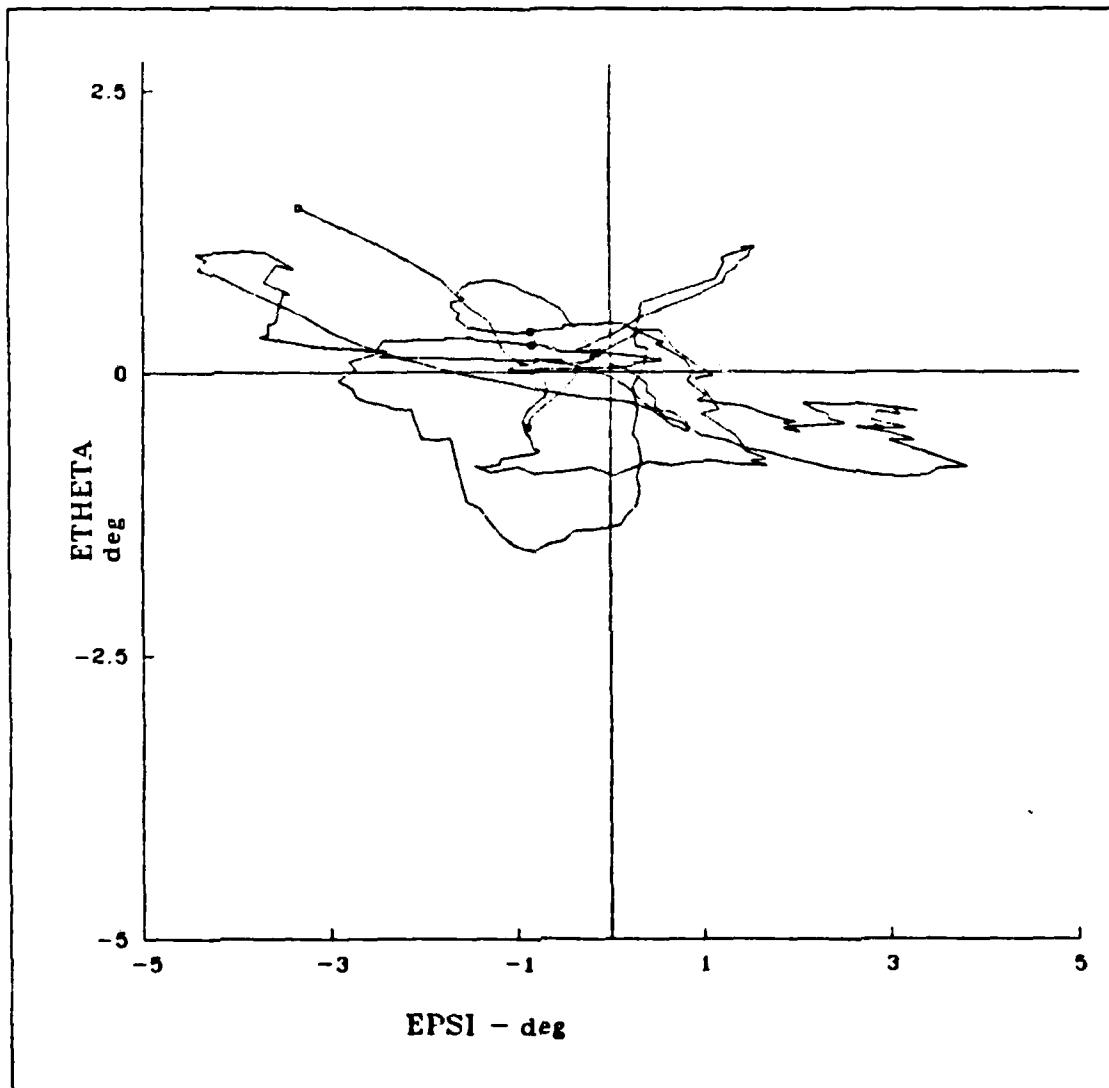
Figure 6.4   Tracking Accuracy Time History over 10 Seconds.

For the statistical investigation, only the time that the fire control was activated was considered. Table 16 lists the results for one pilot by test cell, and includes the percentage of time that the fire control was activated and the mean and standard deviation of the tracking error in elevation and azimuth, respectively.

TABLE 16

STATISTICAL MEASURES OF TRACKING
ACCURACY BY TEST CELL

| Test Cell	% Time Fire Control Active	Mean (deg)		3 sigma (deg)	
		Elev	Azim	Elev	Azim
1	25.6	-0.10	-0.17	3.33	6.69
2	23.9	0.32	0.16	2.13	4.60
3	39.2	-0.08	-0.52	2.80	6.42
4	not available				
5	38.0	0.01	-0.44	2.13	4.05
6	35.1	-0.20	-0.40	2.74	4.38
7	12.5	-0.78	-1.58	3.15	4.29
8	32.7	-0.10	-0.40	3.08	3.63
9	not available				

Unfortunately, a complete set of data was unavailable. A trend is evident, however, for the deviation in azimuth as a function of natural frequency (Test Cells 2,5,8). As natural frequency increased, the tracking precision in azimuth increased.

3. Use of the Turret Envelope

The turret envelope was analyzed graphically by plotting the time history of turret position within its envelope and by determining the means and standard deviations of turret position for azimuth and elevation. sideslip. Figure 6.5 depicts the time history of turret position for a typical run.

To help quantify the time history plots, the mean and standard deviation for turret position were calculated for both azimuth and elevation. Assuming a normal distribution, $\pm 3\sigma$ in azimuth and elevation would yield the portion of the turret envelope within which the turret was in about 98% of the time and that turret usage could then be compared with the turret envelope. The results of a statistical analysis of turret usage for an arbitrarily selected seven runs are shown in Table 17. It can be seen that the restrictive aspect of the turret position envelope was the up elevation. this is evident by the mean value of +7.5 degrees in elevation with 3σ being 11.7 degrees. In other words, the turret was at +7.5 $\pm$ 11.7 degrees in azimuth 98% of the time that the fire control was activated which includes a range only 0.8 degrees from the up-elevation limit.
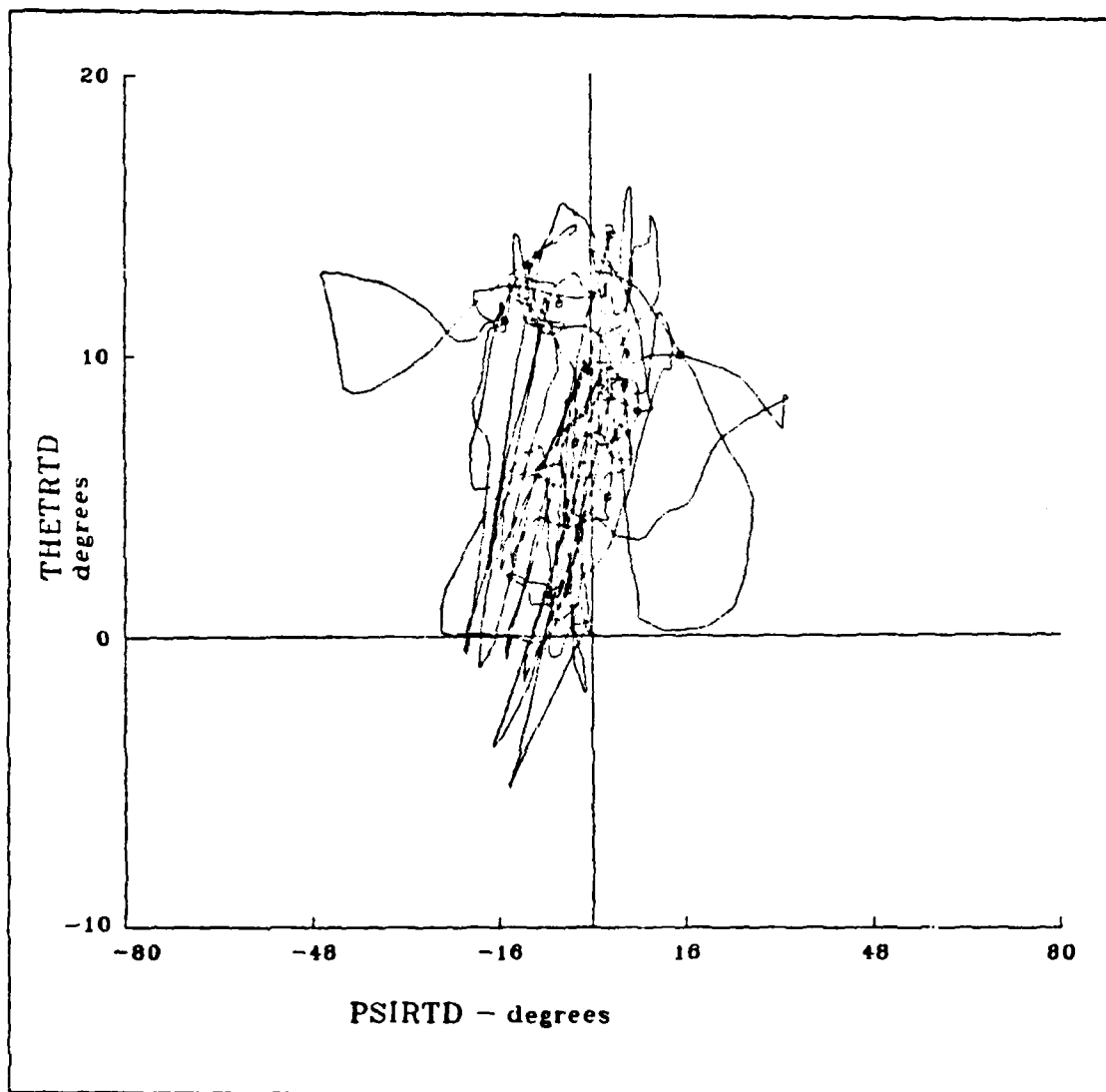
Figure 6.5   Time History of Turret Position over One Run (Full-Traverse Turret).

TABLE 17
STATISTICAL SUMMARY OF TURRET ENVELOPE USAGE
(FULL-TRAVERSE TURRET)

| % Time Fire | Mean (deg) | | 3 sigma (deg) | |
Control Active	Elev	Azim	Elev	Azim
37.4	7.50	-10.72	11.66	42.09

The turret usage in azimuth was not at all close to the limits, however it can be seen that some off-axis engagements were accomplished. Considering that the center-posts between the windows were approximately at ±25 degrees from the nose of the aircraft, engagements would not have been made in that vicinity and may have resulted in a wider use of turret azimuth than if they had not been there. The fact that the mean azimuth position resulted in being 10 degrees off from center may have resulted from the engagements being made in predominantly a counter-clockwise path.

A numerical calculation of turret rates and accelerations demonstrated that the rates and accelerations demanded were consistantly far lower than the assumed maximum values of 80 deg/sec and 120 deg/sec^2 for rate and acceleration, respectively. Figure 6.6 depicts the derived turret rate and acceleration for a typical run.
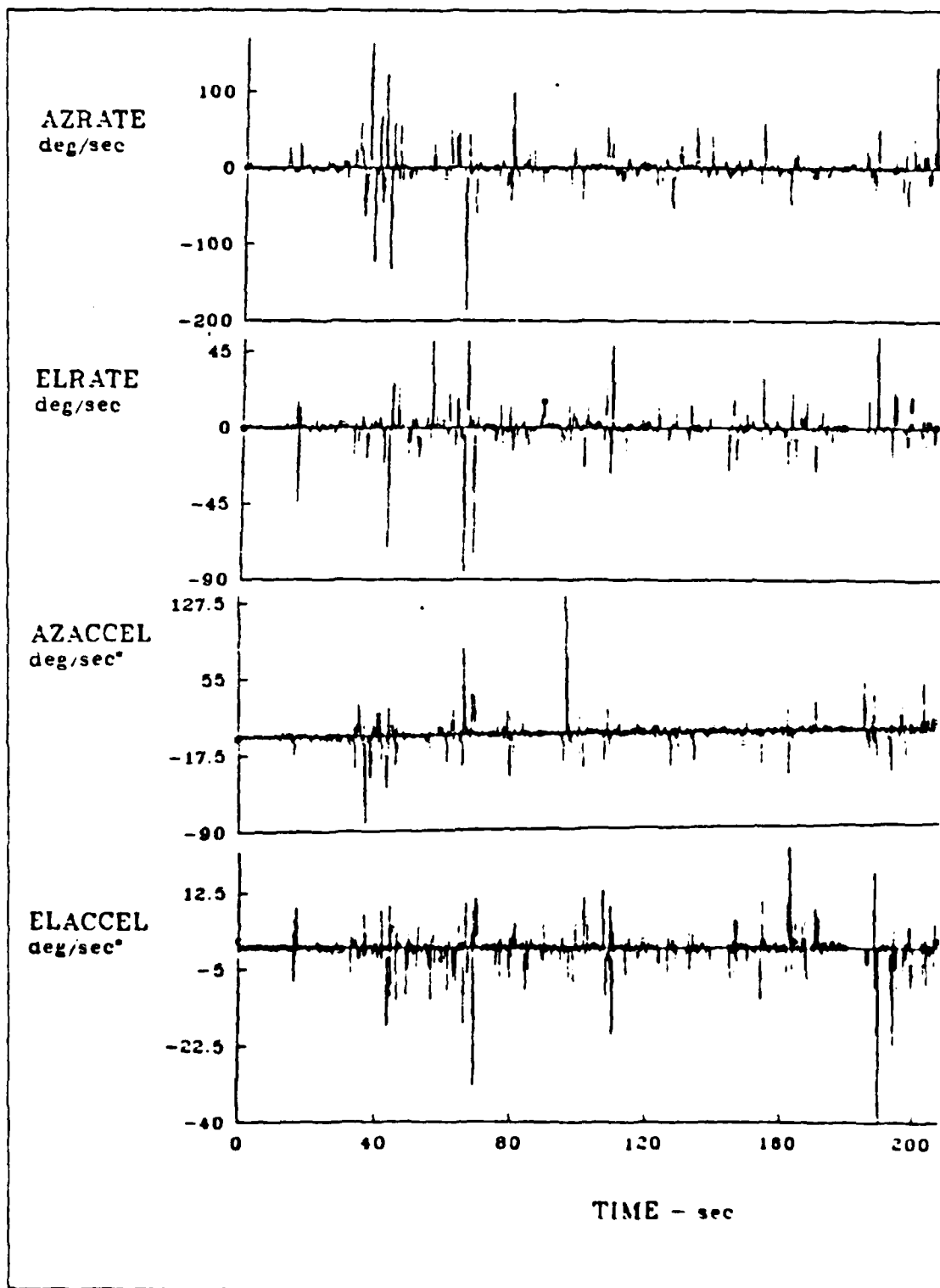
Figure 6.6   Derived Turret Rates and Accelerations over Time.

80

C. WEAPON SYSTEM TYPE

1. Limited-Traverse Turret

a. Cooper-Harper Pilot Ratings

The CHPR's and their associated statistics are shown in Table 18 for both the gross-maneuvering and tracking subtasks. As mentioned previously, data points numbering less than three result in large confidence intervals and, where the standard deviation equals zero, the CI is undefined.

Even though the results may not be statistically significant, graphically plotting the means of the CHPR's as previously done with the full-traverse turret can illustrate possible trends for future investigations. The CHPR means are plotted in Figure 6.7 for both piloting subtasks. The same trends in ratings are evident for the limited-traverse turret as with the full-traverse turret. The sensitivities or gradients of ratings with natural frequency and damping are, however, significantly higher for the limited traverse turret. A possible reason may be that the limited-traverse turret results in a tradeoff in turret maneuver ability for aircraft maneuverability usage. In other words, a decreased maneuver capability of the turret results in the pilot increasing the aircraft maneuvering, and, therefore, the aircraft handling qualities play more of a role. Again, the optimal yaw dynamics for the task were contained in test cell 8. A high yaw natural frequency ($\omega_n \geq 1.5$) and the median damping ratio ($\zeta \sim 1.4$) resulted in Level 1 handling qualities.

b. Tracking Performance

As with the full-traverse turret, no obvious trends in tracking performance over the range of yaw dynamics were present. Table 19 lists, for each test cell, the %time of fire control activation, the mean azimuth and elevation errors and three times the standard deviation in azimuth and elevation. Data for test cell 9 was unavailable.

An obvious difference existed between the tracking errors employing the full-traverse turret and those employing the limited-traverse turret. In fact, the azimuth errors for the limited-traverse turret are over 51% greater than those for the

TABLE 18
CHPR'S AND STATISTICAL MEASURES FOR THE LIMITED-TRAVERSE TURRET
(GROSS-MANEUVERING AND TRACKING SUBTASK)

Gross-Maneuvering Subtask

Test Cell	ω_n	ζ	CHPR's	#pilots	x_m	σ	CI 2
1	1.0	0.7	8,6	2	7	1.41	2.91
2	1.0	1.4	7,6,3	3	5.33	2.08	2.86
3	1.0	2.0	7,7	2	7	0	0
4	1.5	0.7	6,5,6	3	5.67	0.58	0.79
5	1.5	1.4	3,2,2	3	2.33	0.58	0.79
6	1.5	2.0	4,5,2	3	3.67	1.53	2.07
7	2.0	0.7	5,5	2	5	0	0
8	2.0	1.4	2,2,3	3	2.33	0.58	0.79
9	2.0	2.0	7,4	2	5.5	2.12	4.38

Tracking Subtask

| Test Cell	ω_n	ζ	CHPR's	#pilots	x_m	σ	CI 2
1	1.0	0.7	9,7	2	8	1.40	2.89
2	1.0	1.4	7,6,3	3	5.33	2.08	2.83
3	1.0	2.0	7,7	2	7	0	0
4	1.5	0.7	7,4,7	3	6	1.73	2.35
5	1.5	1.4	6,3,7	3	5.33	2.08	2.83
6	1.5	2.0	6,4,2	3	4	2.0	2.72
7	2.0	0.7	6,6	2	6	0	0
8	2.0	1.4	5,3,2	3	3.33	1.53	2.08
9	2.0	2.0	7,6	2	6.5	0.71	1.46
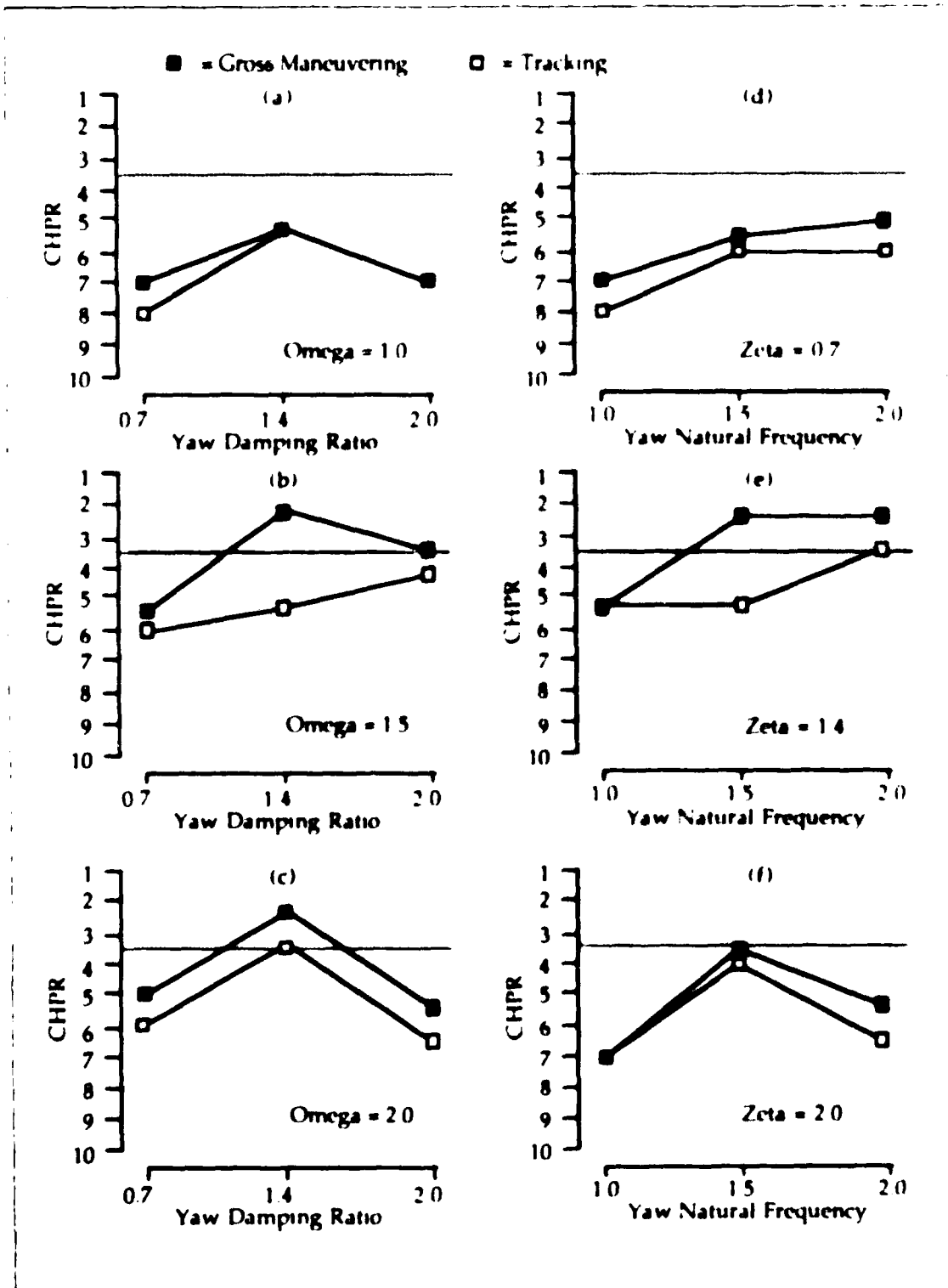
Figure 6.7   CHPR Means for the Limited-Traverse Turret.

TABLE 19

STATISTICAL MEASURES OF TRACKING ACCURACY BY TEST
CELL FOR THE LIMITED-TRAVERSE TURRET

Test Cell	% Time Fire Control Active	Mean (deg)		3 sigma (deg)	
		Elev	Azim	Elev	Azim
1	24.5	-0.08	0.53	3.42	7.38
2	34.2	-0.42	-0.14	3.30	6.09
3	45.6	-0.43	-0.78	2.73	5.85
4	24.9	-0.005	-1.21	3.18	7.74
5	33.2	-0.51	-0.30	2.99	6.56
6	29.2	-1.49	-1.05	5.58	9.63
7	38.9	-0.84	-0.57	4.29	7.74
8	38.1	-0.54	-0.06	3.67	7.84
9	not available				

full-traverse turret. The decreased tracking accuracy was most likely caused by the influence of the up-elevation limit of +10 degrees. As previously indicated, pilot commentary indicated that the decreased turret envelope significantly influenced the ability to maneuver and engage.

c. Use of Turret Envelope

As with tracking performance, a statistical representation of the turret position envelope usage supports the conclusion that the limited up-elevation significantly influenced the ability to perform the task. Table 20 lists the means and three times the standard deviations of the turret position over seven runs. From the data it can be seen that, in elevation, the 3σ (10.18 deg.) added to the mean (5.61 deg.) is greater than the limit. As in the pilot commentary and tracking error analysis, the turret usage analysis shows a significant adverse impact of the decreased envelope in elevation on the piloting task.

To help illustrate the turret usage for the limited-traverse and compare the usage with the full-traverse turret and their respective envelopes, Figure 6.8 depicts usage boxes within which the turret was located 98"o of the time that the fire control was activated (assuming a normal distribution). It is readily apparent from Figure 6.8 that the up-elevation limit was the most constraining, and in the case of the limited-traverse turret, was inadequate for the task. It is also apparent that the location of the window posts

TABLE 20

STATISTICAL REPRESENTATION OF THE
LIMITED-TURRET ENVELOPE USAGE

| % Time Fire	Mean (deg)		3 sigma (deg)	
Control Active	Elev	Azim	Elev	Azim
32.7	5.61	-4.14	10.18	25.7
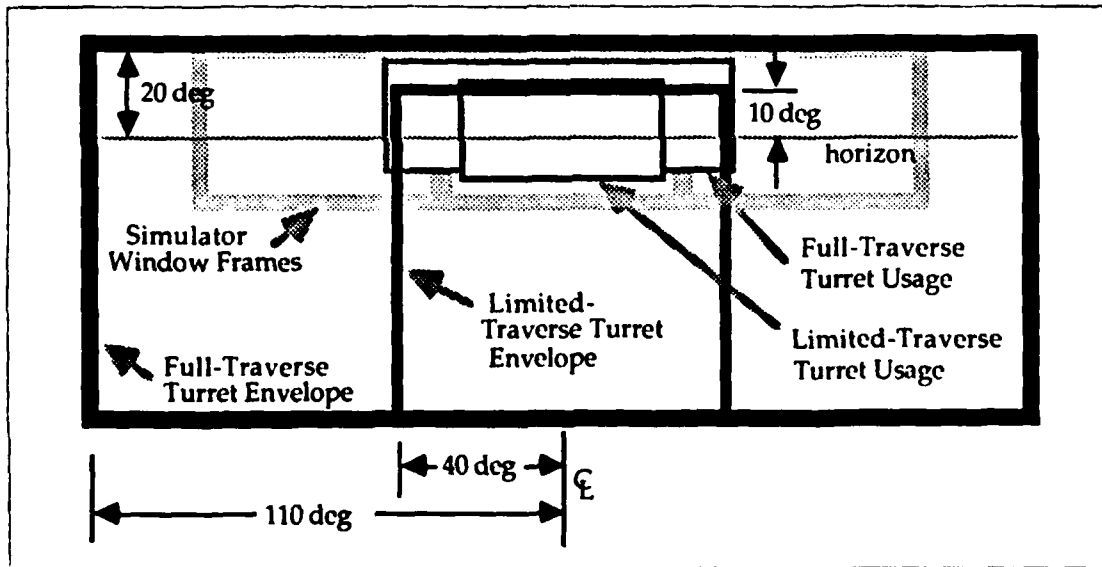
Figure 6.8   Turret Envelope Usage for the Full- and Limited-Traverse Turrets.

85

2. Fixed-Forward Gun

Only limited data was collected on the fixed-forward gun configuration and, for the data that was collected, the pilots were somewhat limited in training time. The data collected is presented here and some comments are made on the data, but it should be recognized that the remarks are highly judgemental and cannot be considered conclusive.

Table 21 lists the CHPR's for the fixed-gun configuration by test cell for the gross-maneuvering and tracking tasks. As with the turreted weapon systems, plots of the CHPR means for the fixed gun are shown in Figure 6.9. Definite trends existed for both yaw damping and natural frequency and the gradients of the ratings were much greater than for the turreted weapons. Unlike the turreted systems, the most desirable handling qualities occurred with the highest damping ratio ($\zeta = 2.0$) and the highest natural frequency ($\omega_n = 2.0$) or test cell 9. Also plotted are the CHPR's from the previous experiment (HAC II) for the same pilot that flew the most fixed-gun configurations for HAC III. Although the data points are limited, the trends are similar between the experiments but the ratings are generally higher for HAC II. A possible reason may have been the fact that HAC II was flown at somewhat higher altitudes with more use of the vertical and terrain avoidance was less of an issue.

Table 22 lists the tracking accuracy statistics by test cell. Surprisely, the tracking accuracy for the fixed-gun is as good, or better, than the turreted weapon systems.

To illustrate a comparison of tracking accuracy for each of the weapon systems, Figure 6.10 depicts the distributions of tracking error in azimuth. A normal distribution is assumed, with the width of the distribution curve depending on the calculated standard deviation (σ).

86
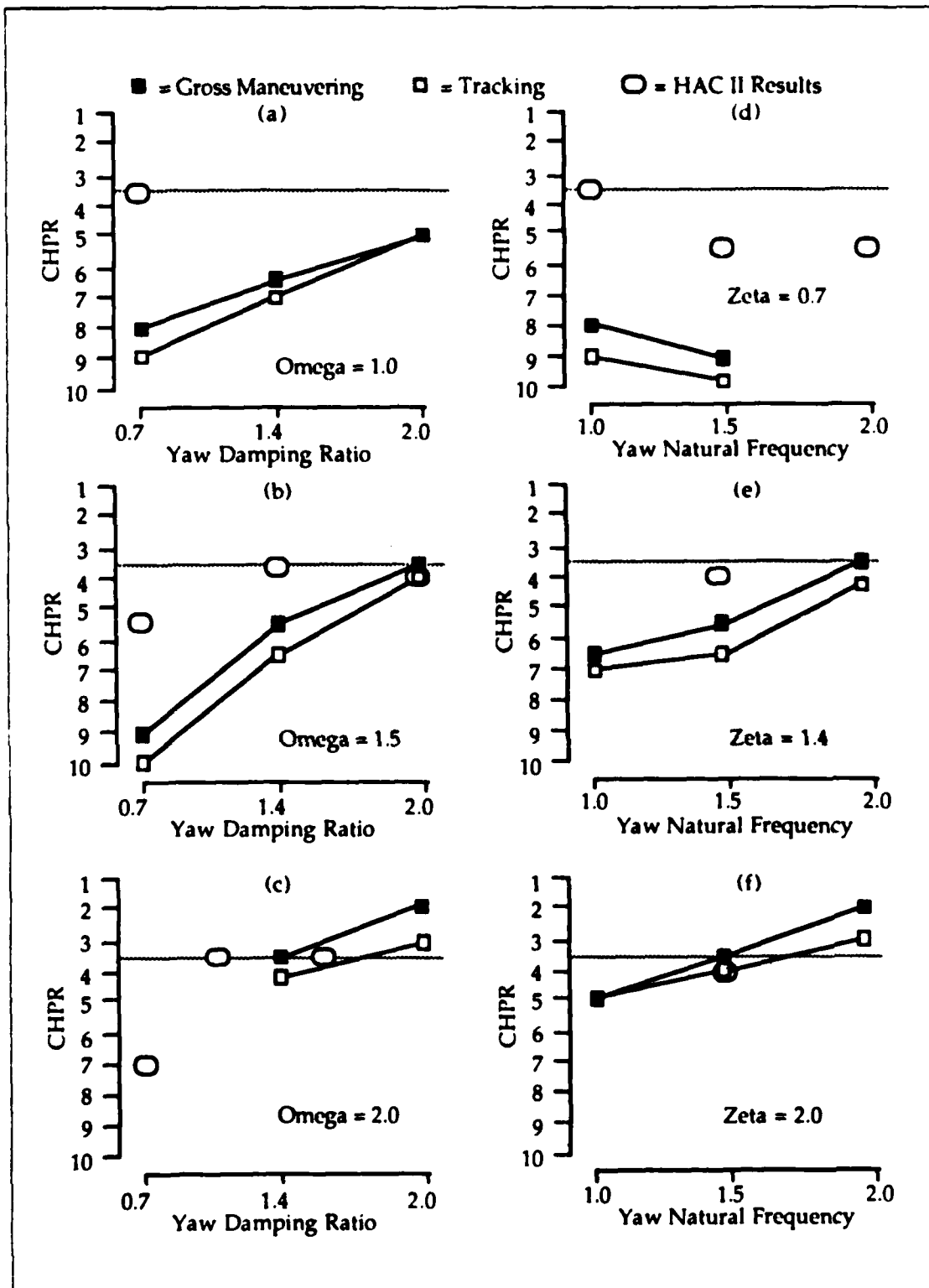
Figure 6.9 CHPR Means for the Fixed-Gun Configuration.

TABLE 21

FIXED-GUN CONFIGURATION CHPR'S

Test Cell	CHPR's	#pilots	Mean
Gross-Maneuvering Subtask			
1	8	1	8
2	7,6	2	6.5
3	5	1	5
4	9	1	9
5	5,6	2	5.5
6	3,4	2	3.5
7	--	0	
8	4,3	2	3.5
9	2	1	2
Tracking Subtask			
1	9	1	9
2	8,6	2	7
3	5	1	5
4	10	1	10
5	7,6	2	6.5
6	4,4	2	4
7	--	0	
8	5,3	2	4
9	3	1	3

TABLE 22

FIXED-GUN CONFIGURATION TRACKING ERROR STATISTICS

Test Cell	% Time Fire Control Active	Mean (deg)		3 sigma (deg)	
		Elev	Azim	Elev	Azim
1	not available				
2	14.1	0.285	-0.39	2.38	5.51
3	not available				
4	not available				
5	18.8	0.755	0.165	3.15	5.96
6	34.4	0.44	0.19	3.72	4.5
7	not available				
8	30.5	0.45	-0.125	2.85	4.52

D.   USE OF THE MANEUVERABILITY ENVELOPE

1. Normal Load Factor

Figure 6.11 depicts the normal load factor (n) distribution for each of the weapon system type configurations. Percent time is plotted against load factor. The load factor envelope appeared to be adequate for the performance of the task at terrain flight altitudes. Very little of the envelope below 0.5 g's and above 2.5 g's was used. Additionally, there were no significant differences among the weapon system types in the use of the load factor envelope.

2. Sideslip

The distribution of sideslip (β) for each weapon system type is shown in Figure 6.12 As with normal load factor, the sideslip envelope appeared to be adequate for the task as defined. Sideslip of less than 50"o of the limit at all airspeeds above 45 knots was predominate and very little of the envelope above 75"o was utilized.

Surprising in the results was the fact that as the weapon system became more restrictive, the use of sideslip in the task performance decreased. This trend was the opposite of what was expected but factors which influenced that trend have been hypothesized. First, training time and the resulting learning curve may have been a factor, particularly with the fixed-gun configuration. Second, the added dynamics introduced with the use of sideslip may have increased the workload requirements for tracking in the terrain flight environment to a point where the pilot was hesitant in using the added degree-of-freedom (DOF). The increased workload was probably even more apparent to the pilots because the fixed-gun scenarios followed the full- and limited-traverse configurations. The added dynamics of sideslip usage employing the full-traverse turret could probably have been compensated for by the turret and pilot's head tracking DOF.

An aspect of sideslip usage which is not known and may be a topic for further analysis is whether the use of sideslip was involved in the gross maneuvering task (and acquisition), the tracking task, or both.

89

Full-Traverse Turret

3-sigma = 14.58 deg

Limited-Traverse Turret

3-sigma = 22.05 deg

Fixed-forward Gun

3-sigma = 15.36 deg

℄
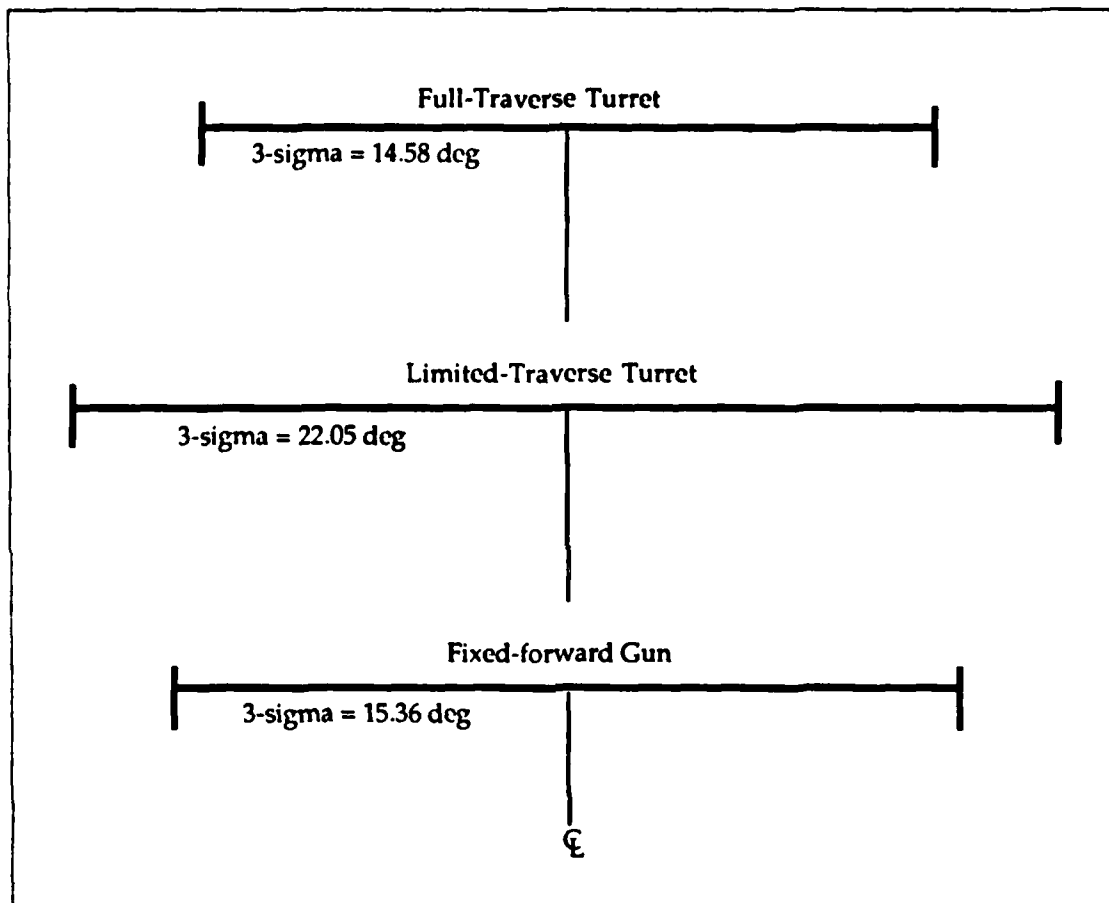
Figure 6.10   Tracking Error in Azimuth versus Weapon System Type.
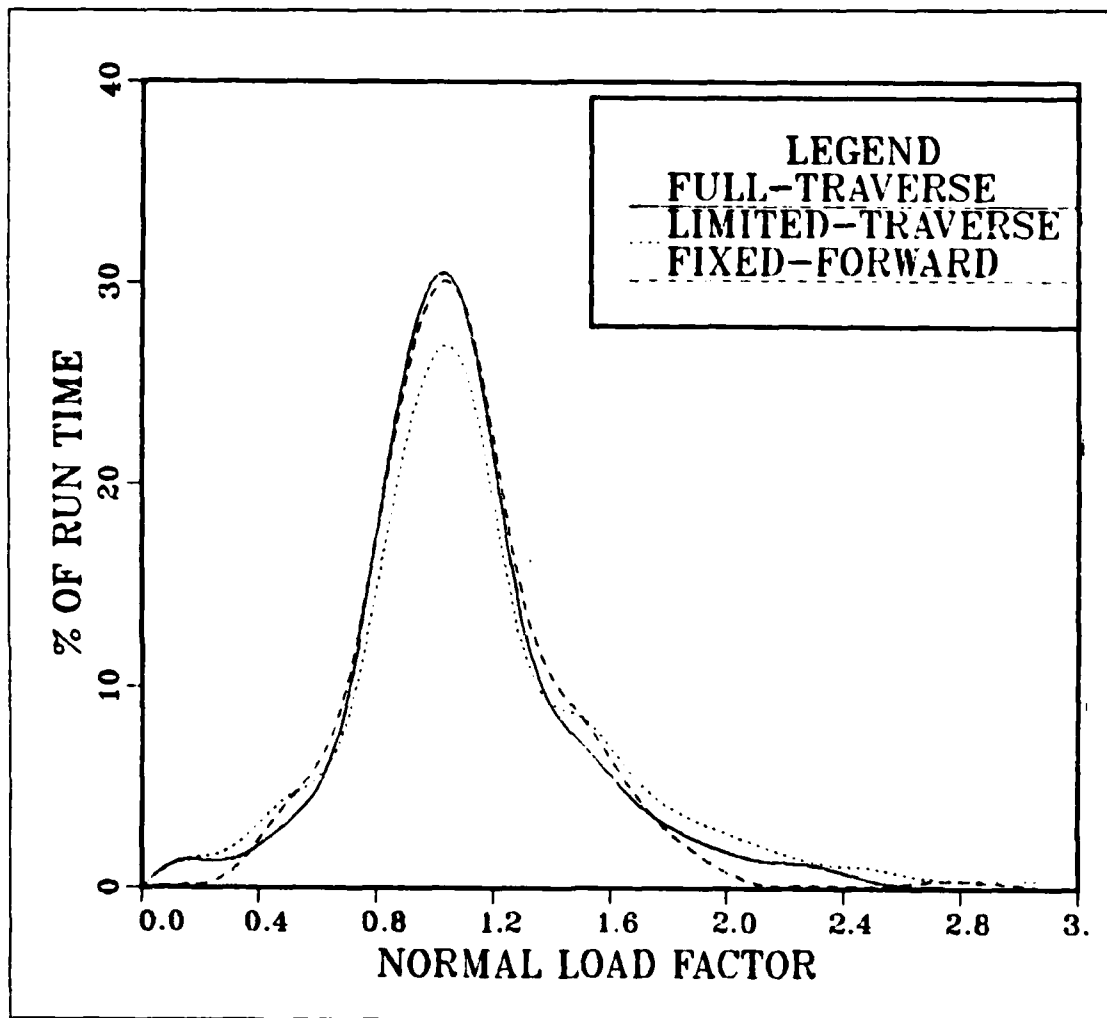
Figure 6.11 Normal Load Factor Distribution vs. Percent Time.
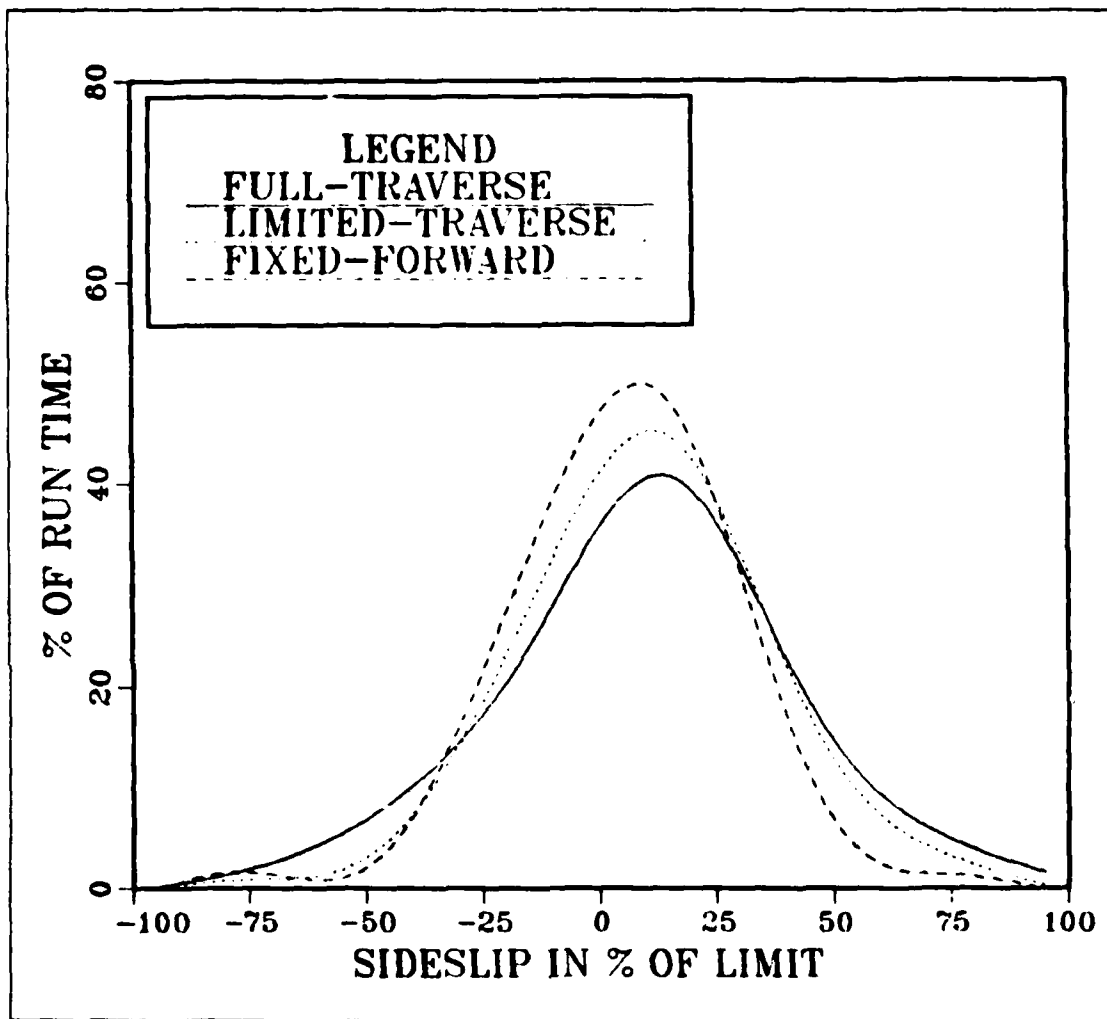
Figure 6.12 Sideslip (β) Distribution vs. Percent Time.

E. CORRELATION WITH ACTUAL FLIGHT

Subsequent to the simulation, two flights were made in an AH-1S performing moderate air combat maneuvering with a relatively passive target (UH-1H) in an attempt to relate the factors influencing the performance of the task in the simulation environment. A targeting pipper was simulated on a helmet visor and the tracking task was performed under varying flight conditions (velocity and turning rates). The following observations and comments resulted from the flights:

1) Because of the increased field-of-view (FOV), and motion and depth cueing in the flight environment, it was easier and more comfortable to utilize the off-axis capability of the turret. Terrain avoidance was less of an issue than in the simulation environment.

2) Although the FOV was better in the aircraft, it was still limited by the cockpit structure and, therefore, was still a hinderance to task performance.

3) The up-elevation limit of the turret was still a significant issue in the actual aircraft especially when acceleration was necessary or the target aircraft was at a higher altitude. A useful cue for the up-elevation limit was the tip-path-plane vice a symbology cue.

4) The additional vibration environment in the actual aircraft appeared to be at a high enough frequency so that it was more or less "in the noise" of the tracking task. (Turbulence was not a factor during the flights.)

5) Unlike the simulation, it was relatively easy to make analog head movements to maintain a track in response to own-ship yaw rates and accelerations and angle-off rates of the target. The increased ease may have been a result of the motion cues, absent in the simulation environment.

VII. CONCLUSIONS AND RECOMMENDATIONS

HAC III was a fixed-based simulation investigating handling qualities and maneuver envelope requirements for a single-pilot helicopter employing a helmet-driven turreted gun in air combat at terrain flight altitudes. A thorough investigation of yaw dynamics for a full-traverse turreted gun was completed as well as a partial investigation into the employment of a limited-traverse turret and a fix-forward gun.

The results clearly indicated that, for a turreted gun, a high yaw natural frequency (ω_n = 1.5-2.0 rad sec) and a relatively high yaw damping ratio ($\zeta \sim 1.4$) yields Level 1 handling qualities. The yaw natural frequency and damping as variables were highly interdependent. For the task as defined, the manuever envelope used (typical of modern combat helicopters) was adequate and was not a limiting factor for both steady-state normal load factor and sideslip. Finally the turret position envelope, particularly the up-elevation limit, significantly effected the task performance. Turret rates and accelerations demanded were far less than current capabilities, and therefore were not issues in the task performance.

Although the quantity of data was low for the fixed-gun configuration, the following possible effects on handling qualities were also identified. As the weapon envelope became more restritive, the CHPR's generally decreased while the desirable yaw damping generally increased. Also, the usage of the aircraft maneuver envelope (particularly sideslip) decreased as the weapon system became more restrictive. This trend was opposite of what was expected and may be a subject for future investigations.

To gain further insight into the experimental results, the following is recommended:

- The available vehicle bandwidth is easily determined from the derived transfer functions. The bandwidth usage can be determined from the demanded vehicle angular displacements and peak rates [Ref. 24.] The bandwidth usage during HAC III should be investigated to determine which, if any, axis is limiting the task performance.

- Continual work should be made to debug the fire control to make available the ballistics and scoring subroutines. Their addition and the resulting feedback loop to the pilot (hit or miss) will change the task and may change the desirable dynamic characteristics.

94

- The aircraft model should be modified for future experiments so that pedal control power at hover does not change with a change in N_r for investigations such as HAC III
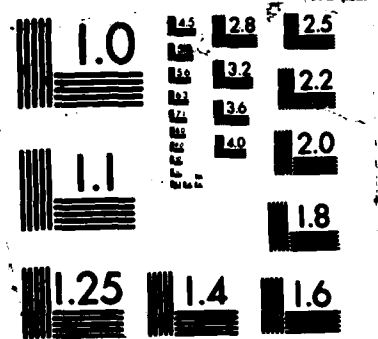
APPENDIX A
AIRCRAFT MATH MODEL

The translational equations of motion for the aircraft model, normalized with vehicle mass and moments of inertia are:

$$\dot{u} = X_u u - g \sin\theta \qquad \text{(eqn A.1)}$$

$$\dot{v} = Y_v v + g \cos\theta - U_0 r \qquad \text{(eqn A.2)}$$

$$\dot{w} = Z_w w + g \cos\theta + U_0 q + Z_{\delta c} \qquad \text{(eqn A.3)}$$

and the rotational equations of motion are:

$$\dot{p} = L_p p + L_\varphi \varphi + L_v v + L_{\delta a} \delta_a \qquad \text{(eqn A.4)}$$

$$\dot{q} = M_q q + M_\theta \theta + M_{\delta e} \delta_e \qquad \text{(eqn A.5)}$$

$$\dot{r} = N_r r + N_\varphi \varphi + N_v v + N_p p + N_{\delta p} \delta_p \qquad \text{(eqn A.6)}$$

1. LONGITUDINAL EQUATIONS OF MOTION AND TRANSFER FUNCTIONS

Transformed into the s-domain, the longitudinal EOM in matrix form become:

$$\begin{bmatrix} -s+X_u & 0 & -g\cos\theta \\ 0 & -s+Z_w & U_0 s \\ 0 & 0 & -s^2+M_q s+M_\theta \end{bmatrix} \begin{Bmatrix} \dot{x} \\ \dot{z} \\ \theta \end{Bmatrix} = \begin{bmatrix} 0 & 0 \\ Z_{\delta c} & 0 \\ 0 & M_{\delta e} \end{bmatrix} \begin{Bmatrix} \delta_c \\ \delta_e \end{Bmatrix} \qquad \text{(eqn A.7)}$$

yielding the following transfer functions:

$$\frac{w}{\delta_c} = \frac{Z_{\delta c}}{s - Z_{w'}} \qquad \text{(eqn A.8)}$$

$$\frac{\theta}{\delta_e} = \frac{M_{\delta e}}{s^2 - M_q - M_\theta} \qquad \text{(eqn A.9)}$$

2. LATERAL EQUATIONS OF MOTION AND TRANSFER FUNCTIONS

Transformed inot the s-domain, the lateral EOM become:

$$\begin{bmatrix} -s + Y_v & g\cos\varphi & -U_0 s \\ 0 & -s^2 + L_p s + L_{\varphi\cdot} & 0 \\ N_v & N_p s + N_\varphi & -s^2 + N_r s \end{bmatrix} \begin{Bmatrix} \dot{y} \\ \varphi \\ \psi \end{Bmatrix} = \begin{bmatrix} 0 & 0 \\ L_{\delta a} & 0 \\ 0 & N_{\delta p} \end{bmatrix} \begin{Bmatrix} \delta_a \\ \delta_p \end{Bmatrix} \qquad \text{(eqn A.10)}$$

yielding the following transfer functions of interest:

$$\frac{\varphi}{\delta_a} = \frac{L_{\delta a}}{s^2 - L_p s - L_\varphi} \qquad \text{(eqn A.11)}$$

$$\frac{\psi}{\delta_p} = \frac{N_{\delta p}(s - Y_v)}{s[s^2 - (Y_v N_r)s + (Y_v N_r + U_0 N_v)]} \qquad \text{(eqn A.12)}$$

$$\frac{\beta}{\delta_p} = \frac{-N_{\delta p}}{s^2 - (Y_v N_r)s + U_0 N_v} \qquad \text{(eqn A.13)}$$

To retain a constant characteristic equation for yaw above 50 knots, N_v was set equal to $K_{N v'} U_0$.

3. STABILITY DERIVATIVE VALUES

For the HAC III simulation the stability derivatives were a function of velocity and had values shown in Table 23. The values for airspeeds between 30-50 knots are simple calculated by a linear relationship between the value at 30 knots and the value at 50 knots. The derivatives are normalized by vehicle mass and moments of inertia, respectively.

TABLE 23

## HAC III STABILITY DERIVATIVE VALUES

		VELOCITY		
	≤ 30 kts	30 ≤ VEQ ≤ 50 kts	≥ 50 kts	Units
L_p	− 5.6	− 5.6	− 5.6	$\sec^{-1}$
L_v	0	0	0	rad/ft-sec
L_φ	− 6.25	− 6.25	− 6.25	rad^{-1}
M_q	− 5.6	− 5.6	− 5.6	$\sec^{-1}$
M_θ	− 6.25	− 6.25	− 6.25	rad^{-1}
N_p	g/u	$0.01908^*U_0 - 0.57235$	0	$\sec^{-1}$
N_r		see Table 8		$\sec^{-1}$
N_v	K_{NV}/u	$K_{Nv}^*U_0^*0.0005924 - 0.02365$	0	rad/ft-sec
N_φ	2(g/u)	$2(0.01908^*U_0 - 0.57235)$	0	rad^{-1}
X_u	− 0.01	− 0.01	− 0.01	$\sec^{-1}$
Y_v	− 0.1	− 0.1	− 0.1	$\sec^{-1}$
Z_w	− 1.0	− 1.0	− 1.0	$\sec^{-1}$

CONTROL DERIVATIVES

|		
$L_{\delta a}$	0.2	rad/sec^2-%
$M_{\delta e}$	0.1	rad/sec^2-%
$N_{\delta p}$	$0.0209 (Y_v N_r + K_{NV})$	rad/sec^2-%
$Z_{\delta c}$	1.5	ft/sec^2-%

APPENDIX B
SAMPLE RUN OUTPUT PLOTS

Included here are example strip charts and cross plots used for the post-simulation analysis for one experimental run. The example used was a free engagement using test cell 5 employing the full-traverse turreted gun.
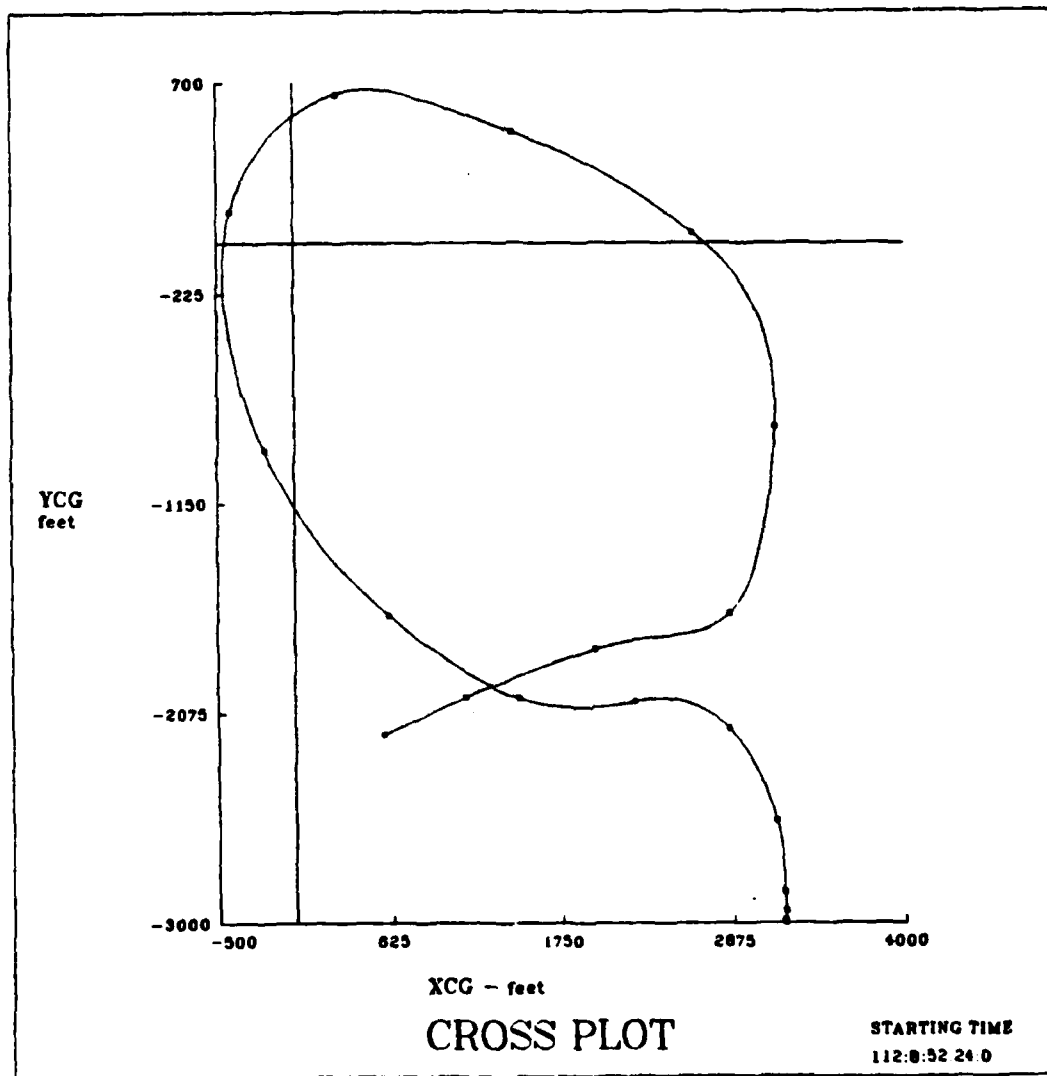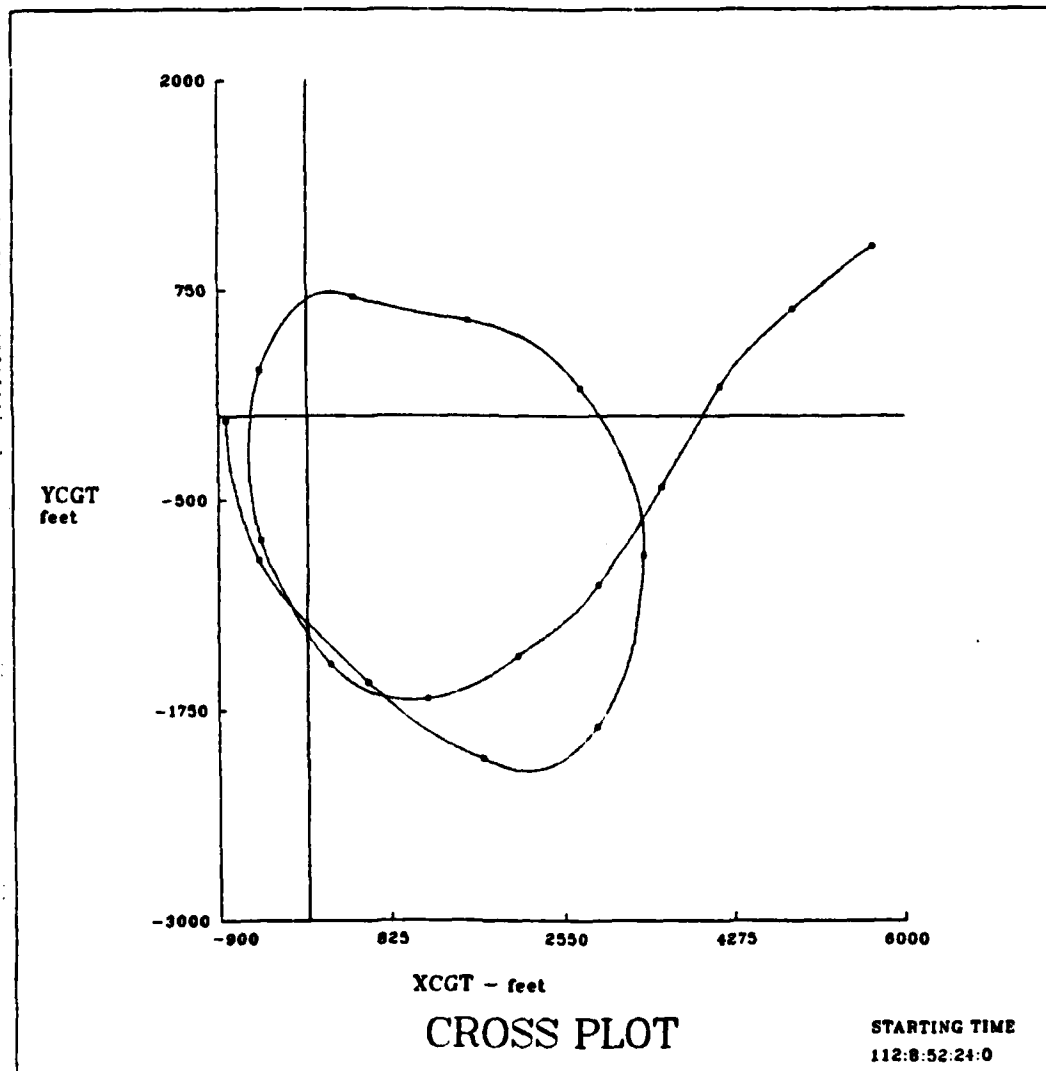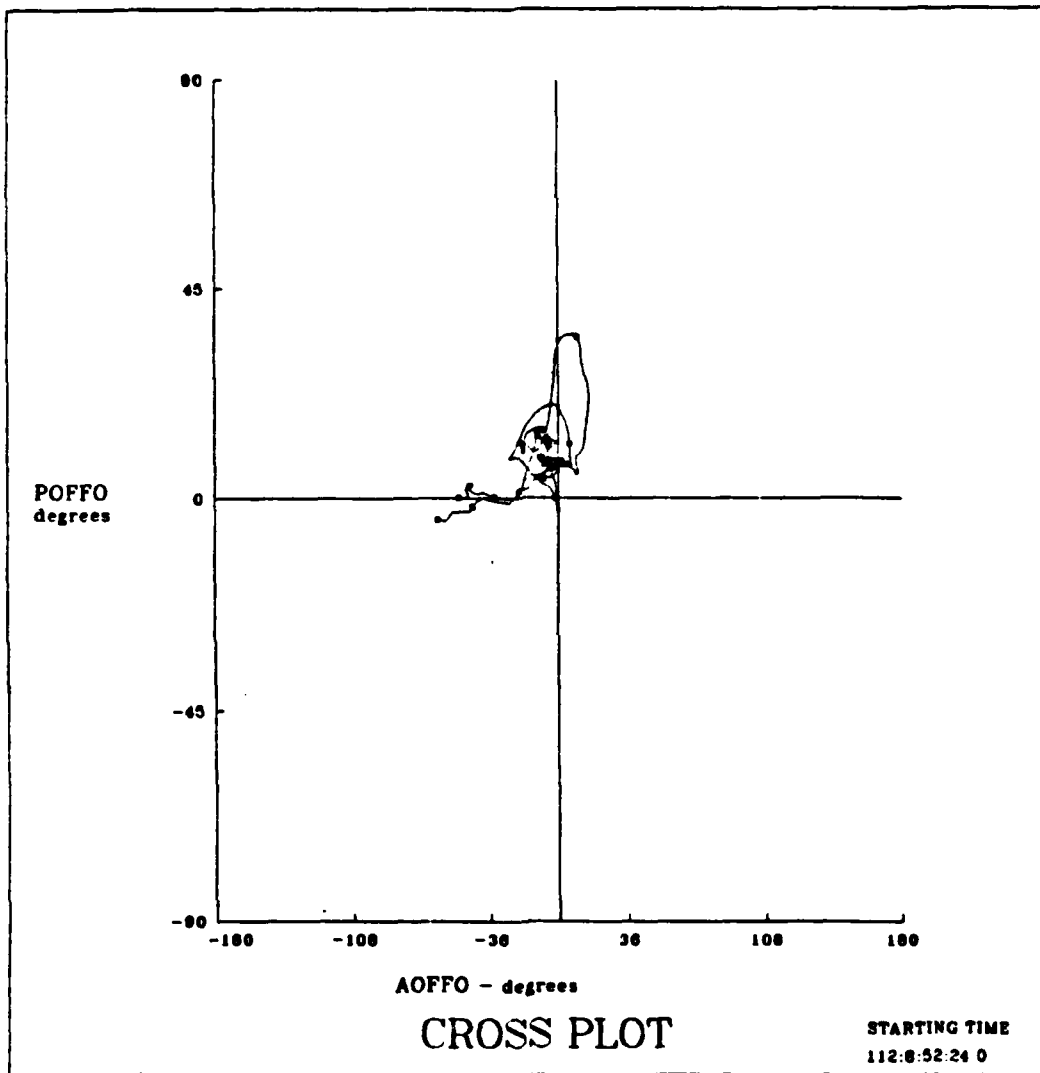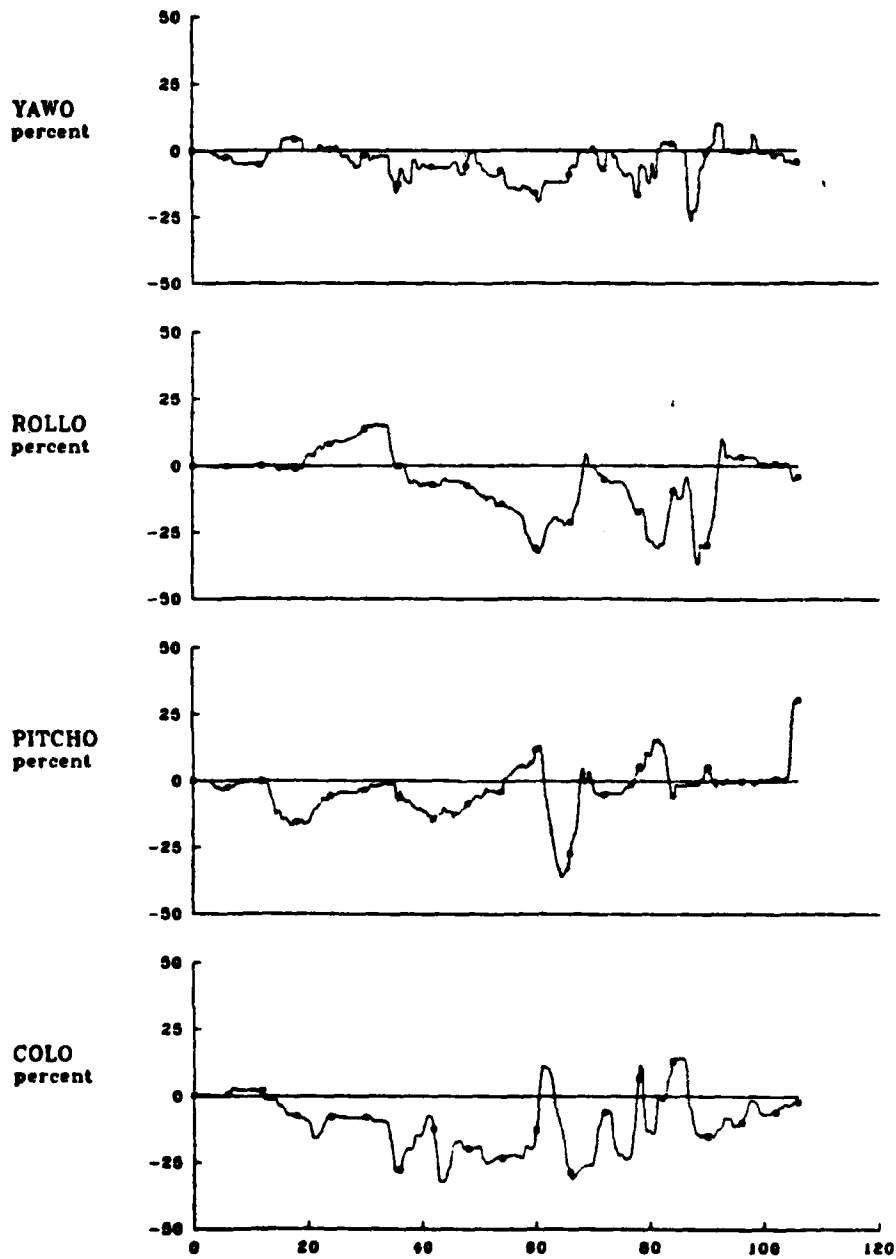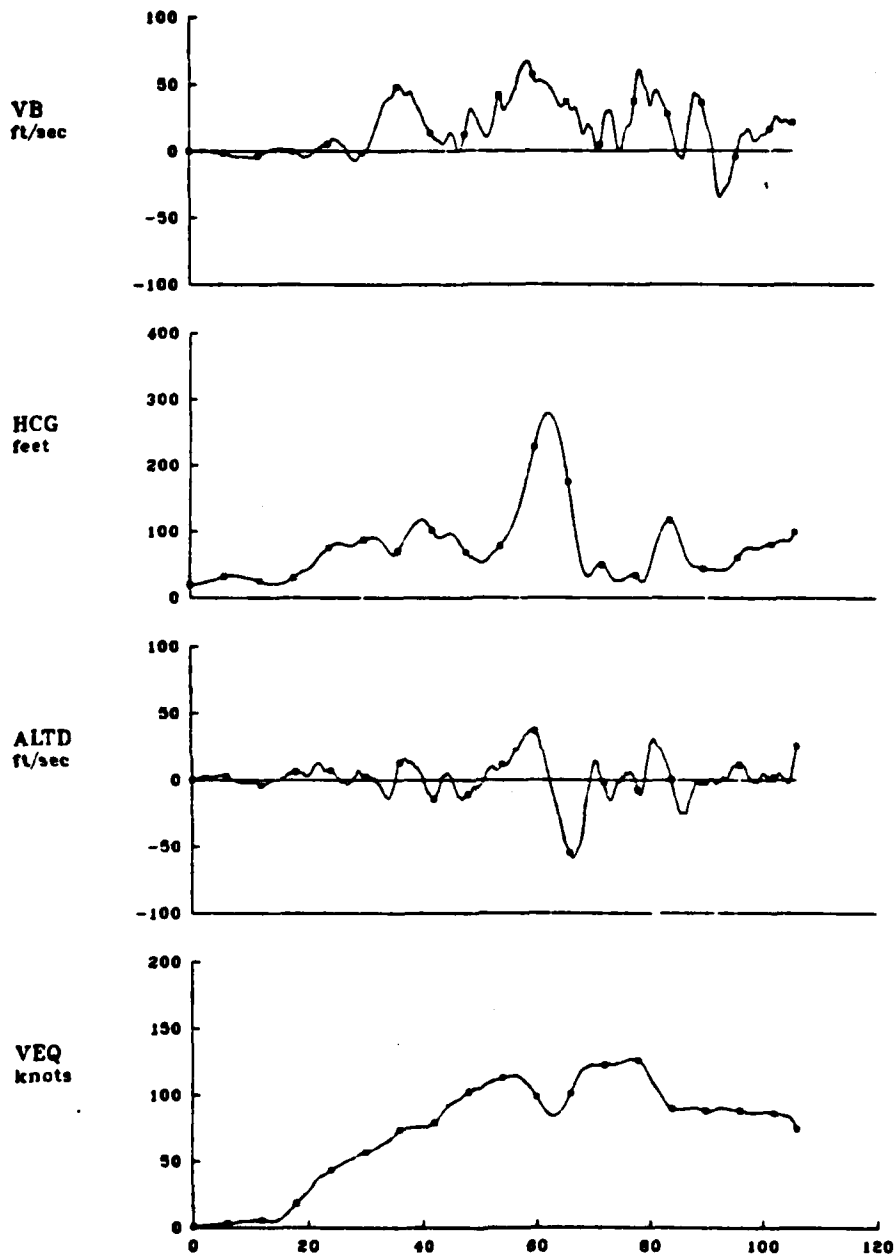

CROSS PLOT

YCGT
feet

XCGT – feet

CROSS PLOT

100

POFFO
degrees

AOFFO – degrees

CROSS PLOT

STARTING TIME
112:8:52:24 0

101

TIME – sec

STRIP CHART

STARTING TIME
112 8.52 24 0

VB
ft/sec

HCG
feet

ALTD
ft/sec

VEQ
knots

TIME – sec

STRIP CHART

STARTING TIME
112.8:52.24 0

103

BETA
degrees

PSI
degrees

THET
degrees

PHIRDM
degrees

TIME – sec

STRIP CHART

STARTING TIME
112.8:52:24.0

104

FTZ
lb-f

PSID
rad/sec

THED
rad/sec

PHID
rad/sec

TIME – sec
STRIP CHART

105

POFFO
degrees

AOFFO
degrees

HCGT
feet

VEQT
knots

TIME – sec

STRIP CHART

STARTING TIME
112 9:52:24 0

106

IFIRECP

THETRTD
degrees

PSIRTD
degrees

SRANGE
feet

TIME — sec

STRIP CHART

STARTING TIME
112 8:52.24 0

107

ITHR3

ITHR2

IFIREB

IFIRECP

TIME - sec
STRIP CHART

STARTING TIME
112.8:52:24:0

108
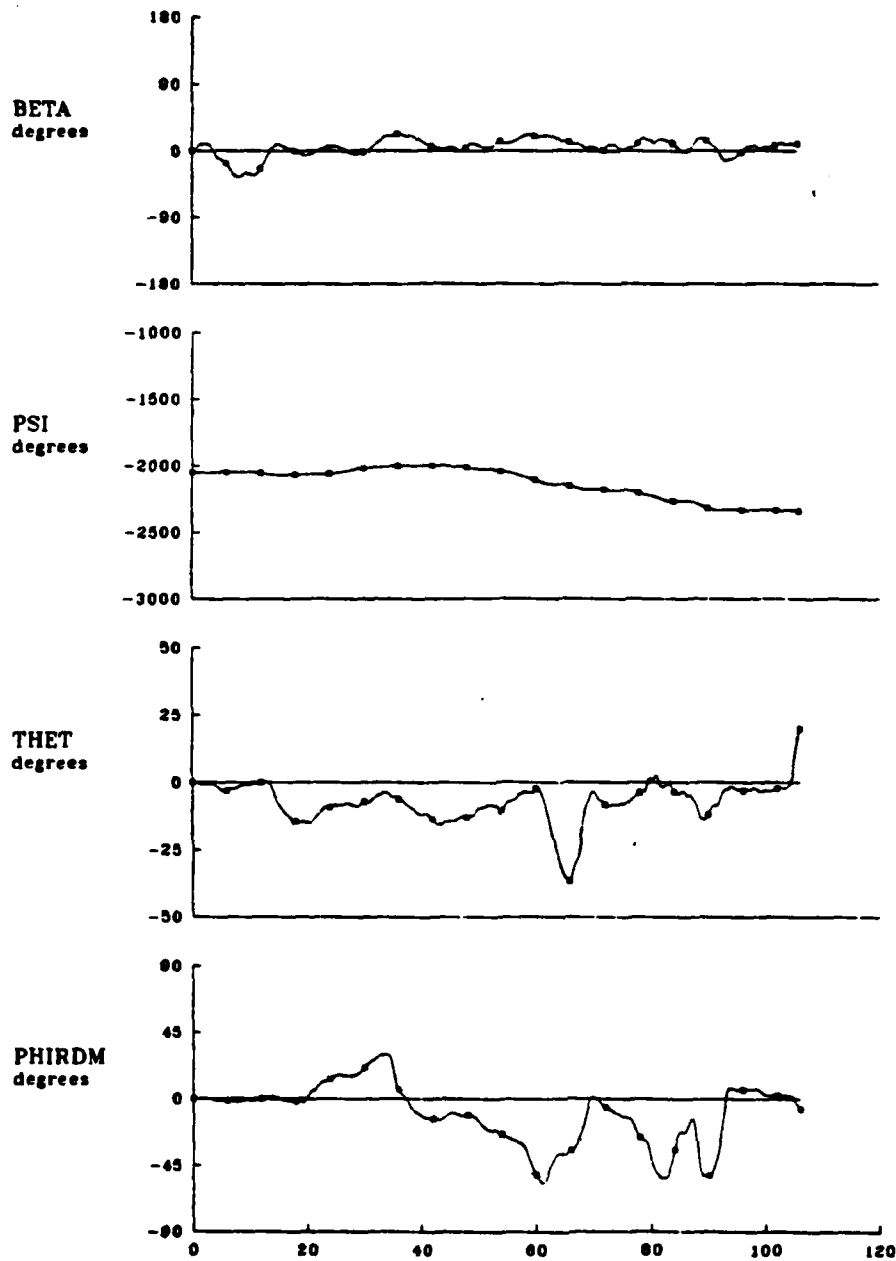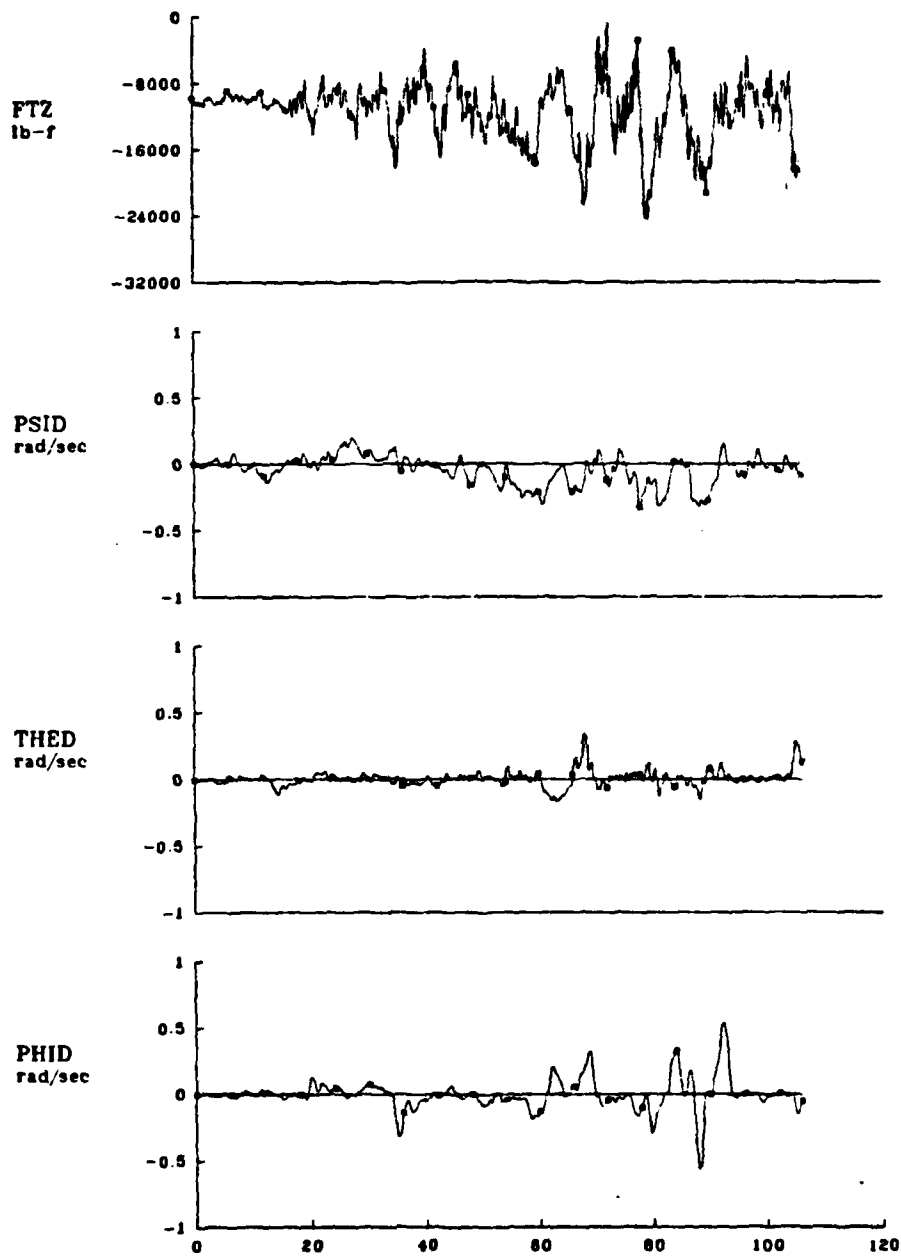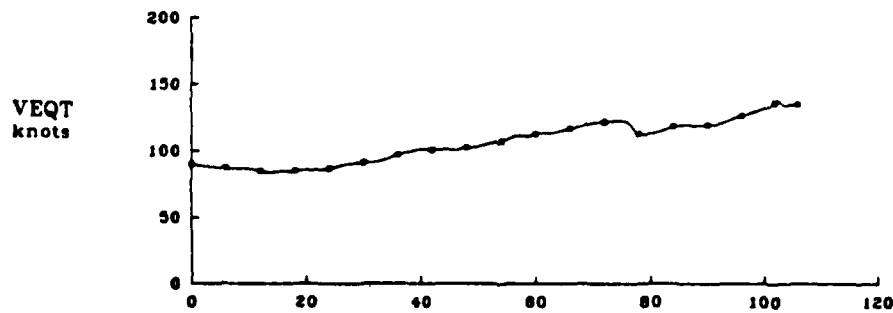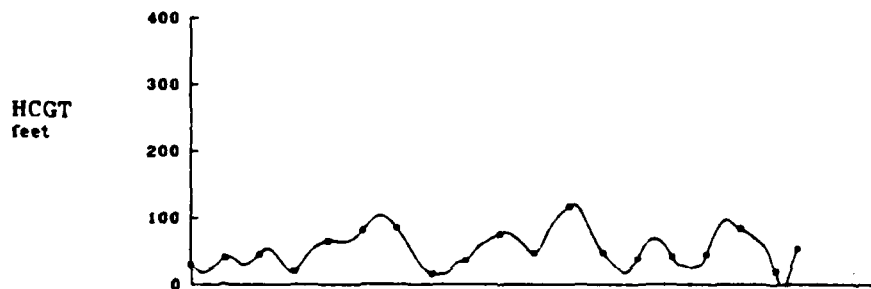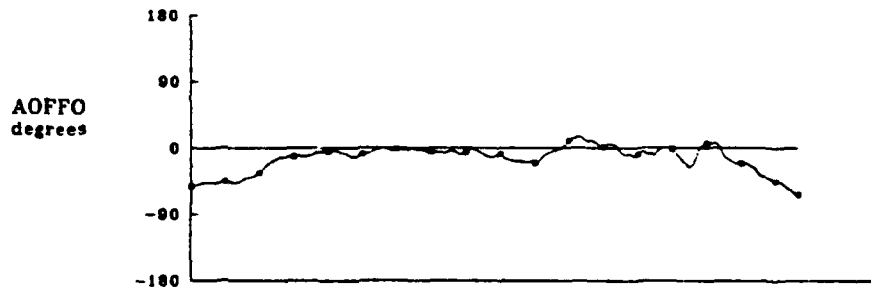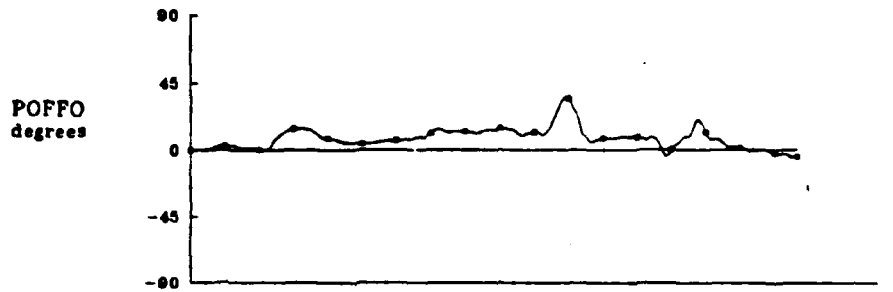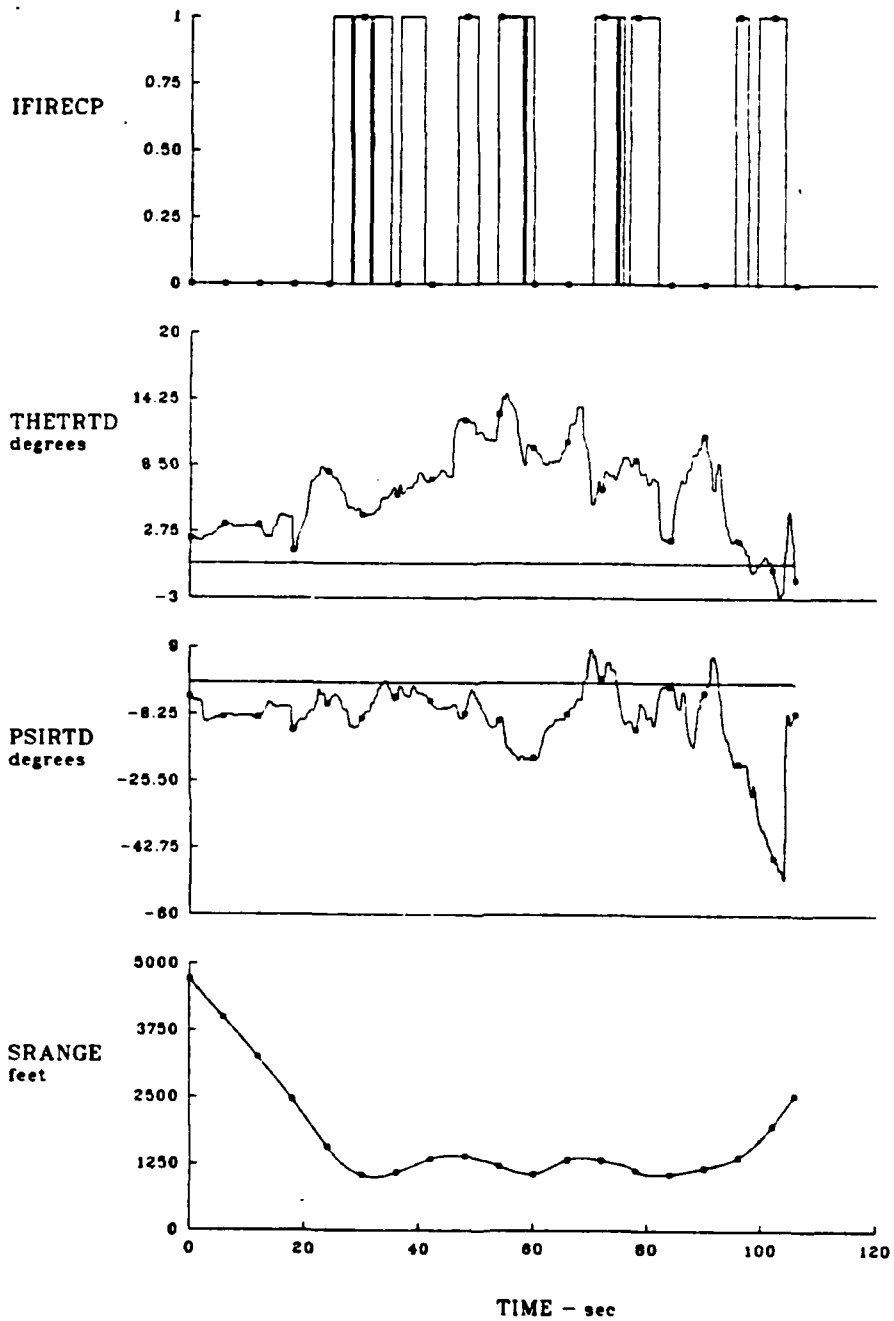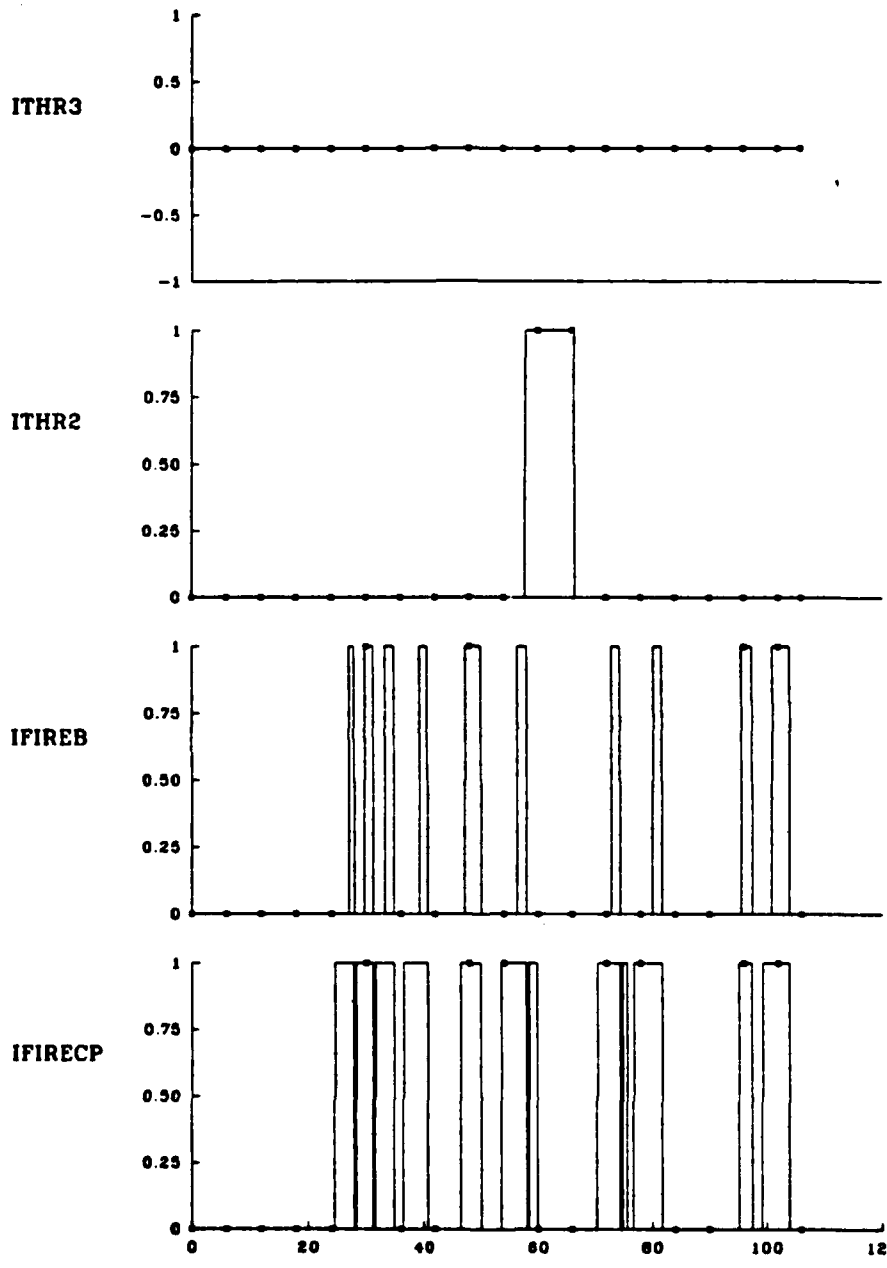
LIST OF REFERENCES

1. Anon, "Assessment of Helicopter Effectiveness in Air-to-Air Combat," Flight Systems, Inc., Newport Beach, CA, June 1981.

2. Kershner, Stuart D. and McVicar, Keith L., "Effect of Improved Maneuverability and Agility on AACT Air-to-Air Engagements," Proceedings 43rd Annual Forum of the American Helicopter Society, 18-20 May 1987.

3. McMillan, D. B., "Helicopter Flight Paths in Simulated Air-to-Air Combat," AMSAA TR-322, April 1981.

4. Vause, R., Harris, M., Falco, M., and Shaw, D., "The Utility of Speed, Agility, and Maneuverability for an LHX Type Mission," Proceedings 40th Annual Forum of the American Helicopter Society, May 1984.

5. Wolfrom, Joseph A. and Fisher, Chris E., "Data Presentation from Air-to-Air Maneuvering Between an S-76 and a UH-60A," USAAVNSCOM TR-85-D-17, September 1985.

6. "Proceedings of the U.S. Army Aviation/Industry Day II," American Helicopter Society and Aviation Systems Command, St. Louis, Missouri, October 1986.

7. Lewis, Michael S. and Aiken, Edward W., "Piloted Simulation of One-on-One Helicopter Air Combat at NOE Flight Levels," NASA TM-86686, April 1985.

8. Cooper, George E. and Harper, Robert P. Jr., "The Use of Pilot Ratings in the Evaluation of Aircraft Handling Qualities," NASA TN D-5153, April 1969.

9. Hoh, R.H., Mitchell, D.G., Aponso, B.L., Key, D.L., and Blanken, C.L., "Proposed Handling Qualities Specification for Military Rotorcraft," NASA Contract No. NAS2-11304, April 1987.

10. Lewis, Michael S. and Mansur, M. Hossein, "A Simulator Investigation of Parameters Affecting Helicopter Handling Qualities in Air Combat (HAC II)," Proceedings 43rd Annual Forum of the American Helicopter Society, 18-20 May 1987.

11. Lewis, M.S., Mansur, M.H., and Chen, R.T.N., "A Simulation Investigation of Parameters Affecting Helicopter Handling Qualities in Air Combat," NASA TM-87****, (TBP).

12. Morris, Patrick M., "AH-1G Sawtooth Climbs and Autorotation Flight Test," Naval Air Test Center, Patuxent River, MD., (unpublished), June 1978.

13. Bill, F.A., "Test Results of Airworthiness and Flight Characteristics Evaluation Conducted on a JUH-1H Helicopter Equipped with the Reconfigured Multiple Target Electronic Warfare System (MULTEWS)", Kaman Aerospace, Corp., RPT T-749, 24 May 1979.

14. Hutchings, Thomas D. and Zak, Adam R., "The Investigation of Dynamic Gun Pointing Errors for Helicopter Mounted Automatic Cannon Systems," Final Report, GEN Thomas J. Rodman Laboratory, Rock Island, IL, November 1976.

15. Kim, Ki Chul, "A Design Method for a State Feedback Microcomputer Controller of a Wide Bandwidth Analog Plant," Masters Thesis, Naval Postgraduate School, Monterey, CA, December 1983.

16. Whyte, R. H., Graham, D. A., and Winchenbach, G. L., "Aeroballistics Range Tests of 25-mm Armor Piercing and Target Practice Projectiles," AFATL TR-82-27, March 1982.

17. Anon, "AH-64 Combat Mission Simulator Ballistics Program Design Specification," The Singer Co., Binghamton, NY, July 1984.

18. Carlson, J., Ellis, D., Parisi, T., and Rizvi, A., "Air-to-Air Helicopter Fire Control Equations and Software Generation," General Electric Co., Burlington, VT., November 1979.

19. Ball, Robert E., *The Fundamentals of Aircraft Combat Survivability Analysis and Design*, American Institute of Aeronautics and Astronautics, Inc., New York, 1985.

20. Tischler, M.B., Fletcher, J.W., Diedmann, V.L., Williams, R.A., and Cason, R.W., "Demonstration of Frequency-Sweep Testing Technique Using a Bell 214-ST Helicopter," NASA TM-89422, April 1987.

21. Heffley, Robert K, "Critical task Performance and Workload Charting," Proceedings of the 22nd Annual Conference on Manual Control, Dayton, OH, 16-17 July 1986.

22. Dukes, Theodor A., "Guidelines for Designing Flying Qualities Experiments," NADC Report 85130-60, June 1985.

23. Holman, Jack P., *Experimental Methods for Engineers* McGraw-Hill, New York, 1984.

24. Heffley, Robert K., et. al., "Study of Helicopter Roll Control Effectiveness Criteria," NASA CR-177404, April 1986.

INITIAL DISTRIBUTION LIST

No. Copies

1. Defense Technical Information Center   2
   Cameron Station
   Alexandria, VA 22304-6145

2. Library, Code 0142   2
   Naval Postgraduate School
   Monterey, CA 93943-5002

3. Department Chairman, Code 67   1
   Department of Aeronautics
   Naval Postgraduate School
   Monterey, CA 93943

4. Professor Donald M. Layton, Code 67Ln   1
   Department of Aeronautics
   Naval Postgraduate School
   Monterey, CA 93943

5. Dr. J. Victor Lebacqz   6
   Chief, Flight Dynamics and Controls Branch
   Mail Stop 211-2
   NASA Ames Research Center
   Moffett Field, CA 94035

6. Director   1
   U.S. Army Aviation Research and Technology Activity
   NASA Ames Research Center
   Moffett Field, CA 94035

7. USAAVNC   1
   Directorate of Combat Developments
   ATTN: ATZQ-CDD
   Fort Rucker, AL 36362

8. William A. Decker   4
   Flight Dynamics and Controls Branch
   NASA Ames Research Center
   Moffett Field, CA 94035

9. CPT Jeffrey N. Williams   4
   Route 1
   Winter, WI 54896

END

Feb.

1988

DTIC